# MASTER OF SCIENCE BY RESEARCH

## Surface treatment of silicon nitride using contact-less energy beams

Shukla, Pratik

*Award date:*
2008

*Awarding institution:*
Coventry University

**MSc by Research Thesis**

# Surface Treatment of Silicon Nitride using Contact-less Energy Beams

**by**

**Pratik Shukla**

**2006 / 2009**

## Abstract

This research investigated the surface treatment of Hot Pressed Silicon Nitride (HP $Si_3N_4$) predominantly using lasers, in order to enhance the surface properties, in particular the fracture toughness ($K_{1c}$). $K_{1c}$ is a fundamental mechanical property that quantifies the resistance of the material to crack propagation. Empirical equations derived by previous workers were used to calculate the $K_{1c}$ from Vickers hardness indentation test.

Conventional Shot Peening of metallic substrates generate beneficial surface compressive stresses by plastic deformation that enhances fatigue properties. Polycrystalline ceramics do not tolerate plastic deformation so the mechanism of mechanical shot peening cannot apply to ceramics. Literature in the field of laser surface treatment of ceramics has identified mechanisms of minimising surface cracks and porosity by softening and redistributing minor amorphous/ glassy phases to in-fill surface defects.

A number of empirical equations, derived by previous workers were assessed and one equation [Ponton 1989] in particular was identified as the most suitable. A low powered $CO_2$ (Carbon dioxide) laser, 2 KW, Nd: YAG (Niodinium, Yittrium, Aluminium Garnet) industrial laser assisted by an industrial Kuka robot, plasma augmented processing and ultrasonics was employed.

As machined (virgin surface) of HP $Si_3N_4$ and ground & polished surfaces were first examined for their hardness and the $K_{1c}$ of the material was calculated prior to the surface treatment using the energy beams. It was found that an average of an 18 % increase was obtained in the materials hardness for the HP $Si_3N_4$ by grinding & polishing in comparison with the “as machined” surface.

Surface treatment using the $CO_2$ laser showed a decrease in the hardness by an average of 35 %. Nd: YAG treatment of HP $Si_3N_4$ also decreased the hardness by an average of 27 %. It was believed that a change in the materials composition occurred due to surface oxidation. It was believed that the treated area of the material was changed from $Si_3N_4$ to silicon dioxide. Crack lengths found after conducting the Vickers indentation test for Nd: YAG processing were much larger than the cracks obtained from $CO_2$ laser processing due to rapid thermal shocking which did not occur with $CO_2$ processing. This decreased the $K_{1c}$ value of the samples treated by the Nd: YAG laser. Although, the value of $K_{1c}$ obtained from the Nd: YAG laser treatment averaged up to 7.12 $MPa\sqrt{m}$ and an average of 14 % of the samples showed an increase in the materials $K_{1c}$. $CO_2$ laser processing was found to be more successful in increasing the $K_{1c}$ in comparison with other energy beams applied.

***To my Parents, whose hard work and sacrifice has made me flourish...***

## Declaration

The work described in this report is the result of my own investigation. All sections of the text and results that have been obtained from other work are fully referenced. I understand that cheating and plagiarism constitute a breach of University Regulations and will be dealt with accordingly.

Signed: ..... Date: 28 / 03 / 07

**Pratik Shukla**

## Acknowledgements

I take this opportunity to express my sincere gratitude to my director of study Dr Colin Page for his valuable advice, guidance and support especially during the times when I needed a push. I would also like to thank Dr Houzheng Wu for giving me the opportunity to undertake this research and pointing me into the correct direction.

Special thanks also go to Dr Philip Swanson who also contributed greatly by keeping this project on track and providing valuable advice and technical assistance. I am grateful to Mr Mike Keough from the laser lab (Coventry University), Niel Burns and Peter Hancocks from Warwick Manufacturing Group, Shanghai Unite Technology (China) for providing ceramic testing material as well as Mr Barry McGrory for his technical advice and Dr David Kirk for providing samples of tungsten carbide for further testing.

I am also thanking my colleague Adel Hajajji for inspiration and valuable advice. Also my flat mate and school friend Syeed (Sid), who paid a big contribution towards my work and has endlessly, supported me throughout the period of my work. Many thanks to Amit Punjani also, who contributed in many different ways. Special gratitude also goes to my colleague Mr David Guiry from AETC Turbines Ltd and another one of my school friend Jignesh Chauhan for moral support and for proof reading some of the draft text from my thesis.

I am forever indebted to my parents for their unconditional love, advice, endless patience and support in every way possible, which has given me the strength, determination and fortitude to accomplish my goal. The moral support which I have received from other members of my family was also very much appreciated.

I express my deep gratitude to one more person who has been very close to me. Tosha. Despite all the hardship, pain and trouble caused over the entire year, I must still confess that the credit should go where it belongs. Her support, contribution, encouragement, the drive and the motivation which she provided will forever be unforgettable. Thank you Toshy…… I will never forget it. Lastly, I am very thankful to those who directly and indirectly helped me in completion of this project.

# Table of Content

# List of Figures

**CHAPTER VI**

# List of Tables

## CHAPTER III



## CHAPTER IV



## CHAPTER V



## CHAPTER VI

**Table 6.3:** The differences in the results obtained by various non- contact energy beams applied to the HP $Si_3N_4$.

## APPENDICES

## Abbreviations

| | |
|---|---|
| Fracture Toughness = | **$K_{1c}$** |
| Carbon Dioxide = | **$CO_2$** |
| Neodinium, Yittrium, Aluminium, Garnet = | **Nd: YAG** |
| Neodinium, Yittrium Lithium fluoride = | **Nd: YLF** |
| Light Amplification Stimulated Emission, Radiation = | **LASER** |
| Gaussian Beam Mode = | **$TEM_{00, 01}$ etc** |
| Continuous Wave = | **CW** |
| Plasma Augmented Laser Processing = | **PALP** |
| Plasma Augment Laser Welding = | **PALW** |
| Scanning Electron Microscopy = | **SEM** |
| X – Ray Diffraction = | **XRD** |
| Surface Roughness = | **Ra** |
| Hardness = | **Hv** |
| Young's Modulus = | **E** |
| Newtons = | **N** |
| Average Flaw Size = | **c** |
| Load (kg) = | **P** |
| Load Impact = | **Pc** |
| Interior Cracks = | **Ic** |
| Metre per minute = | **$m\ min^{-1}$** |
| Cambridge Engineering Selector = | **SES** |
| Hot Pressed Silicon Nitride = | **HP $Si_3N_4$** |
| Reaction Bonded Silicon Nitride = | **RBSN** |
| Sintered Silicon Nitride = | **SSN** |
| Titanium Alloy = | **BSTOA 6 / 4** |
| Yittrium Oxide = | **$Y_2O_3$** |
| Magnesium Oxide = | **MgO** |
| Zirconia = | **$ZrO_2$** |
| Silicon Nitride = | **SiC** |
| Boron Nitride = | **BN** |
| Alumina = | **$Al_2O_3$** |
| Outer Diameter = | **OD** |
| Inner Diameter = | **ID** |
| Kilo gram = | **Kg** |
| Stress Corrosion Cracking = | **SCC** |
| Mega Pascal per Metre Cubed = | **MPa $\sqrt{m}$** |
| Giga Pascal = | **GPa** |
| Kilo Hertz = | **KHz** |

| | |
|---|---|
| Mega Hertz = | **MHz** |
| Kilo Watts = | **Kw** |
| Mega Watts = | **Mw** |
| Alpha = | **α** |
| Beta = | **β** |
| Cubic = | **γ** |
| Micro Metre = | **µm** |

# CHAPTER I

# Introduction to Conventional Shot Peening

## 1.1: Introduction

Shot Peening is a type of surface treatment used to enhance the service life of engineering components. It is a cold working process that fires balls (shot) of steel, ceramics or glass beads at the work-piece (metals in particular) to mechanically pre-stress the material beyond its yielding point [Verpoort 1989]. The localised plastic deformation induces residual stresses into the surface layer of the material. The surface residual stresses are compressive. The induced compressive residual stresses inhibit crack growth under cyclic loading, increasing the material hardness, fatigue life and resistance to stress corrosion cracking (SCC).

Commercial advantages and economic benefits have made the laser systems popular. The benefits offered are high processing speeds, accuracy, shorter process times, deep penetrating treatment (precise control of the thermal input) and aesthetics, which are far too attractive to be ignored.

Laser peening in the recent years has developed and proven its success with steels [Verpoort 1989], aluminium and titanium surfaces, although, minimal research has been conducted on laser surface treatment of engineering ceramics. Applications of ceramics have been limited due to their crack sensitivity and low fracture toughness ($K_{1c}$), however, the use of ceramics have advanced over the years. They are now considered as the new space age material used to manufacture components for the aerospace, automotive and military sectors. Engineering ceramics offer exceptional mechanical properties, which allows them to replace the more conventional materials currently used for high demanding applications [Wright 2005, Verpoort 1989, Hackel 2006, Clauer 1996, Solomah 1993].

Therefore, the focus of this work was to investigate the feasibility of surface treating ceramics by non-contact energy beams in form of industrial lasers, laser assisted plasma augmented processing and ultrasonics to observe if there was a change in the materials $K_{1c.}$ From the family of engineering ceramics; silicon nitride ($Si_3N_4$) was the main material investigated.

The mechanical property under investigation was fracture toughness ($K_{1c}$), since it is a very important property of any material and especially ceramics in particular due to their brittle nature. Ceramics in comparison with metal/ alloys have a low $K_{1c}$, hence it would be an advantage if the $K_{1c}$ of ceramics could be improved. This can open avenues for ceramics to be applicable to high demanding applications where metals/ alloys fail due to their low

thermal resistivity, co- efficient of friction, wear rate and hardness in comparison with ceramics.

$K_{1c}$ is a measure of the materials resistivity to fracture or crack propagation, it is the plane strain fracture toughness. $K_c$ is the plane stress fracture toughness. Materials with high $K_{1c}$ are much softer and ductile. Those types of material can resist cracks at higher stress levels and loading. Materials with low $K_{1c}$ are much harder, brittle and allow crack propagation at lower stresses and loading. Unlike metals, it is difficult for dislocations to propagate within ceramics which makes them brittle. Ceramics also do not mechanically yield as well as metals in comparison which leads to much lower resistance to fracture. The measure of $K_{1c}$ was carried out using the Vickers indentation method which calibrates the hardness of the material and induces a crack. Measured hardness and the crack lengths were then placed into an empirical equation to calculate the materials $K_{1c}$ after and prior to the surface treatment. Surface topography was also measured to observe the change in materials surface finish before and after the laser treatment.

In all cases a comparison from literature was made with the characteristics of the conventional shot peening process to assess the feasibility of surface treating engineering ceramics by the aid of energy beams, to identify if a similar outcome is obtained to that of the conventional mechanical technique. There are three main objectives of the project:

**I**. To evaluate the differences between mechanical and non-contact surface-treatment processes from the literature.

**II.** To Conduct experimental trials on HP $Si_3N_4$ using non- contact energy beams such as industrial lasers, hybrid laser /plasma augmented processing and possibly ultrasonics.

**III.** To analyse the observed changes in the key mechanical property ($K_{1c}$) using an experimental and an analytical approaches.

## 1.2: Early History

Mechanical pre-stressing dates back to the time of the crusades (1100-1400 A.D). Records show objects found near the ancient shoreline of the Persian Gulf, dating back to 2700 B.C exhibiting properties of cold work hardening by controlled hammering. The technique was used on metals such as copper, iron, bronze and steels when manufacturing weapons and tools [London Museums 2007, Bush 1962].

A ball pein hammer was used to work harden the material as it improved the material's resistance to wear and lengthened the life of the treated product. The word "peen", as it is known to us today, originates from the term "pein" [Marsh 1993, Bush 1962]. The term shot peening began from the principle of firing steel shot at the material surface. During early $19^{th}$ century, the process was considered as unpredictable, with its effects being somewhat

unknown. The process then developed over time and continuous research was conducted from 1920's onwards [Marsh 1993, Herbert 1927, Wright 2005, Bush 1962].

From being a remedial process to treat engineering components in the 1980's [Herbert 1993], shot peening is now being introduced into product design specifications for advancing industrial applications and pushing the technology to further limits. Common materials treated by shot peening are carbon steels, alloy steels, stainless steel, aluminium and titanium alloys.

## 1.3: The science and theory of Shot Peening - The Mechanical Processes

The main objective of shot peening is to plastically deform the top surface layer of a material or the component being treated by the impact of steel shot (balls) fired at high velocity. The steel shot fulfilling the purpose of the pein hammer to plastically deform the surface of the component part being treated. During this impact, a portion of the kinetic energy carried by the shot impacts to the material surface generating localised plastic deformation. This results in a small increase in the temperature at the point of impact. The residual kinetic energy carried by the shot enables it to deflect from the surface of the component [Wright 2005].

The level of plastic deformation is dependent on the hardness and the thickness of the material. Therefore, more shot kinetic energy is required for thicker and harder surfaces. This can be obtained by increasing the size or the weight of the shot and its velocity. The type of shot material used also varies the rate of deformation. If steel shot is used, then high deformation energy can impact to the material in comparison with ceramic or glass particles as steel is much denser material [Wright 2005].

The metal shot cause plastic deformation as they are fired onto the surface, which locally expands. The plastic deformation of the stretched surface is resisted by the underlying (elastic) bulk material, which pushes the surface into compression. Hence the core is left at a low level of tension. The system is balanced with respect to forces (stress area) where high surface residual compression exists in the surface region and low bulk residual tension in core. The component part or the material being treated is also reduced in size. This is due to the top layer of the material being compressed. The deformation is dependent on the shot size and velocity.

To understand the effect of shot peening; it is important to analyse the structure under three point bending. When a beam is placed under three point bending the distribution of compressive stress is acting diagonally across its cross section. The top part of the beam is in tension as the material is being bent. Hence, the bottom part of the beam is in compression where the forces are acting in the -ve direction. The point in the centre of the beam is therefore under equilibrium where the forces are balanced. This is presented in Figure 1.2.

If the particular bent surface is shot peened, the distributed stress area is modified to avoid the beam to fracture from tensile stresses, as further presented in Figure 1.1, where the tensile and compressive stresses are equally distributed over the structure. This distribution is called the resultant stress (the sum of the material under three point bending and the peened structure put into three point bending).

The material is compressed during the impact and causes the top layer to stretch and tighten, causing the surface beneath to compress. The compressive layer introduces stresses into the material which are deemed negative as illustrated in Figure 1.1 by the green dotted line. Surface tensile stresses deemed positive (continuous black line, Figure 1.1), would aid the propagation of surface cracks, where resultant tensile stress pre-exist in the core of the material. If a crack is to propagate on the material surface, then the applied tensile stress must first overcome and increase the residual compressive stress induced by shot peening before a crack is generated. A crack will only propagate if applied tension exceeds the induced compression. The material comprises of tensile stresses which exist in the core, hence, it is necessary that the material remains in equilibrium by inducing compressive stresses.

The compressive stresses inhibit surface crack propagation. The tensile forces must overcome the compressive forces in order to propagate a crack on the surface. For example if shot peening induces a compressive force of –200 N/ $mm^2$, the acting tensile stress must be over +200 N/ $mm^2$ for the material to generate a crack. Figure 1.1 presents the distribution of applied and residual stress in 3 point bending after shot penning.

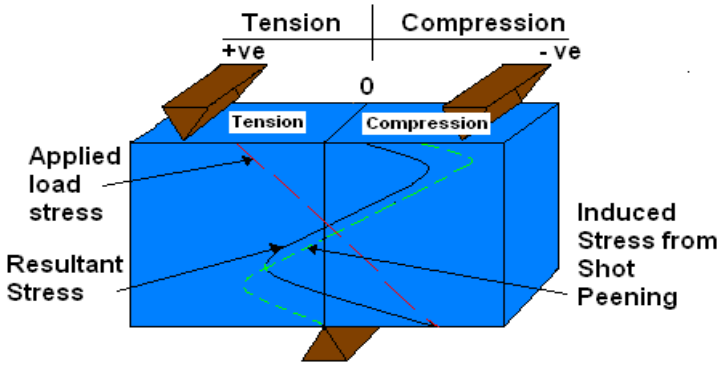


**Figure 1.1: Applied residual stress on the material and distribution of shot peening stress.**

## 1.4: Benefits of Shot Peening

### *1.4.1: Avoids or Prevents Stress Corrosion Cracking (SCC)*

Manufacturing processes such as welding or mechanical fasteners and bolted flanges can leave static stresses in the material. SCC can only develop when the material experiences the following three conditions: (a) tensile stress, (b) susceptible material and (c) corrosive environment. Tensile stress is removed through shot peening by inducing compressive stress in the opposite direction [Wright 2005]. Therefore, one necessary condition from the above three is eliminated, and propagation of surface cracks and SCC can be avoided.

### *1.4.2: Increased Hardness*

Localised surface impact causes the material to stretch and tighten by inducing residual compressive stresses into the surface layer of the material. Hence, the surface hardness increases due to work hardening of the surface layer during shot peening. Work hardening of the material allows plastic deformation and produces mechanical yielding.

### *1.4.3: Improvement in Fatigue Life*

The life span of the engineering components is predicted by either fracture mechanics methods or statistical S/N fatigue test data [Kalpakjian 2001]. Components with fatigue failure predicted at 60 % of its life span were shot peened and then tested. Over 300 % of its predicted life was obtained without further cracking [Wright 2005]. The reason is that shot peening allows the material to become much harder and wear resistant. The wear resistance prevents failure at the early stage and elongates the life span. This is especially applicable to components under frictional and shear stresses.

### *1.4.4: Increase in Load Capacity and Bending Strength*

During bending, tension exists on the top part of the structure and compression would therefore occur on the bottom part. The forces acting on the top layer (Figure 1.2) are pulling the structure apart, meaning that the material under bending has the potential to fracture if the tensile stress reaches the materials UTS (ultimate tensile strength). The bottom part of the structure is under compression which forces the material to compress into its own area. This creates equilibrium in the centre part of the structure under the bending moment as illustrated in Figure 1.2. Shot peening induces additional compressive stress on the top layer where the tensile stress is acting. This would reverse the positive tensile stress into negative compressive stress and prevent the structure from fracturing or being pulled into two parts. It would also enhance the materials resistivity to fracture at higher bending load capacity. Since the material is under compression, the required force to initiate yielding at the top surface (layer) will also increase.

**Figure 1.2: Enhancement in the bending strength due to compressive stress induced by shot peening [Wright 2005].**

Due to shot peening the compressive stress acting on the top layer will mean that the tensile stress produced during the bending moment is required to overcome the compression. This shows that the bending strength of the material is enhanced by introducing a layer of

compressive stress, allowing the material to exhibit higher bending strengths in comparison with the untreated material under the same bending conditions.

## 1.5: Application of Shot Peening in the Aerospace and automotive Industry

Shot peening is applied widely in the aerospace industry where turbine blades and disks used for aerospace and industrial gas turbine engines are commonly peened. Application of shot peening is also common in the automotive industry as the process is used to treat gears, crankshafts, drive shafts and compression springs [Wright 2005].

## 1.6: Other Surface Treatments

### *1.6.1: Shot or sand blasting*

Shot and sand blasting are similar processes to shot peening with a different objective. The only difference is that the shot blasting process employs spherical particles, grit particles or often various grades of rough sand that is fired at the surface to remove corrosive products from many engineering components in general [Marsh 1993]. With shot peening as described previously, smooth round shot are used to induce compressive residual stress by deforming the top layer of the surface. Both of the processes can be carried out on the same machine. It is only required that particles are changed from round shot to spherical shot, grit or sand.

### *1.6.2: Laser peening*

Laser Peening is a recent development in the surface treatment of engineering components. The principle behind the laser peening process is a fairly simple one [Wright 2005]. Typically a Nd: YLF (Neodynium, aluminium, yttrium, lithium fluoride) laser is used to generate a pulsed beam into the material which produces a shock-wave (thermal expansion) through the surface as illustrated in Figure 1.3. The laser pulse can be fired on the work-piece several times to induce compressive residual stress depending on the required depth of the stress. The input of the compressive residual stress is as much as four times larger than of the conventional mechanical shot peening technique. The deep residual stresses induced into the material help to combat fatigue and corrosion failures. Component life and hardness of the material is enhanced in the same way as it would with that of the conventional shot peening technique.

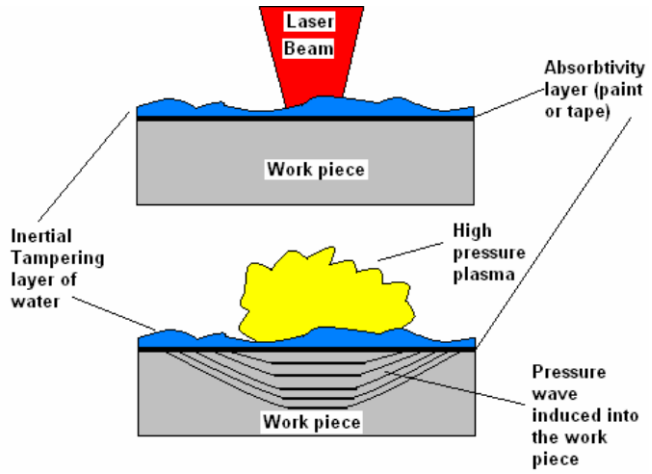


**Figure 1.3: The process of Laser Peening and the residual stress induced by the high pressure plasma.**

## 1.7: Constraints with Mechanical Shot Peening.

Conventional shot peening technique has several constraints that exist within the process as highlighted in the bullet points below. Issues discussed and justified in this section were gained from communicating with the laser peening division at The Metal Improvement Company Limited [Metal Improvement Company Ltd 2006] who are currently the world leaders in providing research & development and job shop applications for mechanical shot peening and Laser peening in particular.

- Changes in the Surface Topography
- Deformation of the Shots
- Change of Shot Size Requires Machine Set Up
- Shot Diameter is only suitable for a Specific type of Nozzle [Marsh 1993]
- Recollection of Shots [Marsh 1993]
- Shot Peening Control and Processing Intensity
- Distortion [Marsh 1993]

## 1.8: Reasons for Implementation of Non- contact Shot Peening

- Penetrating Depth of Residual Stress induced into the material
- Improvement with Surface Roughness
- No Tool Change Require
- No Recollection of the Fired Shot
- Availability of superior motion system and freedom of movement that aids programming of complex shapes and geometries.
- Feasibility for Cooling the work-piece

## 1.9: Cost Comparison

Cost of laser peening is high in comparison with the conventional shot peening systems. However, laser peening is simply a superior process with controllable parameters offering shorter process times. A small/medium size, brand new shot peening machine could cost up to 30000 (GBP). In comparison, an average Nd: YAG or a $CO_2$ high power laser system (brand new) would cost up to 200000 to 250000 (GBP).

Laser Peening is an independent process, which means that it is performed after the component has been manufactured. Most small medium size manufacturers do not invest on laser peening systems for carrying out such a surface treatment. This is simply because the laser systems are far too expensive to run and maintain just for the purpose of a peening application. Manufacturers tend to turn to job shops that specialise in laser peening applications such as The Metal Improvement Company Ltd.

The charges made by the job shops are purely dependant on the component size, shape, geometry, weight quantity, ablative layer, area of peening (number of laser spots) and the customer specification. It was stated by The Metal Improvement Company Ltd that cost estimation of laser peening applications are not specific since the above factors mentioned play a big part in estimating the cost, however, they also state that it is more expensive than the conventional shot peening process and is only performed according to the customer demand and design specification of the component. A typical hourly rate charged by a laser job shop for shot peening a welded heat exchanger was 75 (GBP) per hour in 2005. This included labour, machine set up and variable costs such as electricity wear and tear of the equipment. The current cost for such an application would be higher considering inflation. The number of hours spent on one particular job is again purely dependant on the features of the component. In comparison with laser shock peening rates the typical charges given for the mechanical shot peening process was quoted up to 65 (GBP) per hour in 2008 by Elgamec Ltd (UK) which includes the machine set up time. Elgamec Ltd; is a small job shop which specialises in the conventional shot peening process. The reason for the cost of laser shock peening being higher than that of the mechanical shot peening is due to the machine programming skills required by the operator, which is not needed with a conventional shot peening machine along with the laser system requiring higher costs in general to operate, and also due to laser machinery comprising of more complexity.

## 1.10: Chapter Summary

There are several constraints with the conventional shot peening process which open up avenues for research work to be considered. In order to gain any benefits from the process, it is vital that the material surface yields mechanically and the process of tensile stress is reversed so compression can be induced into the material. This is not common with ceramics as they do not yield and plastically deform readily.

Processes such as laser peening have proved to be successful surface treatment methods for metals and also generate further benefits compared to the more conventional mechanical shot peening technique. Therefore, the aim of this work is to investigate if similar benefits can be obtained from using non-contact energy beams with non-metallic materials such as ceramics.

Existing constraints within the conventional shot peening process could be counteracted if non-contact processes such as laser peening are implemented. The cost of the laser systems is much higher in comparison with the conventional shot peening process. However, laser peening is much superior to the conventional shot peening due to the depth of the compressive residual stress obtainable. Other reasons as previously discussed such as faster processing time, flexibility with treating components of complex geometry and overcoming the constraints existing by mechanical shot peening will attract large manufacturing companies to implement such a system. However, SME's (Small Medium size Enterprises) will most likely revert to sub-contract the process to job shops such as "The Metal Improvement Company Ltd" for their laser peening applications.

Laser peening at the moment is only performed according to the customer demand and component specifications, typically when the product demands deep induced residual stress (automotive gears) for example. The designers and the engineers have to make a choice between processing cost and quality of treatment when choosing either laser peening or the conventional shot peening process.

# CHAPTER II

# Silicon Nitride Ceramics and their Industrial Applications

## 2.1: Introduction

Engineering Ceramics offer a wide range of mechanical and thermal properties. These properties are typically superior to conventionally used metals, plastics and glass [Solomah 1993, Lawn 1975]. It is important to increase the $K_{1c}$ of ceramics so it can open up new avenues for their application. Metal/alloys have higher $K_{1c}$ than ceramics, although, other properties of ceramics are beneficial for use in high demanding applications. If the $K_{1c}$ of ceramics can be improved then it gives an advantage to ceramics for new and demanding applications.

Principle ceramics that are used in industry are alumina ($Al_2O_3$), Zirconia ($ZrO_2$), silicon nitride ($Si_3N_4$), silicon carbide (SiC), and boron nitride (BN). There are also many more which are utilised in various industrial sectors.

## 2.2: Background of Silicon Nitride Ceramics

### *2.2.1: Crystal Structures of Silicon Nitride ($Si_3N_4$)*

Direct contact between silicon and nitrogen at high temperatures form a solid substance known as $Si_3N_4$. $Si_3N_4$ is the main component in the ceramic; about 99 % of the material is $Si_3N_4$. The material has three crystal structures which are designated **α, β**, and **γ**. The designated letters represent the phases of crystals known as **α** = tetragonal, **β**= hexagonal close packed and **γ** = cubic (c), which is a modification of boron nitride, (c-BN). The most common phases of $Si_3N_4$ are **α** and **β** that can be formed under normal pressure conditions [Peng 2004]. In order to produce phase **γ**; synthesis under extreme pressure conditions must be carried out. The **γ** phase has a spinal type structure where the silicon atoms organise six nitrogen atoms octahedrally as well as one other silicon atom organising four nitrogen atoms tetrahedrally [Peng 2004].

All three phases **(α, β, γ)** have hexagonal structures that are constructed by corner sharing $Si_3N_4$ tetrahedra. $Si_3N_4$ exhibits polymorphism that means it can exist as different crystal structures under different combination of temperature and pressure during processing.

### *2.2.2: Characteristics and Properties of $Si_3N_4$*

- Good Thermal Shock resistance
- Very high temperature strength: when exposed to elevated temperatures.

- Good creep resistance: when exposed to or functioning under high cyclic loading/ stresses.
- Low density (3.29 – 3.45 g/cm$^3$): which allows the bulk material to be light weight in comparison with metallic materials.
- Low $K_{1c}$: in comparison with metals/alloys, however, it has reasonable $K_{1c}$ for the relevant applications.
- Hardness and wear resistance: which allows the ceramics to comprise of low friction co-efficient and minimize the heat induced by friction in comparison with metal/ alloys.
- Electrical Resistance: ideal for electrical insulation and earthing materials.
- Good chemical resistance: when exposed to vigorous chemical environments.
- High melting temperature: ideal for high temperature applications such as internal combustion or gas turbine engines.
- Brittle: in comparison with metallic materials due to its high hardness.
- Good thermal insulator: ideal for high temperature applications.
- Good electrical insulator: in comparison with metallic materials.
- Good corrosion resistant: when exposed to water, oxygen and salt.

**Note:** Further mechanical properties of $Si_3N_4$ are presented in the Appendix 11.5, section B.

### 2.3: Types of $Si_3N_4$ Ceramics

$Si_3N_4$ is commercially available in three forms:

- Reaction bonded (RBSN)
- Hot pressed (HPSN)
- Sintered (SSN)

Hot pressed material samples were mainly tested for the purpose of this research. The three techniques available for processing ceramics are stated in [CES 2007].

## 2.4: Applications of Silicon Nitride in the Automotive and Aerospace Industry.

### *2.4.1: Automotive Applications*

Typical applications for $Si_3N_4$ used in the automotive industry are exhaust valves and Clevis Pins, ball/ roller hybrid bearings and Cam Rollers [Mangels 2006, CES 2007].

### *2.4.2: Aerospace Applications*

The use of $Si_3N_4$ as an insulator for the jet engine igniters has come due to failure of the conventionally used alumina ($Al_2O_3$). This is because the $Si_3N_4$ has high thermal shock resistance which is required for jet engine igniters as well as being a good electrical insulator.

$Si_3N_4$ is transparent property to microwave energy. Having high mechanical strength and transparency to microwave energy allows $Si_3N_4$ to withstand erosion from excessive

temperature changes when travelling at high supersonic velocity through the air. The high wear resistance of $Si_3N_4$, minimum requirements for lubrication, and relatively high hardness make it suitable use for as bearings and bushings in the aircraft engines and hydraulic systems [Mangels 2006].

### *2.5: Why Silicon Nitride is used?*

One of the main reasons for the use of $Si_3N_4$ is because of frequent failures occurring with the metal components [CES 2007]. It is therefore important to first address the problems that arise with metal components. Figure 2.1 illustrates the component which comprises a cam roller system. A) Steel cam roller, B) steel cam lobe and C) a bronze pin.

**Figure 2.1: Metal Cam roller system [CES 2007].**

The bronze pin is relatively a soft material and vulnerable to wear by high contact stresses, low level or dirty lubrication and debris accruing from wear. Due to high friction at the pin to metal interface, freedom of rotation is restricted which also causes excessive wear at OD (Outer Diameter) of the pin but ID (Inner Diameter) of the cam roller as the pin is rubbing inside the roller. Sliding of the cam roller causes high contact stress and frictional “stick- slip” which move forward from below the surface to the top of the surface and causes fatigue failures on both the cam roller and the cam lobe. The high contact stresses could also cause pitting, adhesive wear (scuffing and galling) on the metal roller which eventually transforms into wear of the interfacing cam lobe leading to deterioration in performance [CES 2007].

### *2.5.1: Benefits obtained with the $Si_3N_4$ Cam roller System*

$Si_3N_4$ cam rollers contain a steel pin rather than a bronze pin. This allows further resistance to wear and dirty or insufficient lubrication. The steel and the $Si_3N_4$ form a good combination that produces minimum friction, under insufficient lubricated conditions.

$Si_3N_4$ rollers are about 60 % lighter than metal and, this combined with other advantages such as low friction coefficient between the $Si_3N_4$ roller and the metal pin and low rotational moment inertia, allows the $Si_3N_4$ to rotate more freely. Contact fatigue is eliminated and

there is a reduction in wear in comparison to the metal cam roller system [CES 2007]. The reason why the wear is reduced or eliminated is due to the difference in the contact material used as well as the super finishing obtainable with the $Si_3N_4$.

Fatigue damage gradually gets worse with time so over a certain period of its functional life, the performance of the $Si_3N_4$ will be superior as the metal bearings will deteriorate faster in comparison. The wear rate of conventional steel cam rollers is 20 µm, $Si_3N_4$ has a wear rate of 1 µm which is x20 lower in comparison [Mangels 2006]. This also reduces the failure mechanism effect of pitting and spalling which currently exists within the metal cam rollers.

A comparison of rolling contact fatigue shows that the fatigue life of $Si_3N_4$ (147 -31N from Ceradyne's ceralloy) is much greater than of the steel (M50). The $Si_3N_4$ cam roller is able to function for over 8 million cycles, in comparison, the steel reaches up to 4 million cycles which is half of the cycles obtained by the $Si_3N_4$ [CES 2007].

## 2.6: Cost of $Si_3N_4$

Components made from ceramic materials tend to cost more than metal components. This is due to the difficulties with ceramic processing as well as high tooling cost and wear of pressing tools used. $Si_3N_4$ materials cost between £20 – 30 per Kg in comparison with the metal (carbon steels) components which cost typically £0.50 - 0.70 per Kg [CES 2007].

However, the cost of ceramic parts may be considered to be economical if the complete life cycle cost of the component is taken into account. Ceramic parts provide better durability and performance at high operating speed without failing under high pressure and applied cyclic stresses.

## 2.7: Chapter Summary

The use of $Si_3N_4$ components in the automotive diesel engine is now common. Figures from a leading ceramic manufacturer (Ceradyne Ceramics Ltd) show over 2.5 million components being manufactured for the use of diesel engines during 1999 -2001 [Mikijelj 2005, Mangels 2006].

The chapter also addresses the constraints and benefits of using $Si_3N_4$ for such applications as well as justifying why the conventional parts made from metallic materials fail and how the existing problems with such metallic components can be overcome by using the advanced ceramics ($Si_3N_4$ in particular).

However, there is a concern with the cost of the raw materials, processing techniques, ease of processing and machineability of ceramics, ($Si_3N_4$ in particular) since it is hard and the tooling is therefore expensive. However, high cost of raw materials, processing techniques and excessive costing of machining (high tool wear) should not be taken in account if high

product performance, efficiency, reliability, endurance and longer functional life of the product in general are required.

# CHAPTER III

# Effects of Laser Surface Treatments and Conventional Shot Peening on Metals and Ceramics

## 3.1: Introduction

This chapter surveys previous work conducted by various authors in the field of laser Shot (shock) peening (a type of laser surface treatment), conventional shot peening as well as determination of $K_{1c}$ of ceramics using the Vickers indentation method. Literature review was carried out and several key papers were used for the analysis. Related issues from the papers were then extracted and used from this research.

## 3.2: Surface treatment of $Si_3N_4$ using the $CO_2$ laser

Research by Malshe *et al* investigated the possibility of eliminating imperfections within a ceramic material by applying the $CO_2$ laser beam [Malshe 2006]. They found that the fracture behaviour was considerably affected by surface treating $Si_3N_4$ when using the $CO_2$ laser beam. Fracture origins from the machining process were reduced and bending strength was improved. A four point bending test, fractographic analysis and SEM micrographs were used to analyse the materials surface integrity.

Malshe *et al* used a $CO_2$ laser to minimise the detrimental effects caused by grinding as the heat from the sliding motion creates friction. Laser surface treatment was done after severe grinding of the ceramic in order to remove the mechanically induced cracks.

Two types of continuous wave (CW) $CO_2$ lasers were used to treat the $Si_3N_4$ surface. A high power density laser and a lower power laser. It was found that the condition of grinding has a big influence on the fracture strength of the $Si_3N_4$. Longitudinal direction grinding in comparison with transverse grinding direction demonstrated much more resistance to fracture.

The laser used by Malshe *et al* was a square shaped beam. This type of beam usually has a "top hat" end profile which means that the power distribution during its focus would be uniform. Although, this was not clearly defined in [Malshe 2006], as the $CO_2$ laser beams are conventionally of $TEM_{00}$ Gaussian beam mode. The Gaussian configuration of $TEM_{00}$ (comprises of a ring shaped end profile laser beam). So the distribution of power for this type of beam would not be uniform throughout its surface area and this is desirable in order to obtain a uniform effect on the surface during the treatment.

The beam quality has a relation to the outcome of the present work, as the beam quality factor ($M^2$) is taken into consideration. $M^2$ is a numerical expression of the beam quality and is related to the beam divergence [Steen 1998]. It is expressed as $M^2 = \prod \omega_0 \, 0_0 / \lambda$, where ($\omega_0$ = beam waste or (the spot size), $0_0$ = is half the angle produced by the beam divergence, $\lambda$ = *wavelength)* [Cortes 2008]. Various beams as mentioned previously comprise of differing Gaussian or a higher configuration which means that the quality of the beam varies with each configuration. For example beam mode $TEM_{00}$ results to $M^2$ being 1 ($M^2$ = 1) and $TEM_{01*}$ results to $M^2$ being 2 ($M^2$ =2). Higher value of $M^2$ indicates a lower laser beam quality. In case of the present work particularly with laser shock peening; an Nd: YAG beam having a Gaussian mode of $TEM_{01*}$ where $M^2$ = 2, would work better than a $CO_2$ beam with a Gaussian mode of $TEM_{00}$ where $M^2$ =1. This is because the Gaussian mode of $TEM_{01*}$ where $M^2$ = 2 produced by the Nd: YAG laser would have a flat headed beam (top hat, as mentioned previously) which would distribute the laser energy evenly onto the work-piece and is ideal for the laser shock peening process. The concept of $M^2$ however, varies with different materials and the laser process that is required to be performed.

Results from the fractographic analysis showed that there were two types of cracks found; machine induced cracks and inherent flaws from the material (porosity). This should however be the case with $Si_3N_4$ due to its characteristic and material structure. The depth of the machining cracks was between 25 to 50 µm.

Due to the viscous flow of the glassy phase, the surface region of the material has undergone reorganisation and relaxation during $CO_2$ laser processing. Compressive stresses were induced, as residual strain from machining process was released. With longer laser processing time and higher power density, more relaxation of residual strain occurred. The important factor was the difference between the residual stress in the treated samples to the samples which were untreated (as machined). The difference was found within the materials surface morphology, microstructure and uniformity which was not further mentioned in any detail [Malshe 2006]. So the mechanism of the laser material interaction and how the residual stresses were induced was still unknown to the reader apart from the material going through a phase change.

It was assumed that the surface integrity was changed and improved by the secondary glassy phase (YSiA1ON) which underwent a reflowing and rebinding process [Malshe 2006]. This was because the temperature during the $CO_2$ laser processing was measured to be higher than the stable equilibrium upper temperature of the secondary glassy phase. It was found that softening (possibly melting) of the secondary glassy phase caused infiltration in the surface defects. As the laser power density increases, the ability of the secondary glassy phase to rebind and flow also improves. For the purpose of this work softening of the surface was desired in order to enhance the $K_{1c}$, although, complete melting should be avoided since the surface would undergo material removal which is not desired. This was due to the fact

that an increase in surface roughness would occur as well as increased porosity and crack propagation. Therefore, it was desirable to minimise the cracks in order to increase the $K_{1c.}$

For the purpose of this work (Surface treatment of Ceramics Using Contact-less Energy beams), it was not possible to conduct a fractographic analysis or a four point bending test due to the lack of availability of the testing equipment. However, a micrographic analysis was conducted using the SEM and mainly optical microscopy. In comparison to [Malshe 2006]; rather than attempting to eliminate the imperfections, the objective of this work was to introduce energy in form of heat to investigate a change in the materials $K_{1c}$.

For this work diamond grinding and polishing was necessary, as the material surface available from the manufacturer was scarred. In order to reduce the surface scars grinding and polishing was required. Hence, it could be argued in relation to [Malshe 2006] that diamond grinding could potentially enhance the surface strength by minimising the existing surface cracks. The tested surface was therefore ground deliberately in transverse direction to see the effects of $CO_2$ laser surface processing. Grinding in the longitudinal direction was implemented to polish all samples of this work as discussed later in Chapter 5.

The focus for this work is on laser-induced shot peening and therefore it is ideal to use a circular beam concentrated on a small surface area (comparable with the footprint from a conventional shot) to induce residual stresses into the top surface layer of the material by instant input of a thermal shock.

The $CO_2$ laser system used for this work also comprises of similar type of configuration to [Malshe 2006]. However, the shape of the beam was conventionally circular and very fine size ranging from 100 to 200 µm. This was simply used due to the fact that the laser system could only produce of one shape beam. Hence, the results from the work by [Malshe 2006] would differ from the results of this work since the configuration of the beam (shape, size and mode) would differ.

The investigation conducted by Malshe *et al* should be classified purely as a surface treatment process [Malshe 2006]. Shot peening using a laser beam requires a pulsing laser beam. From reviewing Malshe *et al's* work, this was not very well achieved with the $CO_2$ laser as it was designed to perform as a CW. This is why shot peening or laser "shock peening" cannot be conducted to the same effectiveness using a $CO_2$ laser in comparison with a diode pulsed laser and the fact that the element of shock produced by the $CO_2$ laser was very low which purely make it a surface treatment process.

## 3.3: Laser Peening as an Industrial Solution

Significant research has been conducted in the field of laser peening within the last 8 years. Many authors have carried out research in different areas relating to the subject of laser

shock peening [Mannava 1997, Prevey 2000, Altenburger 2002a, Qureshi 2001, Specht 2002, Prevey 2005, Ocana 2005].

Earlier research in the year 2000 by Qureshi *et al* investigated the feasibility and the potential of the process as an industrial solution and compared it with the conventional shot peening technique. Basic comparisons for both of the processes were presented by talking in account the residual stresses induced from each process and the depth of penetration by using metals such as copper, aluminium, zinc, brass, tin and other alloys which all showed promise for future research work [Qureshi 2001].

Altenburger demonstrated the laser peening process performance in comparison with conventional methods and stated that laser peening as an industrial solution could have a great future as an alternative technique since that particular research in 2001 was on the verge from being in the laboratory to larger scale applications. Altenberger in his later work [Altenberger 2002b] established that laser shock peening was a superior technique in comparison with deep rolling, conventional shot peening, and water peening. For this work only metal/ alloy materials were used for experimentation. Results showed that laser shock peening performed for longer life cycles at higher stress amplitudes, deeper residual stress and also proved to be cost effective than other processes as lead-time was minimized due to the superior motion system driving the laser source which eventually resulted in faster delivery time of products to the customers after component manufacture.

Specht (Metal Improvement Company Ltd) in 2002 introduced the process in greater detail explaining the theory behind the subject area [Specht 2002]. In this paper, technical issues are discussed such as the type of laser used, process parameters, and the beam quality aspects. Experiments were conducted using the Almen strip which was also used for conventional shot peening technique to monitor and control the process. The author state that their research can help OEM's (Original Equipment Manufacturers) to successfully use the laser peening process in a production environment and classified the process as a complimentary to the conventional industrial shot peening technique [Specht 2002]. Since then, Metal Improvement Company Ltd have been developing the process that is more applicable to various applications in the industry such as shock peening of automotive gears, shafts, springs, valves and many rubbing components that require high hardness, improvement in fatigue and longer functional life [Metal Improvement Company Ltd 2007, Hackel 2005, McGeachie 2002]. The process used by the Metal Improvement Company Ltd is further described in this chapter.

Research by Prevey *et al* in 2000 described the application of laser shock peening to minimize fatigue, stress corrosion cracking (SCC), enhancement in the materials hardness and improve the microstructural properties of materials. Such improvements were said to maximise the use of the materials for their applications. Further work by Prevey *et al* in 2005 published a paper which described the advantages of the newer high powered laser systems

to better achieve the benefits that are obtained from the more conventional shot peening systems. High powered lasers achieve better surface finish, aesthetics, minimise the process time as well as inducing deep shock waves into the material surface aided by the pulse beam, resulting in deeper penetration. This makes laser shock peening a superior process and more useful towards an industrial application. Qureshi *et al* also gives an example of the aerospace manufacturing sector where laser shock peening is slowly taking over the more classical method of surface treatment [Qureshi 2001].

Laser Shock peening however, is utilised frequently within the aerospace industry to surface treat turbine engine components (turbine blades, rotors and aerofoils specifically) [Mannava 1997, Prevey 2005]. The shock peening process is conducted during manufacturing of the turbine blades. The turbine blades are shock peened to increase fatigue and improve life cycles which enhances the components functional life. The laser shock peening technique is also used as a remedial process to cure damaged turbine blades [Mannava 1997]. The laser shock peened spot is precisely of 0.67 mm diameter and is fired 3 times on the same surface area and the treatment is conducted on both the leading (L/E) and trailing edge (T/E) of the blade. The fan blades are simultaneously shocked peened on both sides also for equal distribution of the induced residual compressive stress [Prevey 2005].

The authors in [Prevey 2005] compare three types of processes such as gravity peening, low plastic burnishing, shot peening, and laser shock peening that were conducted on turbines engine components (Inconel - IN718) supper alloy. The work performed in this research demonstrate that laser shock peening in particular in comparison with the other processes presented better relaxation of the components during their operation at elevated temperatures [Prevey 2005].

From analysing the last 8 years of literature in the field of laser shock peening, it is certain that sufficient research work has been carried out by various researchers around the world and significant improvement has been made from the laboratory environment to the manufacturing set up. At this moment in time the process has many industrial applications in the automotive and particularly the aerospace industry to surface treat metal/alloys. Although, it is yet unknown as to what the end result would be when the process is applied to ceramic materials as no research as yet investigates the laser shock peening of ceramics. It is a new area and demands further research to be carried out. The present work therefore focuses on the feasibility of surface treating ceramics using laser shock peening by employing a pulsed laser beam and a CW beam using two different types of laser systems for the surface treatment.

## 3.4: Laser Peening as a Process

Laser peening technology offers a greater degree of process control, allowing much deeper level of compressive stress as well as maintaining the appropriate quality of the surface finish on metals [Hackel 2005, Metal Improvement Company Ltd 2007]. An intense laser

beam focused to a small spot was traversed over the material surface, creating a tailored thermal shock wave. This thermal shock wave travels deep into the metal and induces residual stresses which can be controlled to the requirement and only on selected areas of the surface of the component. The local region being treated does not introduce any detrimental levels of heat into the bulk material. The enhanced fatigue resistance generated by laser peening was revealed in the experimental results of [Hackel 2005] that compared to the allowable stress amplitude vs. the number of cycles for as machined, shot peened and laser peened aluminium alloy.

**Figure 3.1: Fatigue life cycle graph for laser peening, conventional shot peening and machined aluminium 6061-T6 [Hackel 2005].**

Figure 3.1 revealed that laser peening of aluminium enables much longer fatigue life cycle in comparison with conventional shot peening; the machined aluminium having the lowest fatigue life.

### *3.4.1: Laser Peening of metal alloys*

In work reported by Hackel *et al* stated that a pulsed beam of 25 J for 25 ns was produced by an Nd: YLF (yttrium lithium fluoride) [Hackel 2005]. The beam was focused onto the work-piece and the desired area to be peened was covered with material (black coloured adhesive tape) which acts as an ablative and thermal insulating layer. Water was made to flow over the layer to absorb the laser pulse energy and thermal shocks. Ionization and vaporization are created due to the absorption which forms a plasma on the material being treated which act as a further absorbing mechanism for the remainder of the laser pulse. Gathering of plasma within the water produces pressure that creates the shock waves and immediately penetrate into the surface of the metal, plastically straining the surface. The plastic strain then induces compressive residual stresses into the metal at depth of 1 mm to 8 mm depending on the power density of the focused beam and other system parameters [Hackel 2005]. The concept of using a flowing stream of water was not possible to implement with this work, as the systems described in chapter 5 do not accommodate a supply of

water. Hence, the test sample was placed into a water beaker and the laser beam was fired at the stationary work-piece (ceramic test sample).

The benefit of laser peening has only showed with metal alloys. It was feasible to induce deep residual stresses into the surface. The same effect has not been proven with ceramics to date. This is due to ceramics being brittle: by firing a pulse of laser at the material is equivalent to throwing a sharp hot rod at the material. This increases the potential for the material to crack since it is already brittle and has a porous structure. Metals in comparison are much more ductile and comprise of higher fracture strength (ductility), hence the energy of the laser shock is absorbed well into the material.

Hackel of the Metal Improvement Company Ltd [Hackel 2005], states that laser peening of ceramics has not been performed due to lack of industrial demand. If there was a demand for such applications requiring laser peening then it would be surely considered for research. The work in this research therefore, highlights the potential applications particularly in the aerospace industry. The investigation was partly focused on laser peening by the aid of Nd: YAG laser and $CO_2$ laser, which is considered to be a surface treatment process. The interesting feature to observe is the fracture behaviour of the ceramic under both types of surface treatments. $CO_2$ laser processing is not comparable to laser shock peening and is purely a surface treatment process due to the output beam being CW. However, the Nd: YAG laser could be comparable to the industrial Nd: YLF laser used for laser shot peening [Hackel 2005] as they are both diode pumped lasers and are able to generate a pulsed beam. Although, the effects of the pulsed beam on ceramics are expected to differ from the effects of the CW beam due to the ceramic being brittle and prone to cracking.

## 3.5: Finite Element Simulation of laser Shock Peening

The main focus of the work presented by Braisted *et al* was to analyse finite element simulation in order to predict residual stresses induced by laser shock peening [Braisted 1998]. The laser peened materials were Titanium alloy (Ti- 6A1 -4V) and 35CD4 steel. The peening process was carried out on two sides of the material since one sided peening can permanently deform the materials surface from the untreated side [Braisted 1998]. The schematic in Figure 3.2 presents the way in which two sided peening was conducted.

**Figure 3.2: Schematic of double sided Laser Shock Peening [Braisted 1998].**

Two sided peening was carried out by splitting the beam in half and concurrently peening both faces of the target. A high pressure exists on opposite surfaces during the treatment which balances out and prevents unnecessary deformation of the surface being peened. In order to laser peen two sides it was important to have maximum access to both sides of the parts which was not always possible with complex geometrical parts such as twisted fan blades [Braisted 1998]. The treatment was also not always possible to perform if thicker materials were required to be treated due to splitting of the beam not fully penetrating through the material so due to this reason double sided peening for thicker section was not feasible as it did not adhere to the concept.

This concept was not possible with the capacity of the equipment used for this research due to the thickness of the test sample being far too large to allow the beam to split. It also requires the laser beam to comprise a larger diameter which is not feasible with the low powered $CO_2$ laser. It is possible to generate a beam of large diameter using the ND: YAG laser, although, the power density would decrease as the focal spot of the laser beam is increased. Also the parameters are unknown so, ideally, one sided peening should be practiced and focal spot position of 0 mm should be initially maintained to produce a beam of 2.5 to 3 mm diameter at a relevant power output.

The principles of Braisted *et al's* experiments were the same as the principles described in [Hackel 2005, Metal Improvement Company Ltd 2007, Braisted 1998]. However, the most important issue to be considered was the fact that the author used a pulsed beam of 2 mm by 2.5 mm rectangular shaped beam to conduct the treatment [Braisted 1998, Metal Improvement Company Ltd 2007]. Braisted *et al* employed a rectangular beam profile which has been said to allow more effective processing [Braisted 1998]. It was not stated why this was the case but it can be assumed that the rectangular beam of same length to the diameter of the circular beam would produce coverage on a slightly larger surface area. Hence, the overall treatment on the component would require shorter time and less use of laser pulses which would save the overall process time and the overall cost.

## 3.6: Enhancing the strength of Ceramics by Shot Peening

Pfeiffer *et al* stated that ceramics treated by other surface strengthening techniques such as traditional metal working (pein hammering) or sand blasting tends to develop fractures whereas shot peening of ceramics was more successful due to its process controllability [Pfeiffer 2002]. With shot peening the level of shot size and velocity can be controlled. However, laser peening in comparison with shot peening has much superior process parameter control. The ceramics tested were Alumina and $Si_3N_4$.

### *3.6.1: Benefits obtained by Mechanical Shot Peening on Ceramics*

Primary investigations showed that by using shot peening, high compressive residual stresses can be introduced into the top surface of the $Si_3N_4$ and consequently improvement of load capacity under 4 point bending conditions was obtained [Pfeiffer 2002].

The material properties investigated by Pfeiffer *et al* were residual stresses, bending strength and topography (surface roughness, Ra) [Pfeiffer 2002]. To assess the local strength of the surface; an X-ray diffraction (XRD) method was used which showed limited penetration of the sample surface.

The fracture load was determined by using a ball on plate test in which a 10 mm ball of $Si_3N_4$ was used to strike a plate of $Si_3N_4$ with increasing load until a cone crack on the material was apparent. The examined results revealed that high compressive stresses (in the range of GPa) were present in $Si_3N_4$ accounting for increase in the load capacity (4 point bending) by a factor of 9 [Pfeiffer 2002].

Ceramics exhibit variation in their material properties primarily due to crack sensitivity as a result of inability to relieve crack tip stress by localised plastic flow and a distribution of residual porosity from manufacture.

Two materials, $Si_3N_4$ and $Al_2O_3$, were assessed for residual stress and subsequent load capacity in various surface conditions. The shot peened samples showed compressive stresses up to 1.25 GPa. These compressive surface stresses enabled the load to increase from 3 kN to 9 kN (200 % increase).

The shot peening of the surface of $Si_3N_4$ and alumina increased the roughness up to 0.09 µm (Ra) for $Si_3N_4$ sample and 0.14 µm (Ra) for the alumina samples as presented in Figure 3.3. This was because $Si_3N_4$ is a much harder material than alumina.

This could also be compared with the non-contact peening processes since the surface topography was believed to contain minimum damage due to the fact that there was no physical contact of the laser beam energy or the non transformed plasma arc on the

materials surface, hence the surface should be much smoother in comparison with the conventionally shot peened surface.

**Figure 3.3: Average roughness (Ra) of shot peened $Si_3N_4$ and Alumina samples [Pfeiffer 2002].**

Pfeiffer *et al* proved that conventional shot peening was feasible to induce residual stresses into the ceramic surface in order to gain some of the benefits that were obtainable with conventional shot peening of metals [Pfeiffer 2002]. Pfeiffer et al mention the dislocation of the shot peened surface was affected by two phenomena; localised microscopic surface deformation and appearance of dislocations in the surface crystals. Dislocation multiplication and local surface deformation serve to increase the compressive residual surface stresses and creating a strengthened material surface [Pfeiffer 2002]. Could the same effect be achievable on the ceramic surface using a laser beam? This is an issue to investigate as it is assumed that the effective results from Pfeiffer et al have come from mechanical deformation [Pfeiffer 2002]. The non-contact energy beam does not allow this to occur as the process does not remove physical contact with the material. Therefore, the major property of the non-contact energy beam is considered. This is the heat induced into the material by the laser beam. It is unknown if the input of heat could produce the same dislocation multiplication.

## 3.7: Equations for calculating the $K_{1c}$ for ceramics using the Vickers indentation method

The Vickers indentation test can be used to determine the fracture toughness ($K_{1c}$) of ceramics and glasses from empirical relationships [Ponton 1989]. Preparations of the samples involve polishing in order to create a reflective surface plane [Ponton 1989]. The advantage of the Vickers hardness test is the cost effectiveness, ease of set up and requiring minimum time and effort. The Vickers indentation test was therefore utilised for the investigation and crack lengths were observed using optical microscopy [Ponton 1989].

In this paper 19 empirical equations reviewed were applied (see Chapter 5). Each equation has its origin and application [Ponton 1989]. There are 10 equations that have been selected for the purpose from the 19 equations mentioned in [Ponton 1989], to initially determine the $K_{1c}$ value of the virgin (untreated) ceramic.

***3.7.1: Equations for median (halfpenny-shaped) cracks***: used for high indenter load application. From applying the ten equations to real experimental values, one was then selected (chapter 5) to calculate the $K_{1c}$ value of the tested samples. Tables 3.1 and 3.2 present a summary of the 19 equations that were used in Ponton *et al's* work.

The equations in the tables have been derived by the material's empirical value that has been obtained from experimental means, of ceramic and glass materials [McColm 1990]. The suitability of applying various equations to $Si_3N_4$ in particular was unknown, so it was required that an investigation was carried out in order to determine which equation was best suited for $Si_3N_4$. Chapter 6 presents the results of the investigation carried out to find the most appropriate equation.

**Table 3.1: Equations applicable to calculate the $K_{1c}$, by using the Vickers indentation methods [Ponton 1989].**

**Palmqvist crack equations:** used for low indenter load applications.

**Table 3.2: Equations used for Palmqvist cracks [Ponton 1989].**

**Abbreviations:** Where F= 1.59 – 0.34 B – 2.02 $B^2$ + 11.23 $B^3$ – 24.97 $B^4$ + 16.32 $B^5$ and B = log (c/a). † Where f (E/Hv) = [( $ß^2_{EXP}/\delta$) – 1.5] / 0.75, in which $\delta = 2 (1+3 In ß_{EXP}) / 3$ and $ß_{EXP} = 0.768 (E/Hv)^{0.408}$, **P** = Load (kg), **N** = Load in Newton's (N), **C (c)** = average flaw size, **a** =2c, **Hv** = Hardness value, **E** = Young's modulus. Young's modulus for all untreated samples of $Si_3N_4$ was kept to 250 Gpa $\sqrt{m}$ as obtained from CES [CES 2007].

**Note:** The equations highlighted in bold are particularly used for the investigation in this work in order to determine which equation is best suited for calculating the materials $K_{1c}$.

The profile of a median (halfpenny-shaped) crack is illustrated in Figure 3.4 (a). Median halfpenny shaped cracks occur when high indentation loads are applied [Orange 1887]. Loads applied for this work are exceptionally high (either 490.5 N or 294 N), therefore, it can be predicted that the outcome for most of the crack profiles would be of median halfpenny shape. For cracks that are of median halfpenny-shaped profile; the applicable equations ranges from number 1 to 15. The indention load at which the median halfpenny crack occurs for $Si_3N_4$ was about 3 N [Orange 1887]. This was much lower for the loads applied for this work, hence it could be assumed that the generated cracks would always be halfpenny median crack profiles, so only equation 1 – 15 should be utilised in order to determine the $K_{1c}$. Figure 3.4 (b) illustrates a profile of a Palmqvist crack which tends to occur at low indentation loads [Orange 1887, McColm 1990]. A Palmqvist crack is part of the median halfpenny crack because when a load above 3 N was applied indenter "pop in" occurs; a Palmqvist crack was already produced and further developed into a median halfpenny crack [McColm 1990]. These cracks are shallow and lie in the axis of the indenter as there would be a small extension at the edge of the diamond indenter [McColm 1990]. It is not likely that these cracks will occur for any of the indented surfaces for this work since most of the indentation loads are either 490.5 N or 294 N which are much higher to generate a Palmqvist crack.

**(a) (b)**

**Figure 3.4: Median Half–penny crack (a) and Palmqvist crack (b) [Orange 1987].**

**Note: l** = surface crack length, **2c** or **2a** = length of the diamond indent, **c** = centre of the diamond to the end of the crack tip, **pc** = load impact, **Ic** = interior cracks.

The authors suggested that equation 8 in Table 3.1 has accuracy of 30 to 40 %, for materials which are well behaved in their indentation response [Ponton 1989]. If $Si_3N_4$ does respond well it could be interesting to see if this statement was true (as further investigated in Chapter 5 and later discussed in chapter 6). However, it was first required that a thorough understanding of which crack types could be generated from the Vickers indentation test on the ceramics being tested. If the cracks are of Palmqvist type then equations in Table 3.2 are more suitable to use. Otherwise, if the cracks are found to be halfpenny median type then equations from Table 3.1 are more suitable to use.

It is not certain that the results of the $K_{1c}$ values obtained by the equations are accurate. Chantikul *et al* mention briefly that equation: $K_{1c} = 0.016\ (E/Hv)^{1/2}(P/c^{3/2})$ was ideal for $Si_3N_4$ and has 30 % to 40 % indentation response, although he does not make it convincing and clear why this equation was particularly used for the material. It was therefore required that some of the relevant equations were applied to the tested values from this experiment to determine what sort of results are obtained (this is described in chapter 5). Hardness test was performed on the ceramics assuming that the resulting cracks were of halfpenny median type (due to high applied loads). Ten equations were employed from Table 3.2 to establish which particular one produces the $K_{1c}$ value nearest to the known value for $Si_3N_4$ which is normally between 4 – 6 MPa $\sqrt{m}$ for $Si_3N_4$ [Ponton 1989, Ahn 1996, Braisted 1998].

## 3.8: Chapter Summary

Various research papers have been reviewed which are related to the subject area of this research [Metal Improvement Company Ltd 2007, Malshe 2006, Pfeiffer 2002, Hackel 2005, Ponton 1989, Ahn 1996, Braisted 1998, Mannava 1997, Prevey 2000, Altenburger 2002a, Altenberger 2002b, Qureshi 2001, Specht 2002, Prevey 2005, Ocana 2005]. Several issues have been extracted from each paper and were put to use. However, some of the experimental techniques applied with the previous research were not possible to follow and implement since the availability of the equipment for this work was limited. Therefore, the experiments have been conducted by making the best use of the equipment available to simply analyse the $K_{1c}$ of tested materials.

# CHAPTER IV

# Experimental Development

## 4.1: Introduction

This chapter explains the steps undertaken to develop the experimental procedures in this work. Experiments were conducted by mainly employing two types of industrial lasers ($CO_2$ and Nd: YAG). Plasma Augmented Laser (PAL) processing and ultrasonic energy sources were also employed to broaden the variety of the investigation. All results are discussed and explained in Chapter 6. The material under investigation was mainly $Si_3N_4$ ceramics.

## 4.2: Diamond Grinding and Fine Abrasive Polishing

All ceramic samples were ground using a 201 µm (grit) grinding wheel for a period of 60 to 80 minutes each. The samples were then polished on 3 µm and 1 µm fine abrasive wheels until a surface roughness value (Ra) of 0.040 µm was obtained. Grinding and polishing the material surface can induce compressive residual stress into the top layer [Malshe 2006]. Care was taken with this task since the ceramic can heat up during the process which can influence the behaviour of the material if the surface reaches a sufficient temperature level. It is also important that grinding and polishing of the ceramic is conducted in the longitudinal direction to maintain or enhance the flexural strength. Grinding in the longitudinal direction can increase the flexural strength and reduce the possibility of crack propagation in comparison with transverse directional grinding [Malshe 2006, Timothy 1995]. All samples were ground and polished in the longitudinal direction by applying a stream of water and polishing lubricants to reduce frictional heat generated during the process.

## 4.3: $CO_2$ Laser Processing

### *4.3.1: Surface treatment of $Si_3N_4$ using the high power $CO_2$ Slab laser*

Initial experiments were conducted using the Rofin Sinar®, 2 KW $CO_2$ Slab Laser with 10.6 µm wavelength. The material tested was HP $Si_3N_4$. The laser beam traversed in a straight line by the aid of the work bed of the slab laser traversing into the X direction to create a line of cut. The following section explains the experimental steps undertaken and the parameters that were used, as presented in Table 4.1.

| No | Laser Power (Watt) | Focal Position (mm) | Traverse Speed m min-1 |
|---|---|---|---|
| 1 | 100 | 0 | 2 |
| 2 | 100 | 0 | 10 |
| 3 | 100 | + 10 | 10 |
| 4 | 200 | + 10 | 10 |

**Table 4.1: Parameters from the initial the experiments using $Si_3N_4$.**

**Note:** the gas pressure was kept constant to 0.75 bar and argon was used as a shield gas.

**Trials**

1. The surface treatment penetrated deep into the material, indicating that there was excess power induced into the material which led to the material being cut. Hence, the traverse speed for trial number 2 was increased from 2 m min-1 to 10 m $min^{-1}$, which meant that the power density on the material is decreased.

2. The line of cut was apparent in most areas, however, the beam reflected from the polished surface. This was due to the $Si_3N_4$ surface containing areas of powder coating, indicating that diamond grinding was further required in order to level the surface and induce sufficient level of power density into the top layer. The focal position for the following experiment (trial 3) was defocused to +10 mm so the beam diameter becomes larger and more absorbed by with the material.

3. The cut line produced on this attempt was much finer, obtaining minimum depth; hence, the power density was again increased for the following trial.

4. A fine cut line was obtained with minimum heat dissipation. There was no effect on the polished surface, indicating that the laser beam was reflecting from the work-piece. Therefore, a black marker pen was used to coat the surface to increase laser absorption.

The above observations and findings led further experiments to be conducted bearing in mind the following aspects:

a) The $CO_2$ slab laser was not stable when operating at low power density.

b) The surface of the $Si_3N_4$ ceramic required excessive grinding in order to obtain an even surface.

c) The surface of the $Si_3N_4$ ceramic also required a thin film of black paint or other marking area such as black film or tape in order to increase the laser absorption.

### *4.3.2: Rational of key parameters*

Trials by employing the high powered $CO_2$ slab laser were conducted using the following parameter which performed as a key part for the surface treatment. Laser power (watts), traverse speed (m $min^{-1}$), focal position (mm) and shield gas (l/min) were used as the main processing parameters. The high powered $CO_2$ slab laser was only used for initial trials and proved to be less effective for the surface treatment process in comparison with the low powered $CO_2$ laser marker as further described in section 4.3.6 in this Chapter.

Laser power of 100 to 200 watts was applied to the material surface, simply to investigate the outcome from the laser material interaction and to determine a particular parameter

window as it was unknown regarding what parameters were required to process the ceramic using that particular laser system. With using the above powers along with high beam quality and finer spot size of the beam from the Rofin Sinar high powered $CO_2$ laser (resulting in exhibiting high energy level at the work-piece) it was found that the particular laser head was more ideal for a cutting application rather than surface treatment. A welding head with appropriate optics were not available at the time and therefore resulted in abandoning experiments using the high powered $CO_2$ laser. Rather than the laser beam surface treating the material; it was found that several cutting lines were created and resulted in the material being cut rather than treating the near (top) surface layer.

The focal position was therefore changed due to the occurrence of above; and was focused to + 10 mm to create a larger beam diameter to distribute the laser energy on a broader surface area. However, that was unsuccessful due to the lack of penetration on the material. Hence in this situation, it was apparent that the power lever was required to be increased, however, since the $CO_2$ laser system was better operating at higher powers up to 2000 watts it is likely that the system may not be so stable when operating at lower powers. Hence, further trials were not conducted.

The speed was also ramped from to 2 to 10 m $min^{-1}$, although, ideally it was required that the speed was completely eliminated from the experiments in order to perform the laser shock peening process. As it was initially assumed that a pulsed beam is required rather than a CW beam.

A gas pressure of 0.75 bar was applied using argon as the processing gas. This was because the increase in gas pressure results into too much ablation. Too less of the of the gas pressure results into the beam not being able to couple into the ceramic well and also allows the material to be exposed to the atmospheric gases which results into the ceramic to oxidise. Hence, it was found from previous study that the 0.75 bar was appropriate for the powers used and was not changed throughout the experiments using the high powered $CO_2$ laser.

### *4.3.3: Beam delivery system and machine specification*

Figure 4.1 illustrates the right angle beam delivery system of the $CO_2$ slab laser and Table 4.2 presents the specification of the Rofin Sinar® Slab laser and the integrated Mechatronic® motion system.

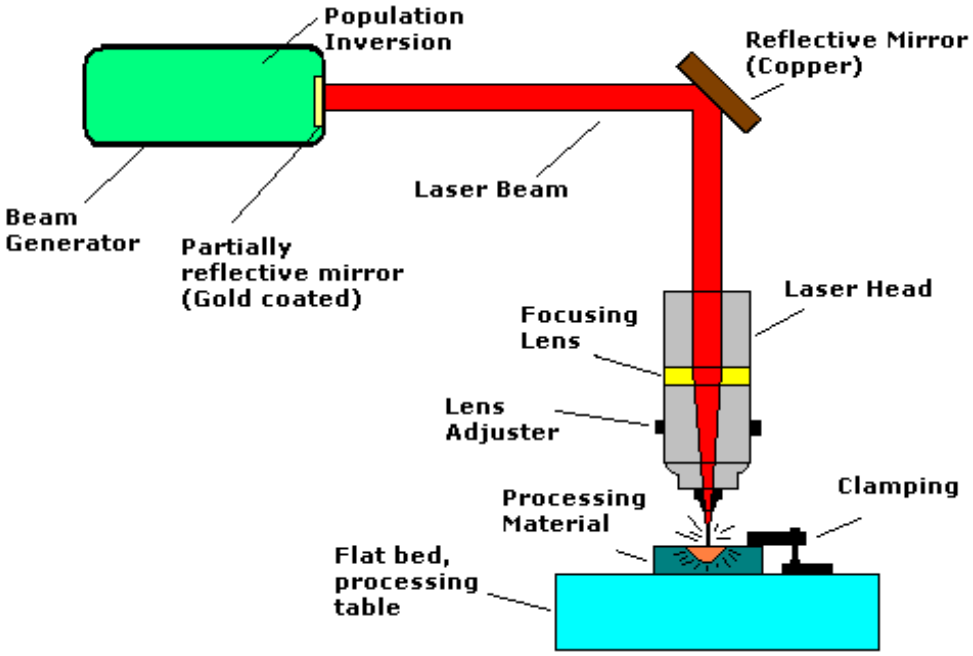


**Figure 4.1: Beam delivery system of the 2 kW Rofin Sinar $CO_2$ Slab laser**

| Features | Details with units |
|---|---|
| **Excitation** | HF |
| **Output power** | 2000 W |
| **Power range** | 200-2000 W |
| **Beam quality factor** | K > 0,9 |
| **Pulse frequency** | 0 or 2 up to 5000 Hz; cw |
| **Laser class** | 4 |
| **Safety class:** | 4 |
| **Field size:** | 1m X 2m |
| **Focal distance:** | 500 mm |
| **Dimensions (L x W x H):** | 500 mm x 300mm x 300 mm |
| **Weight:** | 25 kg |
| **Cooling Type:** | Integrated External Cooler |
| **Ambient temperature:** | 15 to 35 °C |
| **Motion System** | |
| **Size of bed** | 2.5 m x 1.5 m x 1.25 m |
| **Max. Speed** | 100 m/min |
| **Attachments** | Rotary Stand alone fixture |
| **Size** | 200 mm diameter |
| **Max. Speed** | 100 rpm |

**Table 4.2: Specification for 2 kw $CO_2$ Slab Laser and motion system**

### *4.3.4: Surface treatment of $Si_3N_4$ using the low Power $CO_2$ laser marker.*

The 2 KW slab laser system was designed to function effectively and efficiently at high power density and proved to be unstable when operating at low power density. For example when the power was set to 500 watts; it was not certain that the output power at the material surface remained uniform for consistent processing. Therefore, a Rofin Sinar®, 100 Watts $CO_2$ Multi Scan Laser marker was employed to conduct experiments at lower powers with more stability as shown in Figure 4.2. The $CO_2$ laser system is ideal for producing a continuous wave (CW) laser beam, although, it is possible to produce a pulsed beam. For the

purpose of this work, it was ideal that a pulsed beam was produced in order to imitate the typical shot peening process.

In order to treat the surface with a particular path or a pattern for the laser beam to follow, it was required that a CAD (Computer Aided Design) programme(s) was generated on AutoCAD (integrated software that transfers the input of data from the operator to the machine by means of a dxf. or dwg. File). The CAD programme(s) were then used to treat the test material. The CAD programmes were in form of various patterns that would result in treating a particular surface area of the test samples.


**Figure 4.2: Experimental set up of the $CO_2$ Multi scan Laser marker during $Si_3N_4$ processing.**

### *4.3.5: Pattern generation and Selection for $CO_2$ Laser Processing*

A pulsed beam is commonly used for laser peening. In principle, it is not possible to generate the pulsed beam with a lower powered $CO_2$ laser system (Multi Scan Laser marker in particular). Hence, it is not directly possible to produce a comparable impact of the pulsed beam laser that is obtained from the conventionally used Nd: YLF laser to shock (shot) peen metals [Hackel 2005]. This was because it was not possible to generate an effective pulsed laser beam with the low powered $CO_2$ laser marker since it has a fine spot which cannot affect the material in one single pulse. The $CO_2$ laser marker generates multiple pulses at high bandwidth which forms into a CW laser beam. So the programming of the surface treatment was laser carried out by traversing the beam continuously onto the material surface by designing patterns that scan selected areas of the material since the $CO_2$ laser operates as a CW beam. The diameter of the laser beam was around 100 µm to 200 µm; the laser system was capable of pulsing rapidly in order to deliver a CW beam. This beam was therefore programmed to traverse in a spiral pattern, leaving no gaps in between each line (or a spiral). This treatment must be done without leaving significant distance between each of the lines in order to treat the surface of a given dimension for example (8 mm diameter spot). This led to producing a spot of 8 mm diameter that was visually comparable with the spot of a diode pulse laser (ideally used for shot peening). After conducting further trials and visualising the complete pattern under the optical microscopy, it was then found that the surface was being over treated as the lines that produce the spiral pattern were over lapping

one another hence the surface began to melt and increased its roughness. This indicated that the surface was more prone to cracking by increased porosity and developed a potential to fracture.

With the above in mind, it was further discovered that in actual fact the laser beam producing the spiral pattern was not over-lapping. It was the distribution of heat which caused this effect during laser processing. The dimension (surface area of the treatment) of the heat distribution was purely dependant on the level of power output at the surface as presented in Figure 4.3, (the higher the power, the bigger the heat distribution or the heat affected zone (HAZ)).

However, it was important to investigate the effective area which the laser beam could impact so the gap between each line of the pattern could be correctly designed. Hence, lines were created on the $Si_3N_4$ surface at three different power densities (85 Watts as maximum power, 60 watts as median and 48 watts per unit area), to observe the size of the area of impact and the heat affected zone (HAZ) or the distribution of heat, as presented in Figure 4.3.

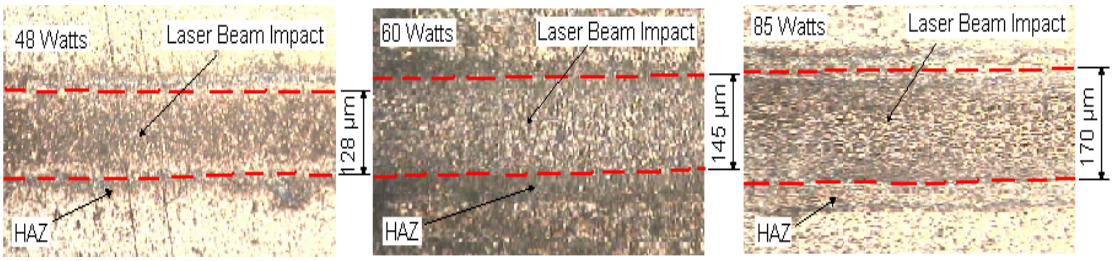


**Figure 4.3: The size of impact of the Multi Scan 100 watts Laser marker on the $Si_3N_4$ material surface as the power density is varied.**

Figure 4.3 shows that as the power density was increased, the HAZ and the impact of the laser beam also increased. In other words the dimension (or the area) covered by the surface treatment was bigger with increasing laser power. Therefore, in order to create a complete pattern which scans a desired surface area, it was important to know the area of the spot size on the surface. This will aid the CAD process prior to laser processing. In order to obtain such an effect, patterns were designed on a CAD system (AutoCAD) which was integrated with the Rofin Sinar®, Multi Scan, and 100 Watts laser machine. These patterns were transferred to the laser machine and used as the potential travelling path for the laser beam.

The gap between adjacent scan lines (tracks) created were dependant on the laser power density used. For example at 85 watts, the pattern was designed with 170 µm gap. Pattern 1 is constructed of several circles with gaps of 128 µm between each line as presented in Figure 4.4. There are 40 circles that make up a spot which was of 8 mm diameter. This means that the beam was switched on and off and impacting the material 40 times. This increased the heat at the material surface by continuous impacts and burnt the top surface of the $Si_3N_4$. This was due to excessive heat produced by continuous laser impacts which

were fired close together. This led to material removal which was detected from the vapours produced during laser processing. Material removal was not desirable since the surface finish of the $Si_3N_4$ deteriorated as the cracks and porosity became larger making the material prone to cracking as predicted from analysing the literature review in Chapter 3 [Malshe 2006]. It was then found that the input of heat was required to be minimised by reducing the processing time of the laser beam acting on the material. This could minimise the heat produced at the surface of the material and avoid or limit the material from melting.

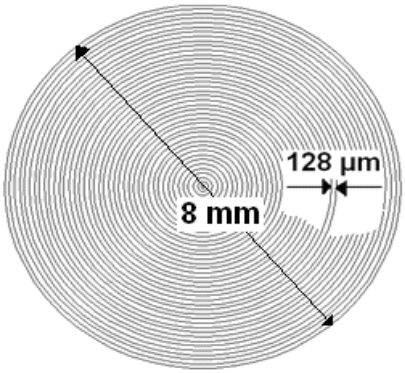


**Figure 4.4: Pattern 1, at 48 watts of laser power.**

If a large surface area was required to be processed then; it is not necessary to overlap or treat the whole surface area of the material being treated. Gaps smaller than the diameter of the circle could well be left untreated. If a surface crack develops in the untreated area; then the areas which are treated would prevent the crack from expanding and developing towards complete failure. By doing this it would also save time to the process and reduce the level of energy input.

Therefore, pattern 2 was created and tested. This pattern as illustrated in Figure 4.5 has a cross hatched shape which contains 41 lines each, in both the X and Y direction. This means that the laser beam would turn on and off and impact the surface 82 times in total. This is much higher than pattern 1 as shown in Figure 4.4, so it was predicted that excess heat would be generated during processing, since the laser beam would spend a longer time on the material surface. The gap in between each line is 128 µm the laser beam first covers the vertical line then over-laps the pattern with horizontal lines. Over-lapping of the pattern would also mean that the pattern was being treated twice, therefore, it increased the processing time as well as the input of heat, causing more melting and material removal in comparison with the pattern in Figure 4.5. This pattern was therefore not ideal and further experimentation was required using various other designs in order to find the correct marking pattern.

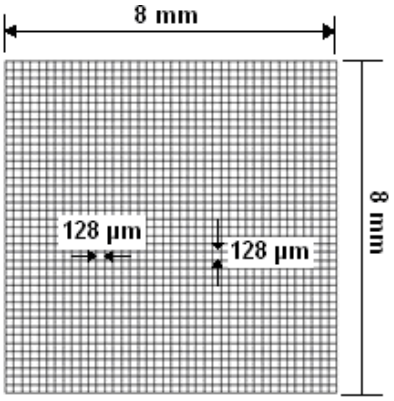


**Figure 4.5: Pattern 2 at 48 watts of laser power.**

Pattern 3 in Figure 4.6 was then designed to eliminate the constraints which existed in the previous two patterns. So the square shape was kept from the previous pattern in Figure 4.5 and the numbers of lines to mark the complete shape were reduced. This makes this pattern unique in comparison with the previous two patterns since one single impact of the laser beam would fully treat the complete pattern preventing the beam from switching on and switching off (start and stop) which produces an unstable beam. The processing time for pattern 3 was also reduced which meant that the generated heat was much lower than the previous two patterns as the laser beam was active on the material surface. It is required that the process time was minimised in order to avoid surface burning and material removal. It was found that the laser beam had the tendency to traverse around sharp corners slower than its normal speed as it travels on a straight line. For example if the laser beam was traversing at 20 m $min^{-1}$ and the beam was required to change directions, then the traversing speed was automatically reduced to 12 to 15 m $min^{-1}$, as the beam approaches the corner and deviates into another direction. The power density induced into the material becomes much higher when the traversing speed is reduced. This creates excess burning around the four corners of the shape as found from Figure 4.6. Due to this reason, this pattern was also rejected.

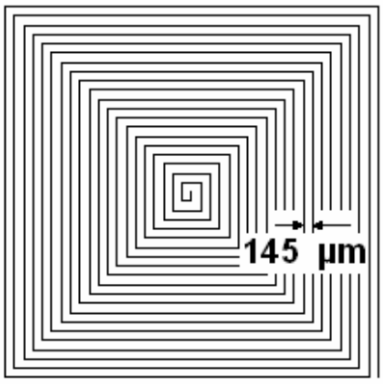


**Figure 4.6: Pattern 3**

Hence, pattern 4 illustrated in Figure 4.7 was designed considering that the laser beam must impact the surface in one single motion, without changing directions since both factors have the effect of over heating the surface and material removal. Pattern 4 is a spiral design which

treats the whole area from start to finish in one single impact (laser beam being executed in one single attempt). This helps to minimise the traverse time to just over 6 seconds in comparison with the previous patterns. The results showed improvements from previous patterns as the burning of the surface and the material removal was non-existent. The circular motion allowed the laser beam to follow a smooth path without the laser beam needing to deviate and cause excessive burning around the corners. Other patterns were also designed and tested to check if there are any improvements with the process quality. However, pattern 4 was the best and could overcome all problems which exist with other patterns such as completing a spot in a single attempt. By doing this, it minimized the processing time. Due to its circular design, the beam can traverse easily around the radius and does not need to change directions in comparison with pattern 1, 2 and 3.

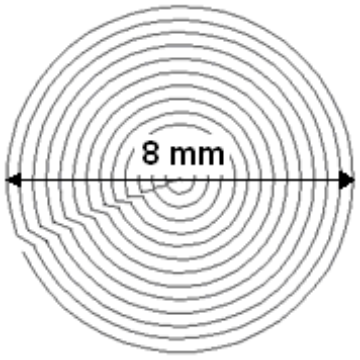


**Figure 4.7: Pattern 4**

Pattern 5 as shown in Figure 4.8 was designed to improve the features of pattern 4 in Figure 4.7. Pattern 5 comprises of one single spot which takes up to 22 seconds to process using the low powered $CO_2$ laser marker. Due to the low powered $CO_2$ laser marker firing the beam as a CW, it was not easily feasible to produce a spot of 8 mm diameter which can impact the material in one single pulse such as the diode pump laser. The spot size of the low powered $CO_2$ laser beam ("foot print" on the material surface) has a maximum diameter 170 µm when operating at maximum power density (80 watts). Therefore, in order to produce a spot diameter of 8 mm the laser beam must impact the surface 47 times in order to produce a spot of 8 mm. This would have meant that there was a possibility of facing the same issues which existed with pattern 1, 2, and 3 (over heating and material removal) as previously described. So due to the nature of the $CO_2$ laser beam delivery system; it was not possible to use this approach. Although, this pattern would be very useful when processing with a high powered laser system such as a $CO_2$ slab laser which can produce a beam of 8 mm diameter as well as an Nd: YAG laser that could produce a single pulse spot.

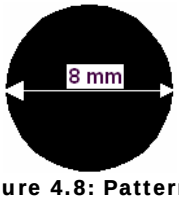


**Figure 4.8: Pattern 5**

Pattern 6 in Figure 4.9 and pattern 7 in Figure 4.10, were constructed to investigate if any improvements can be obtained from pattern 4 in Figure 4.7. Both of the patterns are similar. The only difference between the two was the horizontal and vertical placement of the lines which the patterns were comprised of. However, both patterns comprised of identical features and similarity in the way the Multi Scan laser marker interprets this design for material processing. Therefore, the results also proved to be identical. It was predicted that similar results will be obtained to pattern 2 and 3 since they have similar features to both of these pattern. The laser beam was turned on and off 41 times and impacted the surface. With the pattern in Figure 4.9 and then pattern in Figure 4.10, the laser beam first creates an outer profile. Then the horizontal lines are created (Figure 4.9) and vertical lines in Figure 4.10. The laser beam overheats the corners of the pattern as it changes direction to create the outer box. Then the lines in the centre are marked, with a distance of 148 µm. As each line is marked, the laser beam pauses and moves to the next line. Due to this pause, the burning effect occurs at the beginning and the end of each line.

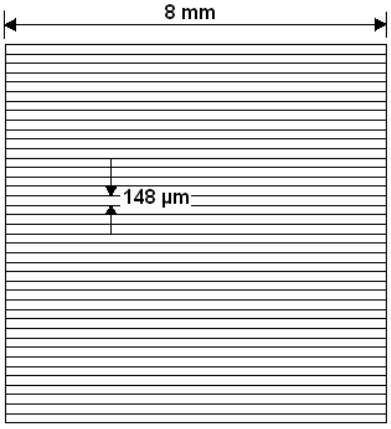


**Figure 4.9: Pattern 6**

These investigations proved that for the low powered $CO_2$ laser marking system, it was required that the pattern was continuous with a smooth curvature, traversing in a circular motion which will minimise the process time for the treatment and avoid any material removal and burning especially when the heat gathers around the corners of the square patterns. From visual observations of the marked patterns, it can be said that the laser beam was stable when operating at longer distance (executing continuous profile or lines) rather than marking small lines with frequent pauses and starts. Each time the laser beam paused; excess power was released which created the burning effect on the edges of the square patterns. This was due to the fact that the laser beam only became much stable during longer runs. Frequent stops and starts led the beam to run unstably hence excess power was released. This was why pattern 4 in Figure 4.7 proved to be more ideal since the beam was running in continuous motion with much stable execution of the power density.

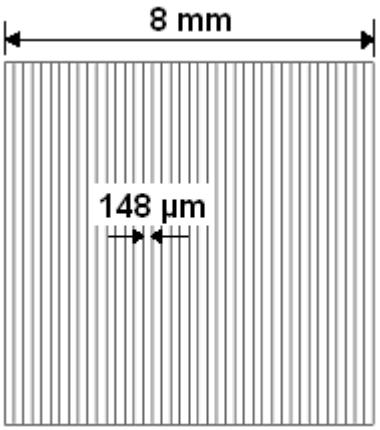


**Figure 4.10: Pattern 7**

### *4.3.6: Parameters for Pattern selection using the $CO_2$ Rofin Sinar® Laser Marker*

Samples were tested under different conditions, with the different patterns as described above. These conditions involved the ground & polished and unpolished test samples to be dipped the under a pool of water [Hackel 2005]. This concept was used by Hackel *et al*, to investigate if water would aid laser absorption much better for ceramic processing. The industrial laser peening process involves placing a black tape over the treating surface or spraying a stream of water with the pulsing (Nd: YLF) laser beam in order to enhance the absorption of the beam [Hackel 2005]. It was not possible to imitate such steps for this work since a stream of water was technically not possible to attach during laser processing. So the concept was repeated by dipping the test samples in a beaker of water. The water was kept at 2 mm -3 mm above the material surface during processing, if the height of the water was kept much higher; then there was a possibility that the beam could fail to have an affect on the material surface since the viscosity of the water could slow down the beam and absorb the laser energy, so a reasonable assumption was required to be made. All other variables such as the frequency, mark speed (traverse speed) and the focal position were kept constant. The parameters are presented in Table 4.3.

| Pattern No | Frequency | Laser Power (Watts) | Focal Position (mm) | Mark speed (mm/sec) |
|---|---|---|---|---|
| P1 – P7 | 2200 | 85, 60, 48 | 143 = (0) | 500 |

**Table 4.3: Parameters used to select the marking patterns for $CO_2$ Rofin Sinar® laser marker.**

**Note:** Pattern 1 to 7 were tested using the above table. All parameters were kept constant with these experiments during the test.

Samples were also polished and tested in the pool of water and outside the pool of water. Otherwise the samples were treated with a surface finish as provided from the manufacturer. Parameters presented in Table 4.4 were executed using pattern 4 (Figure 4.11 presenting the experimental set up). These trials were performed after conducting experiments in Table 4.3.

| No | Laser Power (Watts) | Number of laser impacts (hits) | Sample Condition |
|---|---|---|---|
| 1 | 60 | 5 | Normal |
| 2 | 65 | 5 | Normal |
| 3 | 70 | 2 | Normal |
| 4 | 75 | 2 | Normal |
| 5 | 85 | 2 | In water |
| 6 | 85 | 2 | Normal |
| 7 | 85 | 2 | Polished surface |
| 8 | 85 | 2 | Polished surface, in water |

**Table 4.4: Parameters of the $CO_2$ Laser marker experiments from series 2 – $Si_3N_4$T2**

**Note:** The trials above were only conducted for investigating the absorption of the $Si_3N_4$ to the laser beam when placed in water [Hackel 2005]. The following parameters were kept constant: Pattern number 4, frequency = 2200 (Hz), Focal Position = 143 = 0 mm, Mark speed mm/sec = 500, Number of Laser impacts = 2 and 5 impacts for trial 1 only.

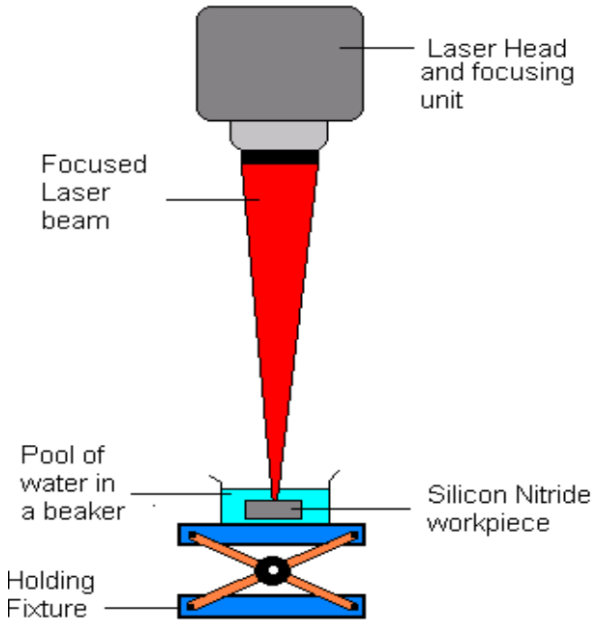


**Figure 4.11: Experimental set up of the $CO_2$ Laser marker processing.**

### *4.3.7: Rational of key Parameters*

The main parameters used with the low powered $CO_2$ laser system were focal position (mm), laser power (watts), frequency (Hz) at which the laser beam was operated at and the mark speed (mm/sec) of the CW beam.

Focal position for all experiments was kept to 0 mm. This was due to the fact that the focused diameter of the laser beam was approximately 150 µm. By defocusing the beam in +ve or –ve direction would increase the beam diameter, however, the laser energy induced

into the material would also distribute onto a larger surface area. Therefore, to keep the laser energy being induced into the material at maximum for the particular power which was set; it was required that the finest spot size was delivered which indicated that the focal position was required to be at 0 mm (143 mm from the lens to the surface of the work-piece).

It was not possible to apply any processing gas with these experiments due to technical constraints with the experimental set up. The processing of the $CO_2$ laser was conducted in ambient temperature with the laser material interaction being exposed to the atmospheric gases. The reason why the shield and the processing gas was not supplied during processing was because the experiments were conducted in a fibre glass protected cage which did not accommodate any space for a gas supply to be included.

The laser power applied to the work-piece ranged from 60 to 85 watts. From initial experiments it was found that no effective penetration or influence was apparent on the material surface below 60 watts. At 60 watts there was some evidence of the laser beam influencing the material surface. The power was then changed in increments of 5 ranging from 60 to 85 watts. Despite the $CO_2$ laser marker being a 100 watts laser system, it was not possible to operate the system at maximum power as the system was capped to generating 85 watts only. However, processing at 60 watts resulted in minor effect on the ceramic surface which was visible under the microscope. Hence, the laser beam was fired 5 times on the same surface area to allow sufficient penetration. For trials ranging from 70 to 85 watts, the laser was fired twice on the same material surface so less heat is induced to prevent cracks occurring by the heat generated from the laser beam.

Mark speed is the speed at which the laser beam is fired within a range of 100 mm diameter optical lens fixed onto the laser head. The beam operates within the 100 mm diameter lens allowing the work-piece to be stationary. The maximum mark speed attained with the low powered $CO_2$ laser system was 1000 mm/sec. However, to minimise the complications due to too many varying parameters; the mark speed was kept constant throughout the experimentation which was 500 mm/sec. Varying the mark speed would either increase or decrease the processing time and change the temperature of the heat being induced into the ceramic material surface. So to avoid this change in temperature it was required that the mark speed remained constant.

Frequency was another parameter which was kept as a constant. It is the pulse frequency of the laser output which ranges from 100 to 5000 Hz for the particular low powered $CO_2$ system used. Frequency can control the average laser power executed at a constant percentage. A particular frequency required is dependant on the percentage of the output power that is delivered. For example for powers ranging from 60 to 85 watts; the frequency cannot be set to below 1500 Hz. So the frequency was set to 2200 Hz for all experiments as determined from the initial experiment, which proved that 2200 Hz was a median mark and

appropriate for the range of powers levels used (60 to 80 watts). The frequency would however vary, if the power was changed. This means that for lower powers the laser cannot operate at higher frequency and for higher powers, low frequency cannot be used which in other words mean that there is a small operating window for the frequency and was dependant on the input of the laser power that was set by the operator.

### *4.3.8: Beam delivery system and machine specifications*

Figure 4.12 illustrates the low power laser marker beam delivery system and Table 4.5 presents the technical specification for the system.

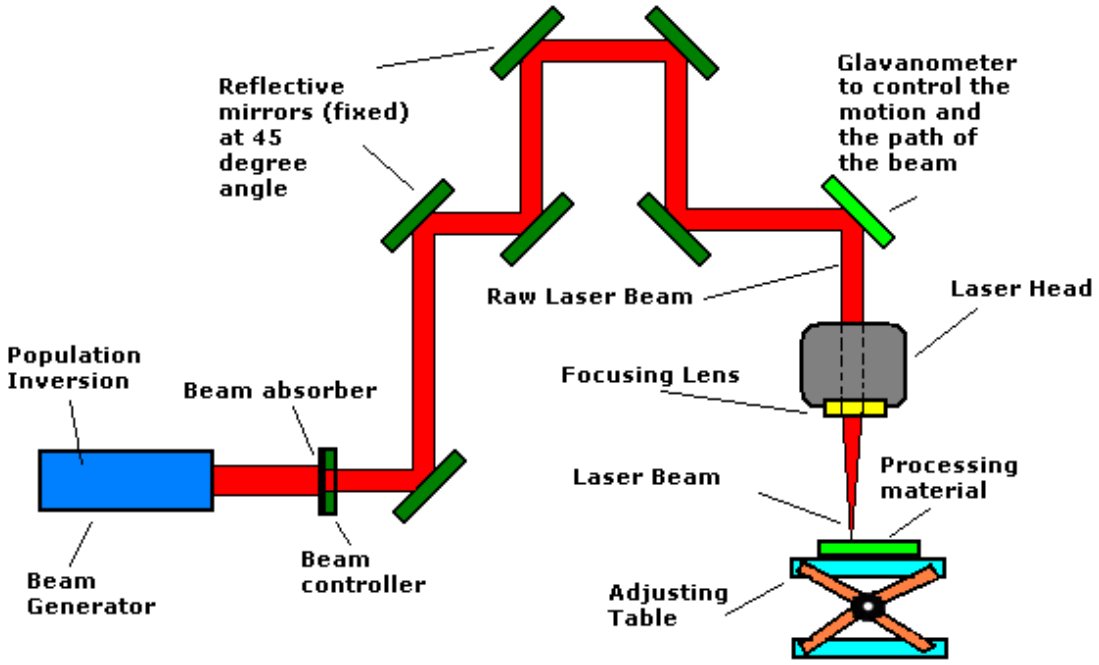


**Figure 4.12: Presents the beam delivery of 100 watts $CO_2$ laser marker.**

| Features | Details with units |
|---|---|
| **Wave length:** | 10.64 µm |
| **Pulse frequency:** | 0 - 200 kHz (at 10.64 µm) |
| **Laser class** | approx. 25 kg |
| **Safety class:** | 4 |
| **Field size:** | 100m diameter |
| **Focal distance:** | 60 x 60 mm (other field sizes on demand), 100 mm (other focal distances on demand) |
| **Dimensions (L x W x H):** | 167 x 118 x 200 mm |
| **Weight:** | approx. 3.5 kg |
| **Dimensions** | 167 X 118 X 200mm |
| **Cooling Dimensions:** | 610 mm x 19" x 6 HE; approx. 50 kg |
| **Cooling Type:** | Integrated air cooling |
| **Power supply:** | 230 V ± 10%,; 1 P / N / PE; 50 Hz / 60 Hz |
| **Connection:** | max. 1.9 kVA |
| **Ambient temperature:** | 15 to 35 °C |

**Table 4.5: Specification for 100 w $CO_2$Multi-Scan Laser marker.**

## 4.4: Nd: YAG Laser Processing

Trials were conducted using the 2 KW, Nd: YAG laser with a 1.06 µm wavelength, assisted by a KC 25 Kuka industrial robot. This configuration differs from the $CO_2$ laser beam

configuration since the $CO_2$ laser beam is ideal for producing a CW beam as previously stated. To imitate the shot peening process, it is required that a top hat beam was used so the output energy of the laser beam was distributed evenly on the surface of the material. The Nd: YAG laser was comparable with the diode pumped laser used in as it was able to pulse similarly to the industrial laser shot peening process [Hackel 2005, Metal Improvement Company Ltd 2007]. However, the frequency of the pulse differed as the Nd: YAG laser was able to generate pulses up to milli seconds only and the industrial Nd: YLF laser generated pulses up to nano seconds (this is further discussed in the next chapter).

### *4.4.1: Robot Programming*

The first step of the experiment was to programme the robot to traverse from its home position to the desired area to be laser peened. Once the robot reaches the set position (6mm above the work piece), set up is presented in Figure 4.13. The laser was then fired in the pulse mode for 10 ms and traversed up-wards (away from the work-piece) and then back to its home position. Industrial Nd: YLF laser used pulses in nano-seconds [Hackel 2005], which could not be obtained using the Nd: YAG laser (Figure 4.13) as the system could not pulse for such short period of time. Some trials involved the operator to manually switch the laser shutter on and off so the treatment was still comparable to the industrial laser [Hackel 2005]. To drive the robot, it was required to create a simple programme by the aid of the teach pendant and the imbedded Kuka programming software. The teach pendant was a wired remote control that was used to generate the programme commands.

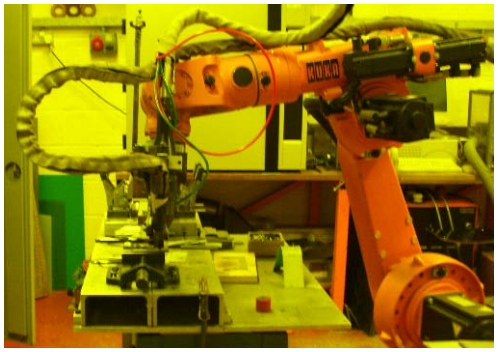

**Figure 4.13: Nd: YAG Robot and laser peening of $Si_3N_4$, placed on a holding fixture.**

## 4.5: High Power Nd: YAG Laser Alone Experiments

| No | Laser Power (Watts) |
|---|---|
| 1 | 400 |
| 2 | 500 |
| 3 | 600 |
| 4 | 520 |
| 5 | 550 |
| 6 | 575 |
| 7 | 600 |

| | |
|---|---|
| 8 | 575 |

**Table 4.6: Parameters used for Nd: YAG laser treatment of HP $Si_3N_4$**

**Note:** As the power was varied other parameters were kept constant: Spot Size = 8 mm, Pressure Shield Gas (l/min) = Argon @ 25 l/min, Focal position = 38.4 (mm).

### *4.5.1: Rational of key Parameters and steps taken*

The main parameters used for Nd: YAG laser processing were, laser power (watts), focal position (mm), pulse time (ms). Shield gas was used however, was not varied and was kept to 25 l/min as a constant. This was because too much gas pressure would have resulted in the material being blown away and too less would result in the material being oxidised.

Initial experiments began from 400 watts and proved that beyond 450 watts there was yet no effect on the material surface. Hence, the power was increased in trial number 2 to 500 watts. It was initially unknown with regards to what the effect of the Nd: YAG laser was going to exhibit on the $Si_3N_4$ surface using the pulsed beam. So 400 watts being 20 % of the maximum capacity of the laser system was applied. At 500 watts (trial number 2); there was yet no effect on the surface so the power was again increased. At 600 watts (trial 3), there were surface cracks which were breaking up the top layer of the material. This indicated that the window of parameters which were required to produce a crack-free laser peened surface was between 600 and 500 watts. So 525 watts in (trial 4) was therefore applied and found to produce no cracking. Hence, the power was increased to 550 and then 575 watts (trial 5 and 6) also showed no sign of cracking. For trial number 7, the power was therefore, raised to 600 watts where surface cracks began to appear again. Finally, trial number 6 was repeated again, to make sure that the results obtained in trial 4 were repeatable.

An 8 mm diameter spot was used by applying the pulsed Nd: YAG laser, which was comparable with the 8mm diameter pattern from the $CO_2$ laser processing. For the Nd: YAG laser system to generate an 8 mm diameter spot it was required that the focal length from the lens to the material surface was 38.4 mm. It was a compromise that was made as the spot of a smaller diameter would have concentrated the same energy in a smaller area and would have resulted in the surface being cracked and a larger spot size would have required more laser power to be generated on the material surface. A smaller diameter spot, however, would not be comparable with that of the $CO_2$ laser treatment. Therefore, the focal position was kept as a constant throughout the experiment and the laser power was only changed.

From the preliminary study on $Si_3N_4$ it was found that 1 second long laser pulse was far too long to be executed on the material surface. This resulted in a small crater being produced on the material surface rather than a circular 8 mm diameter spot. A crater ranging from 2 mm to 3 mm diameter was produced with a longer pulse cycle as the laser pulse operating on and off, being 1.5 seconds, 1 second and 0.5 second long were experimented. Therefore,

a smallest pulse size was applied and proved to be effective when the material was observed under the optical microscopy. It was found that there was a sufficient energy going into the material at 10 ms. Hence, a 10 ms of the laser pulse was therefore used as a constant for all experiments with only varying the laser power.

### *4.5.2: Beam Delivery system and System specification*

Figure 4.14 presents a Rofin Sinar® 2KW Nd: YAG laser beam delivery system. Table 4.7 presents a technical specification for the beam delivery system and Table 4.8 presents a technical specification for the motion system.

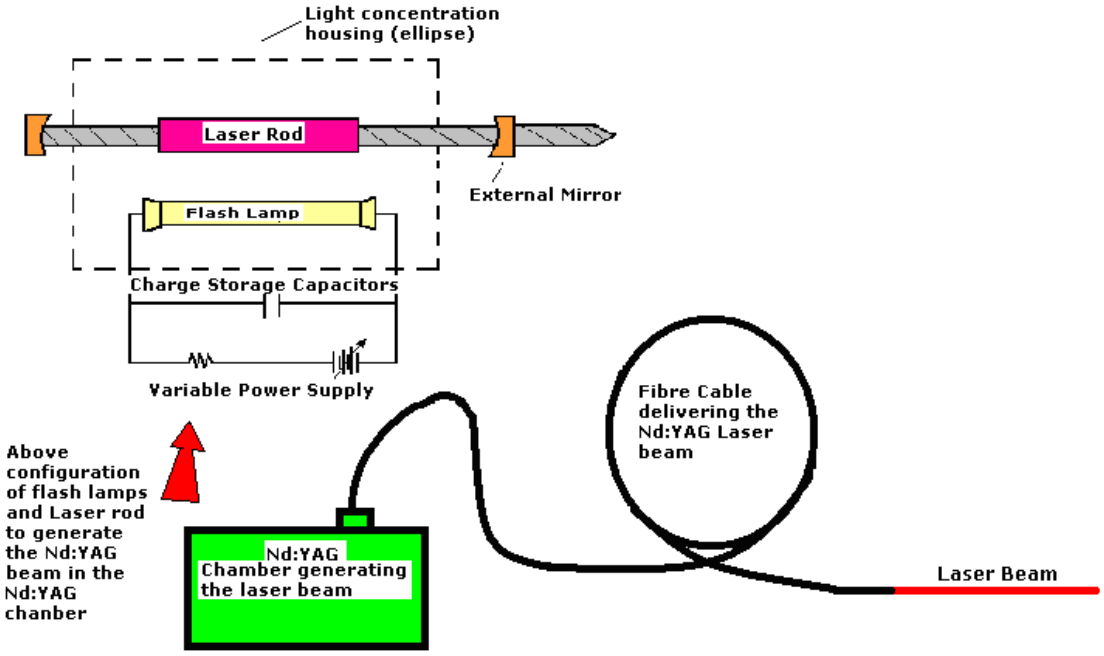


**Figure 4.14: Beam delivery system of the 2 kW Nd: YAG laser.**

| Features | Details with units |
|---|---|
| **Output power** | 2000 W |
| **Power range** | 100-5000 W |
| **Beam quality factor** | K > 0,9 |
| **Pulse frequency** | 0 or 2 up to 5000 Hz; cw |
| **Laser class** | 4 |
| **Safety class:** | 4 |
| **Field size:** | 1m X 2m |
| **Focal distance:** | 500 mm |
| **Dimensions (L x W x H):** | 500 mm x 300mm x 300 mm |
| **Weight:** | 25 kg |
| **Cooling Type:** | Integrated External Cooler |
| **Ambient temperature:** | 15 to 35 °C |

**Table 4.7: Specification for 2 kw Nd: YAG Laser.**

| Features | Details with units |
|---|---|
| **Robot Type** | Kuka- KC R25 |
| **Number of axis** | 6 |
| **Wrist** | 30/45/60 |
| **Rated Payload** | 25 Kg |
| **Suplimentary load with rated payload** | 30 Kg |
| **Max. Total Distributed load** | 60 Kg |
| **Max rotation on all 6 axis** | 270° |

| | | |
|---|---|---|
| **Max. Speed of rotation on axis 1** | 153°/ sec | ± 185° |
| **Max. Speed of rotation on axis 2** | 106° / sec | +90°<br>-40° |
| **Max. Speed of rotation on axis 3** | 152° / sec | +68°<br>-210° |
| **Max. Speed of rotation on axis 4** | 240° / sec | ± 350° |
| **Max. Speed of rotation on axis 5** | 226°/ sec | ± 163° |
| **Max. Speed of rotation in axis 6** | 298° / sec | ±350° |
| **Weight** | 867 Kg | |
| **Working Envelope** | 20 $m^3$ | |
| **Product Colours** | Base: Black, Moving Parts: Orange, Gripper: Special paint finish | |
| **Gripper Specifics (axis 1)** | | |
| **Over pressure in arm:** | 0.1 Bar | |
| **Compressed Air:** | Free of oil water and Oil. | |
| **Air Consumption:** | Approx 0.1 $m^3$ /h | |
| **Threaded Union:** | M5 | |
| **Pressure Reducer:** | 0.1 – 0.7 bar | |
| **Pressure Gauge:** | 0-1 bar | |
| **Filter** | 25 – 30 µm | |

**Table 4.8: Kuka- KC R25 robot technical specification.**

## 4.6: Laser Alone and Plasma augmented processing – (PAL)

The plasma torch was attached to the robot adjacent with the laser head as shown in the schematic in Figure 4.15, where the laser head and plasma torch were set 45° apart from each other. This setting can be adjusted depending on the experimental materials, output laser power and the output current on the plasma torch. The distance of the plasma torch was set at 6 mm above the test material surface which can also be adjusted to a ± position; however, it is kept constant throughout this experiment. In Figure 4.15; the schematic presents the set up of PALP torch attachment with the laser head onto the Kuka robot in its required configuration for laser processing as shown in the schematic below and Table 4.10 presents a technical specification of the DC plasma kit.

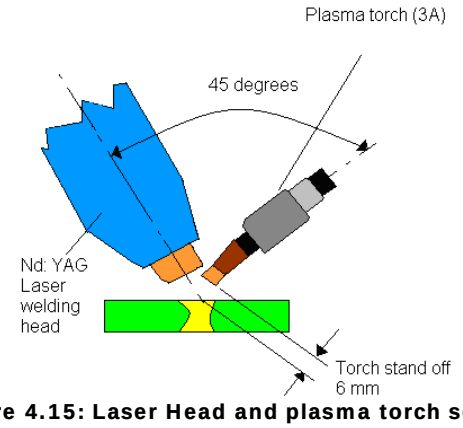


**Figure 4.15: Laser Head and plasma torch set up.**

It is important that the laser and the plasma torch fire at the same time with equal distribution of heat energy on to the materials surface so both of the devices are set to the above configuration in order to dissipate heat on one single spot by coupling in together.

| No | Laser Power (watts) | Pulse Time (milli sec) |
|---|---|---|
| 1 | 550 | 10 |
| 2 | 500 | 10 |
| 3 | 490 | 10 |
| 4 | 450 | 10 |
| 5 | 400 | 10 |
| 6 | 375 | 10 |
| 7 | 300 | 10 |
| 8 | 300 | 10 + 3 sec Pilot arc |
| 9 | 300 | 10 + 10 sec Pilot Arc |

**Table 4.9: Parameters of the high powered Nd: YAG laser using the PAL Processing of RB $Si_3N_4$.**

**Note:** Laser Power was varied with the pulse time (for trials 8 and 9), all other parameters were kept at constant: Focal position = 38.4 mm, Spot Size = 8 mm, pressure Shield Gas (argon) = 30 (l /min).

### *4.6.1: Rational Of the parameters and Steps taken*

Reaction Bonded (RB) $Si_3N_4$ and HP $Si_3N_4$ both tested. Same power settings were applied on material types. However, there was a difference in how the materials behaved. The area of impact showed some signs of cracking and, therefore, lower powers were applied until a crack-free laser peened area was found at 300 watts. This was different in comparison with the other trials attempted with HP $Si_3N_4$ since the spot size of the laser beam was much larger so it required extra laser power. The spot size of these trials was also kept to 8 mm at a focal length of 38.4 mm to keep a comparable size of the Nd: YAG laser alone treatment and the treatment using the $CO_2$ laser also being 8 mm diameter.

At 300 watts (trial 8 and 9), a plasma pilot arc was applied, for 3 seconds and then 10 seconds with the laser beam firing for a period of 10 ms only. Trial 9 showed excess burning of the outer area of the impact with evidence of surface flaws. The results with trial 8 showed crack-free surface and some evidence of surface burning.

The gas pressure with all trials for laser augmented plasma processing was increased by 5 l/min from the Nd: YAG laser alone trials and was conducted at 30 l/min due to protecting the lens and to prevent the debris going up into the laser head. This was necessary as the plume generated by the laser and the plasma beam interaction with the ceramic being much larger than that of the Nd: YAG laser alone trials.

### *4.6.2: Specification for DC Air Plasma Kit LG-100*

| Features | Details with Units |
|---|---|
| **Model** | LG-100 |
| **Power supply voltage** | AC 380±15% V / 50~60 Hz |
| **Power supply capacity** | 15 kVA |
| **Current range** | 20-100 A |
| **Duty cycle** | 60% |
| **No-load voltage** | 260 V |
| **Power output voltage** | 120 V |
| **ARC strike** | Contact /Non- Contact |
| **Power factor (η)** | 0.93 |
| **Protection** | IP21 S |
| **Insulation** | B |
| **Air pressure** | 6 Mpa |
| **Cutting Thickness** | 35 mm |
| **Weight** | 35 kg |
| **Dimensions (mm)** | 300 x 540 x 600 |

**Table 4.10: Specification of the DC Air Plasma Kit LG-100**

## 4.7: Laser Peening of $Si_3N_4$ using the Lumonics® Nd: YAG Marker

| No | Number of Pulses & rate (ms) | Laser Power (Watts) | Speed m min -1 | Spot Size (mm) |
|---|---|---|---|---|
| 1 | 5 for 5 ms each | 100 | 0 | 10 |
| 2 | 10 for 5 ms each | 200 | 0 | 10 |
| 3 | 7 for 5 ms each | 300 | 0 | 10 |
| 4 | 10 for 10 ms each | 400 | 0 | 3 |
| 5 | 5 for 10 ms each | 400 | 0 | 3 |
| 6 | 5 for 10 ms each | 350 | 0 | 3 |
| 7 | 5 for 10 ms each | 300 | 0 | 3 |
| 8 | 5 for 10 ms each | 300 | 0 | 5 |
| 9 | 5 for 15 ms each | 400 | 0 | 5 |
| 10 | 5 for 10 ms each | 400 | 0 | 8 |
| 11 | 5 for 12.5 ms each | 400 | 0 | 8 |
| 12 | 5 for 12.5 ms each | 400 | 0 | 8 |
| 13 | 5 for 12.5 ms each | 400 | 50 | 8 |
| 14 | 5 for 12.5 ms each | 400 | 500 | 8 |
| 15 | 5 for 12.5 ms each | 400 | 750 | 8 |
| 16 | 5 for 12.5 ms each | 400 | 1 | 8 |
| 17 | 5 for 12.5 ms each | 350 | 0 | 8 |

**Table 4.11: Parameters used on $Si_3N_4$ from the Nd: YAG Lumonics laser marker.**

**Note:** Frequency for all parameters was kept to 10 Hz, the gas pressure was kept very low for all trials. For trials 1 to 3 the beam spot size was kept to 10 mm diameter, for trial 4 to 7 the spot size was kept constant at 3 mm. The spot size was found to be too small so it was increased for trial 8 and 9 to 5 mm. For trial 10 to 17 the spot size was the increased to 8 mm diameter.

### *4.7.1: Rational of Laser parameters and the steps taken*

From 100 to 300 watts the spots created were not visible and have a small impact on the materials surface when observed under the magnifying lens. Hence, the power was increased until an impact was visible onto the materials surface (trial 2 and 3). At 400 watts (trial 4) the spot was visible, and the crater was produced in the centre of the spot. As the power increases the crater in the centre of the spot become significantly large. To avoid this effect, the numbers of pulses fired were reduced to 5 for trial number 5.

For the following trials (6, 7, 8) the power density was decreased and the beam spot size was increased so the occurrence of the crater can be avoided. With trial number 10; a beam spot size of 8 mm was set and an evenly spread heat dissipated impact was obtained. Trial 11 was conducted to attempt an improved spot in comparison with the previous trials. However, kinks and ridges began to occur with the ceramic cracking in the centre part of the impacted area hence, it was established that trial number 10 proved to be most successful.

The traverse speed was kept to 0 for most of the trials. Only trial 13-16 were varied to see the wider effect using the same power and spot size for each of the four trials. Variation in the traverse speed as a parameter was avoided due to the idea of imitating the laser peening process and keeping all the spot sizes comparable (8 mm) so the laser beam was made to pulse over a certain surface area. However, variation of the spot size was made from 3 mm to 10 mm, although, it was found that the smaller spots size was digging into the material due to the increase of energy focused in a small surface area and the larger spot sizes of 10 mm were having no significant impact on the material unless if the power was raised. So the 8 mm diameter spot was used for most trials with variation in the laser power.

**Note:** All trials were conducted using argon as the processing gas due to no other gas being available during the period when conducting experiments.

### *4.7.2: Beam delivery system and system Specifications.*

Figure 4.16 illustrates the beam delivery system for the 400 watts Lumonics® laser and Table 4.12 presents its technical specification.

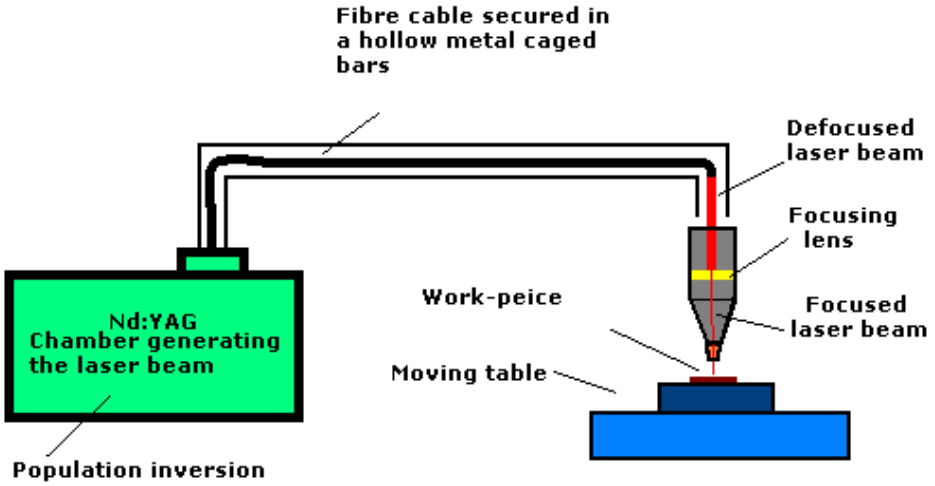


**Note:** Beam is transported through a fibre cable with a moving bed integrated with the inbuilt Lumonics software.

**Figure 4.16: Beam delivery of Lumonics 400 watts laser.**

| Features | Details with units |
|---|---|
| **Model** | JK 401SM |
| Average Power (W) | 400 |
| Max. Modulated Peak Power (W) | 800 |
| Number of Lamps | 2 |
| Beam Quality ½ Angle Radius (mm. mrad) | 16 |
| Laser response time (ms) | 1.5 |
| Modulation Frequency (Hz) | 100 – 1000 |
| Output Mode | CW, Sine, or Square |
| Fibre Core Diameter (µm) | 400 |
| Standard Spot Size (nominal) (mm) | 0.16 – 0.60 |
| Standard Fibre Length (m) | 5, 10, 15, 30 , 50 |
| Max. Fibre Length (m) | 50 |
| Beam Deliver Options | Up to 4 T or 3E or 2T x 2E combination |
| Timeshare Switching Time (ms) | > 50 |
| Focusing Head Options | Straight or right angle |
| Process Tool Options | CCTV viewing, welding nozzles autofocus cutting modules |
| Cooling water temperature & flow rate | 25 l/min @ 15 °C, 5.3 US gal/m feed input |
| Max. Pressure drop at 18° C | 2.5 bar |
| Max. Inlet Pressure | 7.5 bar |
| Cooling Capacity (kW) | 19 |
| Electrical Requirements | 380 – 415 V ± 10 % @ 50/60 Hz |
| Supply Rating (kVA) | 20 |
| Max. Power Consumption (kW) | 19 |
| Ambient Temperature (C°) | 5 – 40 |
| Max. Humidity | 95 % RH @ 20 °C, 50 RD @ 40 °C |
| W x H x D (mm)/ (inches) | 1495 x 1216 x 770/ 58.8 x 47.9 x 30 |
| Weight (kg) | 444 |

**Table 4.12: Specification for Lumonics® 400 watts laser.**

# CHAPTER V

# Analysis of Fracture Toughness

## 5.1: Surface Roughness Measurement (Topography)

Surface roughness of all the samples was measured by using the Taylor Hobson Talysurf measuring equipment. The measurement was carried out for three different conditions.

1. Virgin rough surface
2. Virgin Polished surface
3. Treated surface (using the energy beams)

The aim of this investigation was to examine the surface roughness of all samples under the above conditions for the comparison, in order to analyse and justify the effects of the energy beams executed on the material surface. The function of the Taylor Hobson Talysurf as illustrated in Figure 5.1 is simple; a mechanically-controlled probe with a sharp needle is made to travel on the treated or untreated material which would measure the smallest peaks or troughs (in the + ve or – ve direction) on the material surface [Shukla 2007]. Programming of the machine was carried out by the use of the integrated Taylor Hobson Tallysurf software which drives the mechanically-controlled probe. The probe is sensitive to the smallest variation in the material topography, hence producing results in form of graphs which present **Ra** value in units of micro meters (µm).


**Figure 5.1: Taylor Hobson Talysurf –Surface measurement equipment.**

## 5.2: Vickers Hardness Test

An indenter of a specific shape made from a diamond material was used to indent the surface of the material being investigated [Clauer 1996]. The diamond was pressed on to the top surface of the test piece and the load was then released. Hence, a diamond indent was created onto the surface which was measured in size. The surface area of the indentation was then divided by the applied load to calculate the hardness value.

The diamond indenter was in the form of a square based pyramid comprising of 136° between its faces as shown in Figure 5.2. The faces of the diamond are smooth with a sharp tip, well polished and free from any type of surface defects or imperfections. The applicable load varies from 1 to 120 kg. For the purpose of this investigation loads of 5, 20, 30 and 50 kg were applied.

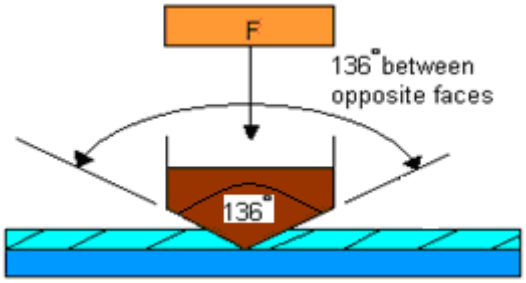


**Figure 5.2: Schematic of the diamond indentation procedure.**

The indentation depth was pressed to about 1/7 of the diagonal length. So if the indentation has 0.5 mm diagonal length the depth of the indentation would be about 0.071 mm.

The Vickers hardness number obtained used units of (Hv). There are two ways of obtaining the Hv value. It was more practical and easy to use existing charts that present the values depending on the size of the indented surface. The size of the indented surface was measured using the dimensions illustrated in Figure 5.3. This approach could be used for obtaining all Hv values from Vickers indentation test. The second approach was to calculate the Hv value by using a formula. This method was not used since it was more time-consuming in comparison with the first method using charts to obtain the Hv value. This was the ratio of the load applied to the indenter to the surface area of the indentation:

$$\mathbf{HV = 2P \sin [\theta/2] / D^2 = 1.8544P / D^2}$$

Where **P** was the load applied in kilograms (Kg), **D** was the average diagonal size of the indentation in mm and $\boldsymbol{\theta}$ was the angle between opposite faces of the diamond indenter being 136° with less than ±1° of tolerance. The indentation produced is always symmetrical as shown in Figure 5.3.

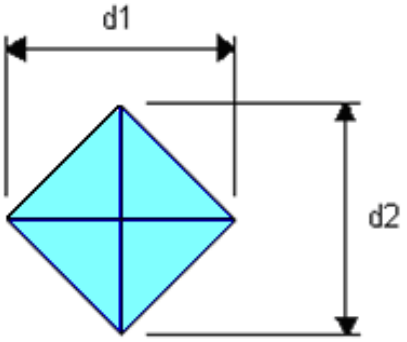


**Figure 5.3: Symmetrical Diamond Indentation.**

Diamond indentation creates crack propagation on the surface of the ceramics due to their brittleness. With the aid of the optical microscopy and SEM equipment, it was possible to measure the lengths of the cracks in order to calculate the $K_{1c.}$ In an ideal situation, cracks are generated on all four edges of the diamond indent as illustrated in Figure 5.4. These cracks were measured in length with the aid of scales that measure the lengths in micrometers (µm). The length of C1 and C2 are added and divided by 2, to obtain the average length of the propagated surface cracks in the four corners from the diamond indentation.

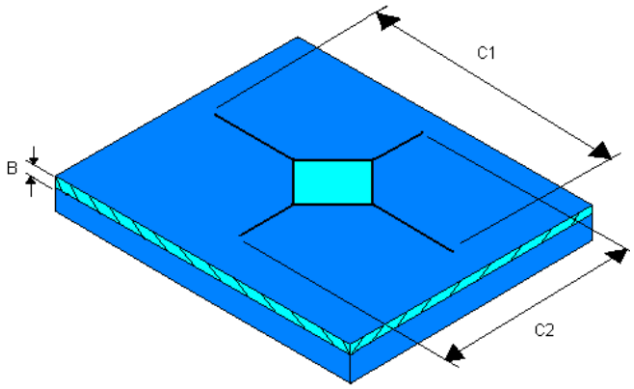


**Figure 5.4: Schematic of a Vickers diamond indentation with propagation of the cracks.**

## 5.3: Optical Microscopy

Optical microscopy was used to view the morphology and the texture of the material treated by the energy beams. There are various lenses which vary the level of magnification. The images taken for this project mainly utilised the x 100 and x 200 magnification lenses. The Vickers indented surface was viewed under the optical microscope. Each of the measurable indents was then printed as (10 cm x 13 cm) images using a standard printer. The scale was also printed at the same size and then put against the diamond indentation and the propagated cracks to accurately measure their lengths. There are various scales available for the measurement. It was purely dependent on which lens was used for taking the microscopic image. If a lens of x 100 magnification was used, then it was essential that a correct scale was also utilised in order to obtain an accurate measurement of the surface cracks. The magnification used for most of the images was x 100. On various occasions, magnification of x 200 was also utilised. Figure 5.5 presents images of both scales.

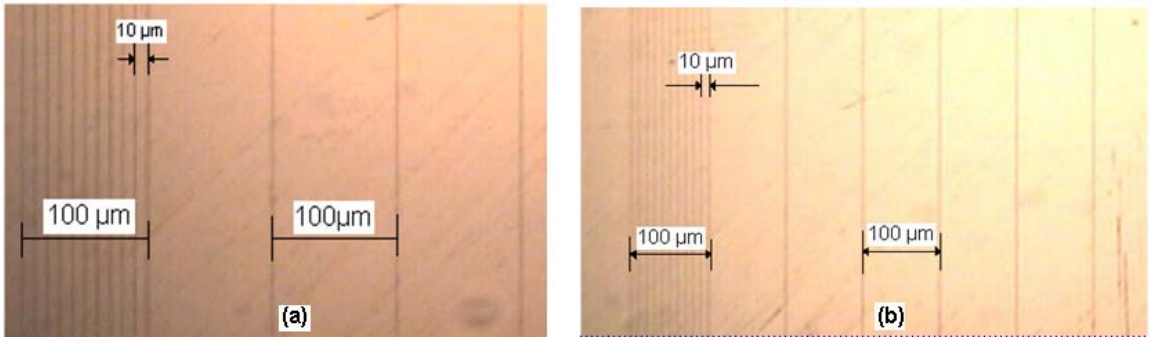


**Figure 5.5: Images of the scales used to measure the crack lengths from the indentation (a = x 200 and b = x 100 magnification).**

### *5.3.1: SEM*

Scanning Electron Microscope otherwise known as the SEM is a tool which is used to observe objects at a much larger, magnified scale than optical microscopy [Kell 2006]. All materials tested under the energy beams were viewed using the SEM. The SEM, manufactured by Joel Advanced Technology Ltd is illustrated in Figure 5.6. The magnification was varied from x 500 to x 8000 depending on the quality of the image visible and the desirable comparison of different images.

**Figure 5.6: The SEM Equipment**

The SEM operates in a triangulated configuration so the material under investigation must be a good electrical conductor. Stainless steel and tungsten carbide performed exceptionally well under this investigation. However, $Si_3N_4$ as a ceramic has low conductivity in comparison with metals so it required a thin coat of gold since gold is a good electrical conductor. This was not possible due to lack of funds and facilities available to carry out the task. Therefore, an best attempt was made to clean the samples with acetylene in order to conduct as much current as possible and form a loop in the system to produce a valuable image that can be viewed for evaluation.

## 5.4: Determination of Fracture Toughness ($K_{1c}$)

As stated in the literature review, ten equations were initially utilised to determine which were best suited for calculating the $K_{1c}$ [Ponton 1989, Ahn 1996]. Virgin surface of the $Si_3N_4$ was first tested for its hardness. Twenty indentations were produced on one particular surface of the $Si_3N_4$ from various test samples. Calibrated hardness was then recorded and a mean average was taken for its virgin surface hardness.

Each indentation was then viewed at microscopic level by the aid of optical microscope and SEM, in order to observe the surface morphology. Surface flaws were also measured using scales suitable for the magnification as mentioned above. The length of the surface flaws, produced by the indentations were then placed into the various $K_{1c}$ equations with its calibrated mean hardness.

**Note:** The true $K_{1c}$ value of non-treated (virgin) $Si_3N_4$ was between 4 to 6 Mpa$\sqrt{m}$ [CES 2007].

Various equations can be used to calculate the value of $K_{1c}$ for ceramics depending on the different material type and experimental conditions. The equations used for this investigation are for half-penny median cracks and are presented below. It was found that the cracks found from the Vickers indentation test were half-penny median cracks so other equations illustrated in Chapter 4, Table 4.7 for Palmqvist cracks were not used.

$$K_{1c} = 0.0101\ P/\ (ac^{1/2}) \quad (1)$$

$$K_{1c} = 0.0515\ P/C^{3/2} \quad (2)$$

$$K_{1c} = 0.0824\ P/c^{3/2} \quad (3)$$

$$K_{1c} = 0.0134\ (E/Hv)^{1/2}\ (P/c^{3/2}) \quad (4)$$

$$K_{1c} = 0.0330\ (E/Hv)^{2/5}\ (P/c^{3/2}) \quad (5)$$

$$K_{1c} = 0.0363\ (E/Hv)^{2/5} (P/a^{1.5})\ (a/c)^{1.56} \quad (6)$$

$$K_{1c} = 0.095\ (E/Hv)^{2/3}\ (P/c^{3/2}) \quad (7)$$

$$K_{1c} = 0.022\ (E/Hv)^{2/3}\ (P/c^{3/2}) \quad (8)$$

$$K_{1c} = 0.035\ (E/Hv)^{1/4}\ (P/c^{3/2}) \quad (9)$$

**Abbreviations: P** = Load (kg), **N** = Load in Newton's (N), **c** = average flaw size, **a** = 2c, **m** = length in meters, **Hv** = Vickers material Hardness value, **E** = Young's modulus. (Young's modulus for all untreated samples of $Si_3N_4$ was kept to 250 GPa √m as obtained from CES [CES 2007].

All the above equations have been used to calculate the $K_{1c}$ value for the virgin surface of $Si_3N_4$. The results have been tabulated and are as following tables. The equations were set up using Microsoft Excel which made it easy to be able to input three major parameters from the full equation. These values were hardness, crack length and the Vickers indention load. It can be seen that all the values range between 4 and 6 MPa √m, which make the equation accurate and useable.

Different values for $K_{1c}$ were obtained. The $K_{1c}$ value of untreated $Si_3N_4$ is known to be between 4 and 6 Mpa √m so the values that do not lie between 4 and 6 Mpa √m were not considered as acceptable and therefore those equations were discarded. The investigation is presented as follows:

**Key:**

= Invalid and unacceptable values

= Acceptable values, hence the equation is accurate and usable

| $K_{1c}$ (MPa √m) |
|---|
| 8.69 |
| 13.76 |
| 12.09 |
| 12.80 |
| 12.88 |

**Table 5.1: Equation 1[$K_{1c} = 0.0101\ P/\ (ac^{1/2})$]**

In Table 5.1 presents values highlighted in red for the calculated $K_{1c}$ were too high for the required range.

| $K_{1c}$ (MPa √m) |
|---|
| 0.02 |
| 0.02 |
| 0.02 |
| 0.02 |
| 0.02 |

**Table 5.2: Equation 2 [$K_{1c} = 0.0515\ P/C^{3/2}$]**

The values obtained were very low hence the equation was not acceptable.

| $K_{1c}$ (MPa √m) |
|---|
| 187825.85 |
| 374233.33 |
| 308358.76 |
| 335911.64 |
| 339172.90 |

**Table 5.3: Equation 3 [$K_{1c} = 0.0824\ P/c^{3/2}$]**

This equation was also not acceptable since the values were far too high.

| $K_{1c}$ (MPa √m) |
|---|
| 3.63 |
| 5.02 |
| 4.56 |
| 4.76 |
| 4.78 |

**Table 5.4: Equation 4 [$K_{1c} = 0.0134\ (E/Hv)^{1/2}\ (P/c^{3/2})$]**

The values in Table 5.4 were reasonable and lie within the range of (4 – 6 MPa √m); hence this equation was acceptable and could be considered for use if other equations do not present more consistent result.

| $K_{1c}$ (MPa √m) |
|---|
| 0.18 |
| 0.25 |
| 0.23 |
| 0.24 |
| 0.24 |

**Table 5.5: Equation 5 [$K_{1c} = 0.0330\ (E/Hv)^{2/5}\ (P/c^{3/2})$]**

Values for the equation in Table 5.5 were high, hence the equation was unacceptable.

| $K_{1c}$ (MPa √m) |
|---|
| 0.0031 |
| 0.0041 |
| 0.0037 |
| 0.0039 |
| 0.0039 |

**Table 5.6: Equation 6 [$K_{1c} = 0.0363\ (E/Hv)^{2/5}(P/a^{1.5})\ (a/c)^{1.56}$]**

Values in Table 5.6 were too low hence, the equation was unacceptable.

| $K_{1c}$ (MPa √m) |
|---|
| 572.12 |
| 745.55 |
| 676.75 |
| 706.34 |
| 709.76 |

**Table 5.7: Equation 7 [$K_{1c} = 0.095 (E/Hv)^{2/3} (P/c^{3/2})$]**

The values found were too high in Table 5.7, hence, the equation was unacceptable.

| $K_{1c}$ (MPa √m) |
|---|
| 132.49 |
| 172.65 |
| 156.72 |
| 163.57 |
| 164.36 |

**Table 5.8: Equation 8 [$K_{1c} = 0.022 (E/Hv)^{2/3} (P/c^{3/2})$]**

Equation in Table 5.8 was unacceptable since the values do not lie within the required range.

| $K_{1c}$ (MPa √m) |
|---|
| 6.04 |
| 8.19 |
| 7.44 |
| 7.76 |
| 7.80 |

**Table 5.9: Equation 9 [$K_{1c} = 0.035 (E/Hv)^{1/4} (P/c^{3/2})$]**

The figures were close to the required values in Table 5.9, however, they are still considered too high, so the equation was also unacceptable.

| $K_{1c}$ (MPa √m) |
|---|
| 4.33 |
| 6.00 |
| 5.44 |
| 5.68 |
| 5.71 |

**Table 5.10: Equation 10 [$K_{1c} = 0.016 (E/Hv)^{1/2} (P/c^{3/2})$]**

The $K_{1c}$ values in Table 5.10 were reasonable and comply within the desired range so the equation was accurate and useable.

**Note:** These equations were only ideal and specialised for ceramics. So they cannot be applied to the metallic materials. For further details on the above results, please check Appendix 11.6, section C.

Each of the equations was set up by the aid of an Excel spreadsheet. The experimental values obtained were an input into the equation such as the indentation load, flaw size created by the Vickers diamond indentations and the calibrated hardness.

The equation that generated the most accurate result was equation 10 in Table 5.10. However, it was first established that the above equation (10), could be used manually to obtain a realistic $K_{1c}$ values. An example is presented below on the next page. It was time consuming to determine each $K_{1c}$ value of the treated or untreated surfaces so to make the analysis consistent and as accurate as possible, a Microsoft Excel file was created to determine each $K_{1c}$ value of the treated and untreated ceramic test samples.

Abbreviations: 0.016 = Constant (K), E = Young's Modulus, Hv = Vickers hardness, P = indentation load, crack length (flaw size).

$$K_{1c} = 0.016\ (E/Hv)^{1/2}\ (P/c^{3/2})$$

$$= 0.016 \times (28300/\ 1521)^{1/2} \times (490.5\ /(0.000755\ /\ 2)^{3/2})$$

$$= 0.016 \times (18.6018014^{1/2}) \times (490.5\ /(0.0003775^{3/2}))$$

$$= 0.016 \times (4.312982031) \times (490.5\ /\ 0.000007334)$$

$$= 0.016 \times (0.069007712) \times (66880283.61)\ /\ 1000000$$

$$= 4.615255383$$

$$= \mathbf{4.615\ MPa\ \sqrt{m}}$$

Values obtained using equation 10 were most accurate in comparison with the other equations. Hence, this equation will be used from this point onwards to determine the $K_{1c}$ of the $Si_3N_4$ for treated and untreated test samples.

The $Si_3N_4$ surface was first treated with the $CO_2$ laser beam. The $K_{1c}$ values were then calculated using the above equation and the results are presented in Table 5.11. Due to the experimental conditions of the $CO_2$ laser processing; it was found that there was an effect of oxidation on the material surface (discussed in the later chapter). Hence, the Young's modulus was then changed to 300 Mpa √m, for the treated samples only. This was because the ceramics materials are isotropic (meaning the Young's modulus of the material not being uniform around all orientations of the material) which occurs due to certain manufacturing impurities and further modifications. So when the material is exposed to a laser beam (thermal energy) which leads to further changes within the material by the thermal stress induced meaning that the change of the Young's modulus was ideal after conducting the laser treatment.

| $K_{1c}$ (MPa √m) |
|---|
| 6.61 |
| 7.44 |
| 6.65 |
| 6.81 |
| 7.25 |

**Table 5.11: Calculation of $K_{1c}$ for $CO_2$ Laser treated $Si_3N_4$ using equation 10.**

## 5.5: Chapter Summary

The chapter demonstrates the use of both high and low powered $CO_2$ and Nd: YAG industrial lasers, ultrasonic and PAL processing to carry out the investigation. The results were put together and analysed by the optical microscope and the SEM. Vickers hardness testing, surface roughness tests and analytical means of calculating the $K_{1c}$ were used. Ten equations especially designed for calculating the $K_{1c}$ were also employed. One equation was applied throughout the analysis [Ponton 1989], from the ten equations that were used. The following section demonstrated the findings and the results obtained from the above activities. The objective in the end was to analyse the change in the materials $K_{1c}$ value if

any (after the treatment), presented with key findings in the later chapters after applying the energy beams.

# CHAPTER VI

# Experimental Results and Evaluation

## 6.0: Introduction

This chapter presents the results and discussion of the experimental work as described in chapter 5. The results were collected in the form of numerical values derived from the Vickers hardness tests, microscopic images obtained mostly from the optical microscopy and SEM. Also, empirical equations were used to calculate the $K_{1C}$ of the treated and "as machined" (untreated virgin surface) of HP $Si_3N_4$. Further investigations also include analysis of the surface topography which is presented by the aid of graphs. Detailed experimental data is presented in the Appendix 11.9 onwards.

## 6.1: Results from the analysis of as machined (virgin surface), ground and polished HP $Si_3N_4$

The hardness of ground, polished and the unpolished surfaces was obtained to understand the behaviour of HP $Si_3N_4$ under atmospheric conditions. It was found that the hardness of ground and polished HP $Si_3N_4$ was much higher in comparison with the as-machined surface. Increase in hardness achieved by grinding and polishing was 11 %. The values were obtained from taking 20 indentations by the Vickers diamond indenter over a distributed surface (30 mm) of the HP $Si_3N_4$ test sample. Twenty indentations were made to ensure repeatability and inconsistency of results and an average hardness of the surface was derived (this applies to all treated samples).

The indentations were made over a small surface area; the resulting values were found to be similar and closely linked. For example the hardness values were not far apart from each other for the indentation number 3, 4, 5 in Table 11.24 Appendix 11.9.1 (ground and polished HP $Si_3N_4$) and the hardness of the indentation number 6, 7, 8, 9, 10 in Table 11.19, Appendix 11.9.1 for "as machined" HP $Si_3N_4$. This was because the indentations made on the surface of the test sample were conducted closely as shown in Figure 6.1. A gap of 2 mm to 3 mm was left between each indentation; however, the surface hardness did not appear to change within that distance. A space of four diamonds is required to be left between each indentation as mentioned in [ISO 6507-1 2005]. In case of the present work in Figure 6.1, a gap of only two to three indentations were left from each. This was not left according to the [ISO 6507-1 2005]. However, from observing the diamond indentations under the optical microscopy demonstrated that the cracks produced by the diamond indentations were independent to each other (cracks not being connected) and were not affected.

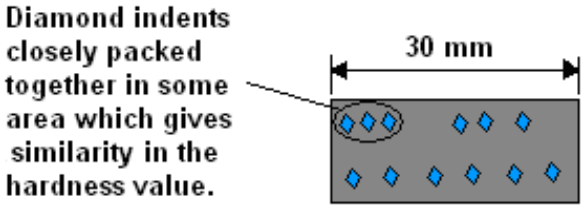


**Figure 6.1: The spread of indentations on the HP $Si_3N_4$ test samples**

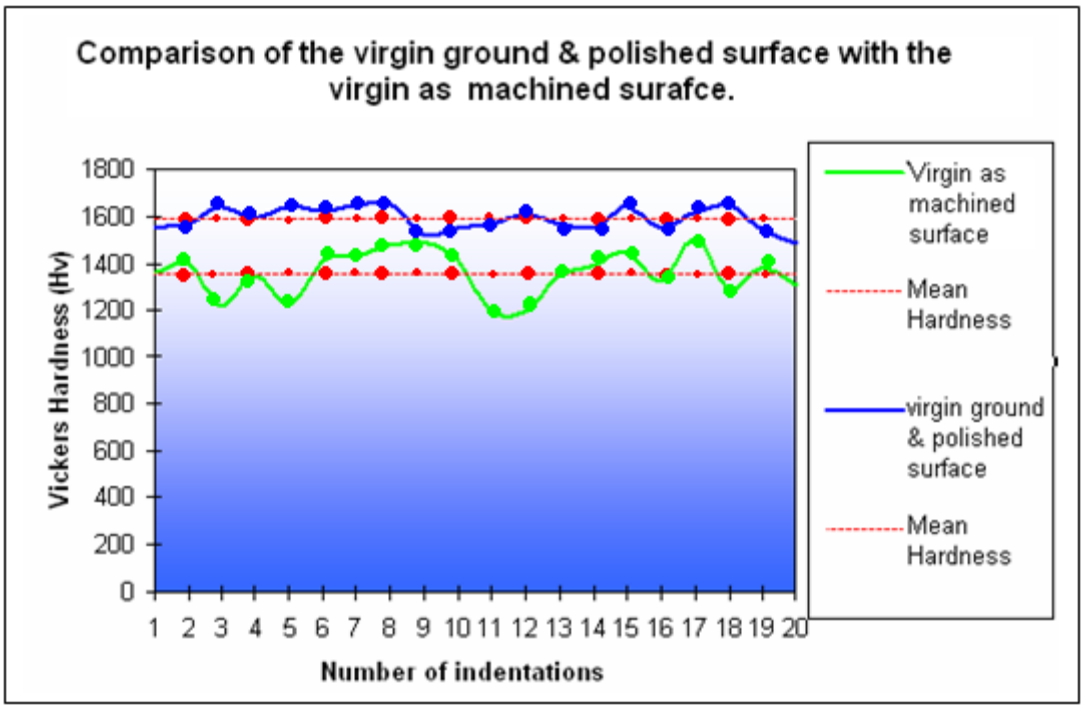


**Figure 6.2: Comparison of the virgin ground & polished surface with the virgin machined surface.**

The fluctuation in the hardness values was a result of the material not being uniform throughout its surface area for “as machined” (unpolished) surface which featured induced machining marks from drilling and milling. This surface was “as machined” in the condition obtained directly from the manufacturer. Some areas on the surface were highly scarred which could have been a possible cause of this fluctuation as the average surface hardness was lower than the average surface hardness of the ground and polished surface. It is thought that stress concentration generated at the machining marks aided crack propagation as the indenter moved into the material. As a consequence, the indentations were larger, hence it generated lower Hv value.

It was stated by McColm *et al* typical expected variation in the Vickers hardness test results could be around ±10 % of the nominal hardness value of the material [McColm 1990]. The nominal hardness value of the ground, polished HP $Si_3N_4$ was found to be 1587 (Hv) as presented in Table 11.19 in Appendix 11.9.1. 10 % of this nominal hardness value was 158 (Hv) allowing a tolerance of ± 158 (Hv). The values in Table 11.19 Appendix 11.9.1 and the graph in Figure 6.2 present the difference between the highest and the lowest hardness value for the ground and polished surface being 166. Therefore, the fluctuation of the ground

and polished curve in Figure 6.2 was out of tolerance by ±1 % and can be considered as a non-conformance but in cases can also be acceptable.

### *6.1.1: Vickers Indentation of the Ground, Polished and as machined Surfaces of HP $Si_3N_4$*

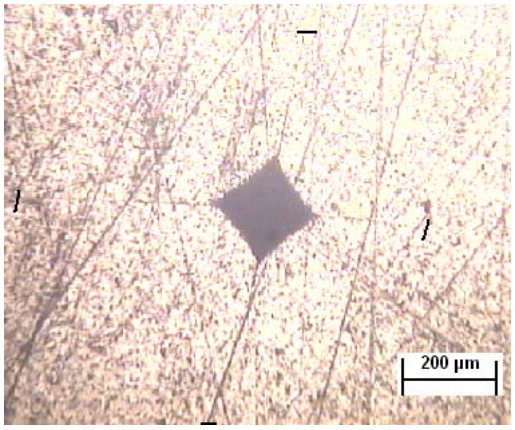


**Figure 6.3: Un-polished "As machined" HP $Si_3N_4$, Crack Length = 825 µm, average hardness = 1355 (Hv)**

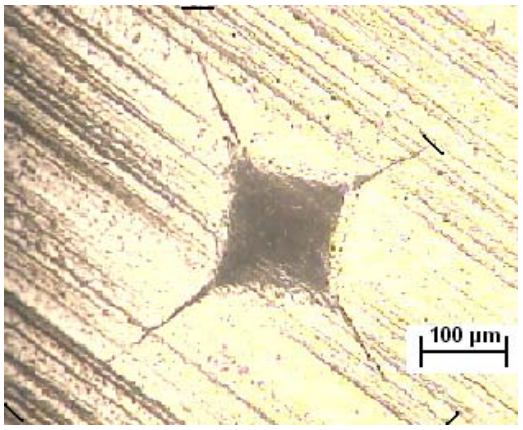


**Figure 6.4: Polished HP $Si_3N_4$ Crack length = 600 µm, average hardness = 1521 (Hv)**

From the microscopic observation it was found that the unpolished (as machined) surface contained machining scars as presented in Figure 6.3. The scars were caused by machine tools and featured localised tensile stress. This agreed with the work presented in [Strakna 1996]. Figure 6.4 presents the polished surface of $Si_3N_4$ with less scars and higher surface hardness. It was believed that the tensile stress can lead to the propagation of cracks on the surface during the diamond indentation. This residual stress aided crack propagation associated with the indentation of the surface during hardness testing and hence resulted in longer indents, producing a lower hardness value.

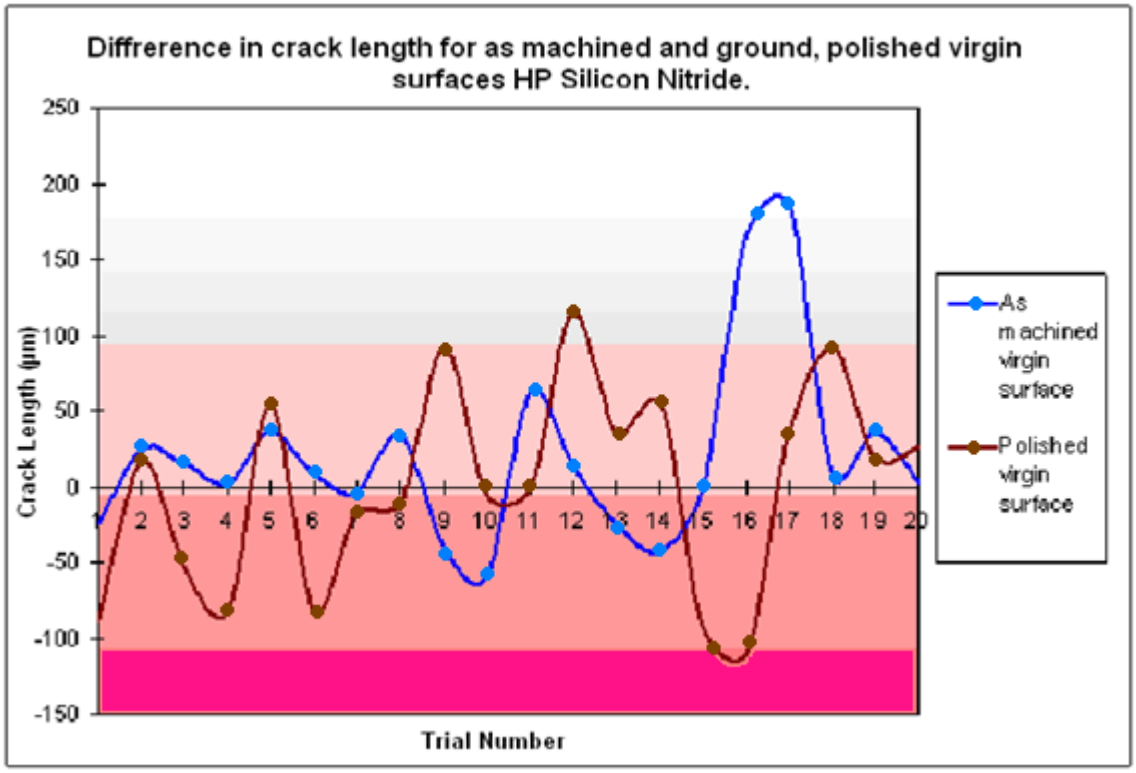


**Figure 6.5: Crack length values generated during hardness testing of "as machined" vs ground, polished virgin surfaces of HP $Si_3N_4$.**

Figure 6.5 illustrates that the crack length generated by the ground and polished surface after the Vickers hardness test. The average crack length of the "as machined" virgin surface was 745 µm and the hardness obtained after grinding and polishing was 596 µm. The average crack decreased by 150 µm after grinding and polishing of the ceramic. This decrease in the crack length was achieved from removing the surface macro-cracks by grinding and polishing which resulted in the surface obtaining more strength from the induced compressive stress by grinding & polishing which also allowed the material surface to become more resistant to cracking.

### *6.1.2: Surface Topography of ground and polished and untreated $Si_3N_4$ Surfaces*

Figure 6.6 reveals the surface roughness profile of "as machined" virgin surface was a mean value of 4.82 µm. The curve on the graph shows that there are areas of high peaks in the positive direction and areas of troughs in the negative direction. This could be in form of the microscopic machining scars, surface flaws and porosity that pre-existed due to the nature of the brittle ceramic.

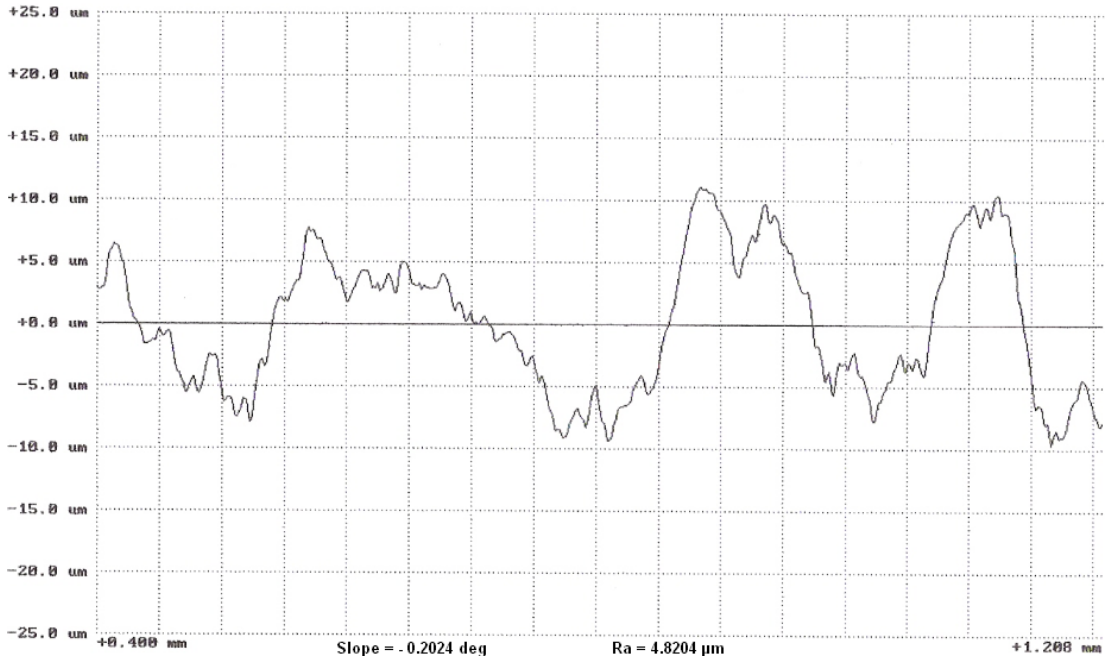


**Figure 6.6: Surface Roughness graph of virgin as machined HP $Si_3N_4$ (Ra = 4.82 µm).**

It was important to observe the surface roughness of the HP $Si_3N_4$ during each stage of testing. Grinding and polishing enhanced the surface quality and decreased residual surface defects from machining. The smoother ground & polished surface is a disadvantage with respect to absorption of the incident beam. Therefore to enhance beam absorption into the ground and polished surface a black marker was used to generate an absorptive layer [Metal Improvement Company Ltd 2007, Hackel 2005].

The surface finish (Ra value) of both "as machined" virgin surface, ground and polished virgin surface (Figure 6.6) as well as treated surfaces by the energy beams were measured, which then allowed a comparison between each of the conditions. The untreated surfaces (ground & polished and "as machined") were both much more resistant to propagation of a surface crack during the laser treatment by the thermal shocks as later discussed in this chapter.

Figure 6.7 illustrates the surface roughness profile of the ground and polished virgin surface of HP $Si_3N_4$. The average surface roughness measured was 0.07 µm. This in comparison with the machined virgin surface was much lower, meaning that the surface has become much smother from the result of grinding and polishing. The graph shows that the positive peaks and the negative troughs (asperities) have become much sharper and closely compacted, indicating that the porosity, surface flaws, and machining induced scares of the HP $Si_3N_4$ surface has decreased. This was purely due to the fact that the surface has been ground and polished.

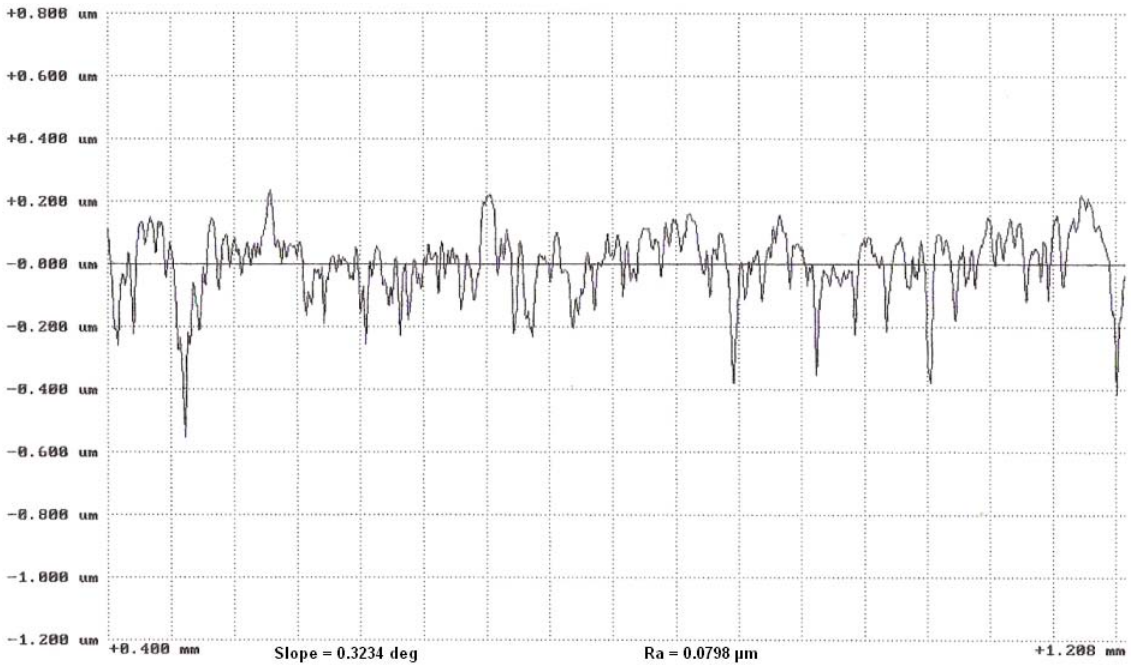


**Figure 6.7: Surface finish of virgin ground and polished HP $Si_3N_4$ (Ra = 0.07 µm).**

### *6.1.3: $K_{1c}$ of untreated ground, polished and as machined untreated Surfaces*

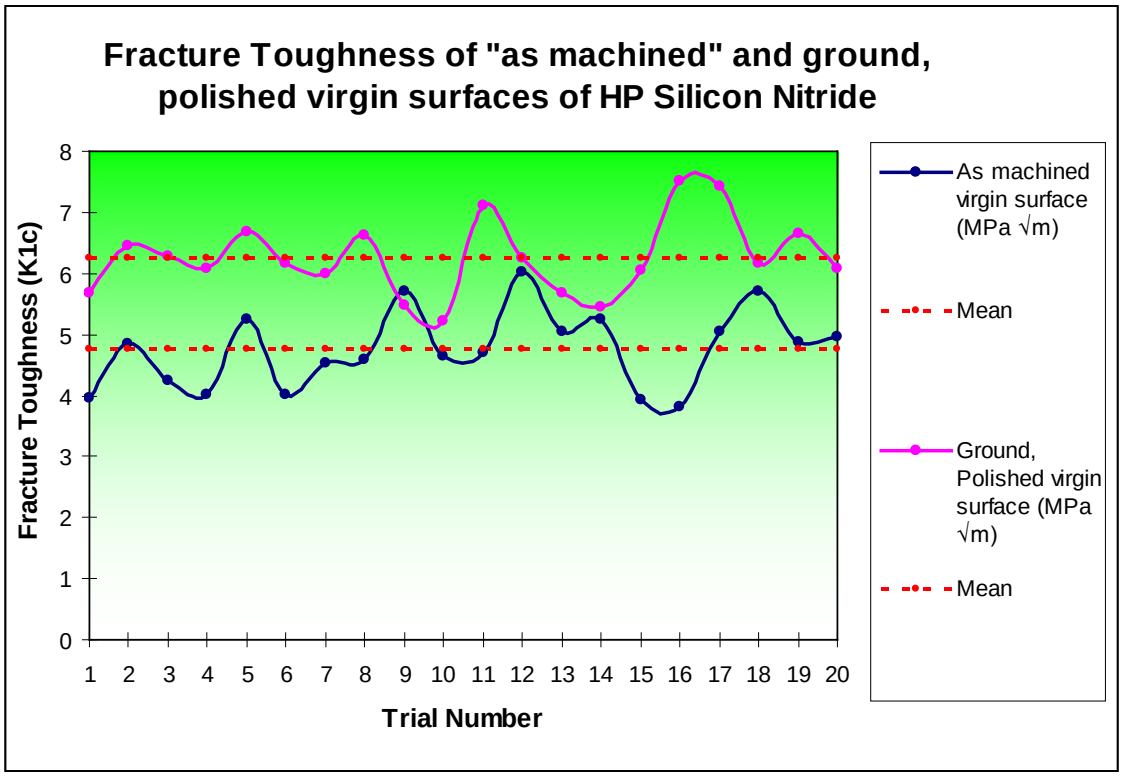


**Figure 6.8: $K_{1c}$ value for as machined and ground, polished virgin surfaces if HP $Si_3N_4$.**

**Note:** Further results of the $K_{1c}$ calculations are presented in Appendix 11.6 onwards.

It was assumed from literature [CES 2007] that the $K_{1c}$ of both types of virgin surfaces were found between 4 – 6 MPa √m (standard range). Although, the value of the ground polished virgin surface (Figure 6.8) was slightly above the predicted result. This was due to polishing that minimised the surface scars as well as porosity and increased the hardness of the top layer of the HP $Si_3N_4$. The calculated $K_{1c}$ of the "as machined" virgin unpolished surface was in the region which was acceptable from literature [Mangels 2006, Mangels 2006, CES 2007, Metal Improvement Company Ltd 2007, Kalpakjian 2001, Morgan Advanced ceramics Ltd 2007]. $K_{1c}$ of the virgin ground and polished surface was calculated to be 8 % above the "predicted range". This can be justified by stating that there was a lack of consistency in accurately measuring the crack length created by the Vickers indentation as the accuracy of the length of the cracks measured is dependant on the human eye. Hence, experimental errors were possible to take place. This could have led to a small increase in the crack lengths, influencing the final $K_{1c}$ value.

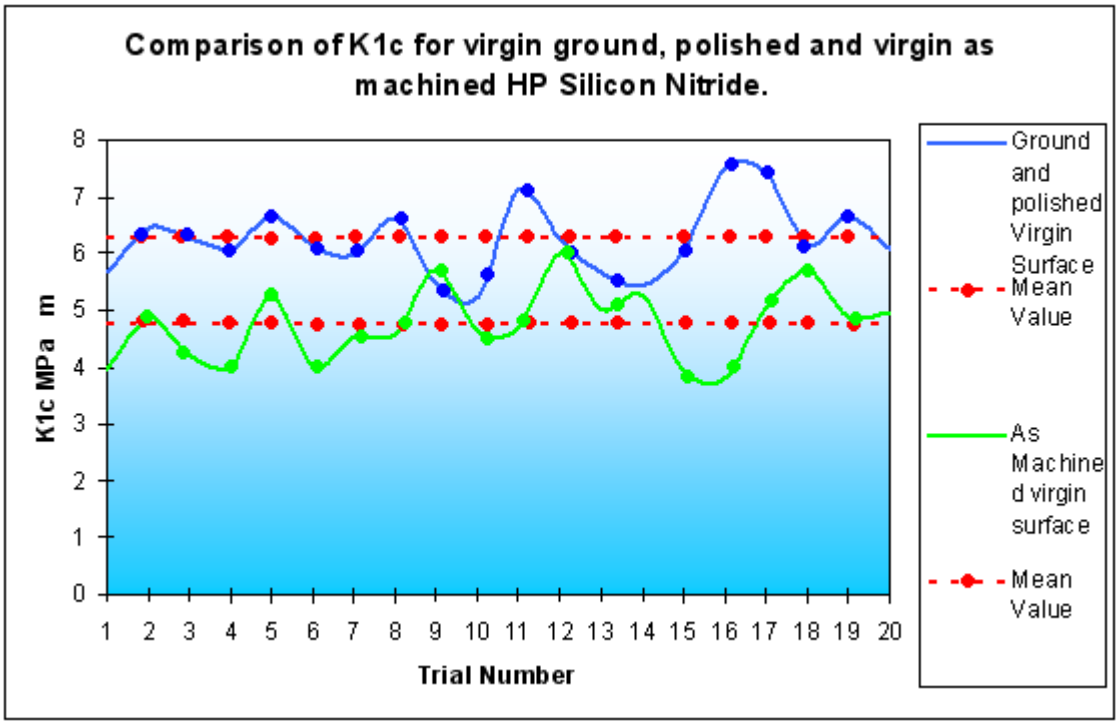


**Figure 6.9: Comparison of the $K_{1c}$ between the virgin ground, polished and virgin as machined HP $Si_3N_4$.**

Figure 6.9 shows a comparison of the two different samples that were initially tested. The mean $K_{1c}$ value of the virgin ground and polished surface was 6.27 MPa √m and in comparison, the value of the as machined virgin surface was 4.75 MPa √m. The fluctuation in both of the curves in the graph was a result of non uniform surface topography (throughout its area). Due to the fluctuation in the hardness as previously illustrated in Figure 6.2, it was expected that the value of $K_{1c}$ would differ for both conditions. These results are in agreement with the findings of Malshe *et al* that machining processes such as turning, milling and grinding which induce scars and microscopic flaws on the material surface could reduce the surface strength of the ceramic [Malshe 2006] . However, grinding followed by polishing

would enhance the surface strength. Hence, the surface flaws are minimised, so it could be predicted that some residual compressive stress on the top layer of the material was also induced (this complies with the work in [Ahn 1996, Strakna 1996]. The porosity and the microscopic surface flaws that exist prior to grinding and polishing were also closed off and compacted to generate a smoother surface layer. The smooth layer would be ideal for enhancing the $K_{1c.}$

Ponton *et al* stated the accuracy of the equation (10) was between 30 to 40 %. From applying the equation to the virgin surfaces (ground & polished and as machine), it was found that up to 80 % of the values were within the expected range as stated in [Ponton 1989]. The equation performed within the expected value (4 – 6 Mpa $\sqrt{m}$) for HP $Si_3N_4$ which meant that the method was acceptable and was used for all other treated samples throughout the analysis.

## 6.2: $CO_2$ Laser Processing Experiments

Higher surface roughness values obtained from $CO_2$ laser processing as compared to those from the Nd: YAG can be attributed to a greater degree of material ablation generated by the CW $CO_2$ beam relative to the pulsed Nd: YAG laser.

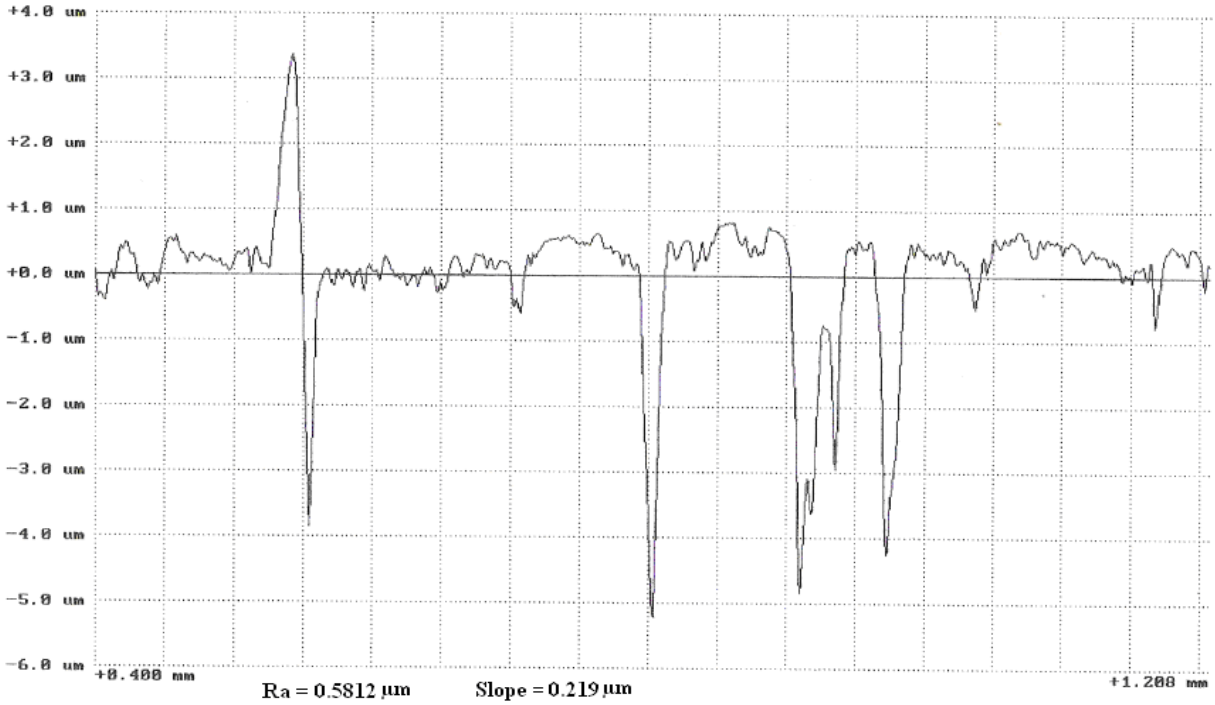


**Figure 6.10: Surface topography of the $CO_2$ laser treated HP $Si_3N_4$.**

The following results were obtained from scanning the $CO_2$ laser beam in a spiral pattern as detailed in Chapter 4, section 4.3.3 (pattern 4). The hardness was measured from one edge to the other edge of the spiral, across the diameter, as illustrated later in this chapter.

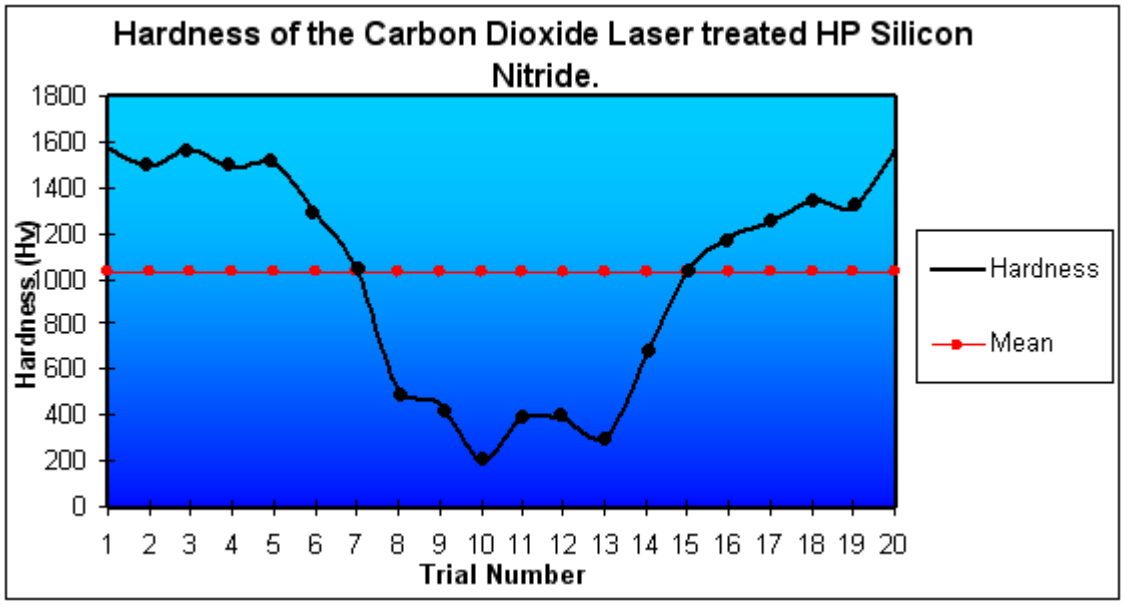


**Figure 6.11: Hardness of $CO_2$ laser treated HP $Si_3N_4$.**

The graph in Figure 6.11 presents the distribution of hardness for $CO_2$ laser treatment of HP $Si_3N_4$. A reduction in the hardness was obtained after the surface treatment, although, it was found that the hardness fluctuated throughout the treated area which could have occurred due to the surface ductility not being uniform throughout the treated surface. As well as variation of the defect in fill by glassy phase as it was re- distributed by the laser thermal input. In other words; the top layer of the HP $Si_3N_4$ surface was excessively softened in some areas compared to other areas to obtain a reduction in the hardness.

Hardness was measured across the diameter of an 8 mm spot treated by the $CO_2$ laser power beam as illustrated in Figure 6.12. The indents were carried out from the left hand to the right hand side of the circle in a single line.

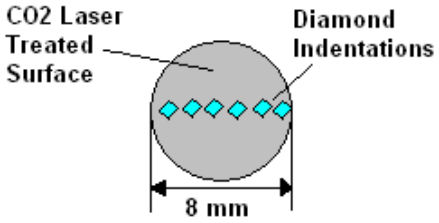


**Figure 6.12: Indentations conducted on the $CO_2$ laser treated surface.**

The hardness profile across the 8 mm spot area illustrated in Figure 6.12 and Figure 6.13 was due to concentration of thermal input in the central core of the treated area causing local softening. The $CO_2$ laser beams were executed as a CW and was acting on the material surface for times ranging from 6 to 22 seconds depending on the laser parameters. The reason for the hardness being low in the centre of the circle has occurred due to a decrease in the radius of the beam path which has caused an increase in thermal input in the centre of the circle, so it has softened the top layer.

As the treated surface was indented across the diameter of the 8mm circle, the hardness was reduced from 1569 Hv (outer edge) to 212 Hv (core). At this point, the indentations only covered half of the treated circle. As further indentations were made, the hardness gradually began to increase from 212 Hv (core) to 1564 Hv (outer edge). This is presented in Table 11.20 Appendix 11.9.2 and Figure 6.13.

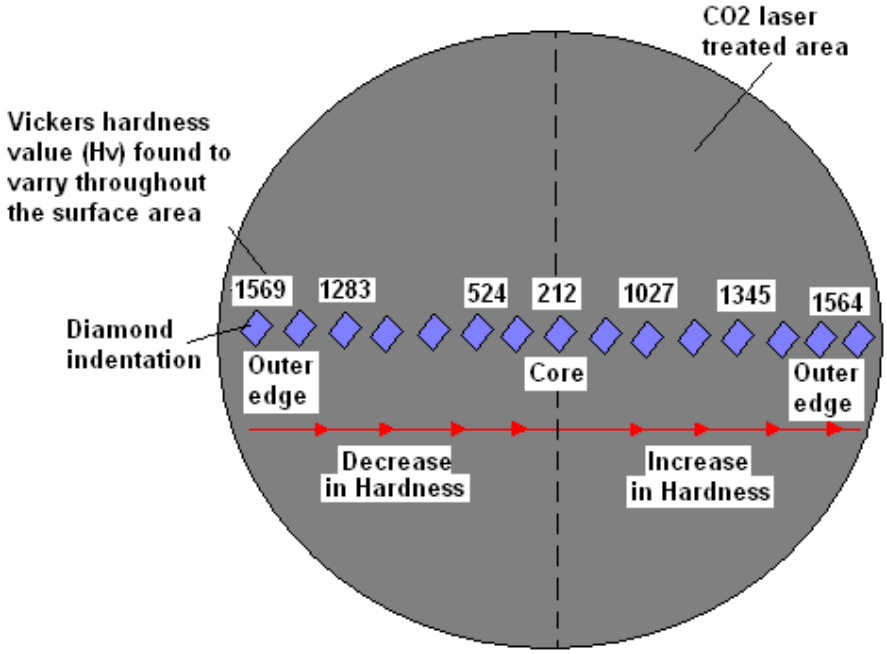


**Figure 6.13: Trend in hardness across the $CO_2$ laser treated surface of the 8mm diameter spot HP $Si_3N_4$.**

### *6.2.1: Crack Lengths*

The measured crack lengths are represented in a graphical format in Figure 6.14. The cracks obtained from $CO_2$ laser treatment were much smaller in comparison with the Nd: YAG treated surface as further illustrated in section 6.4 onwards. This meant that the $CO_2$ laser treated surface became (much more ductile and) resistant to fracture. The cracks were found to be much smaller in the centre part (core) of the 8mm spot which reflects the low hardness value from the Vickers indentation test.

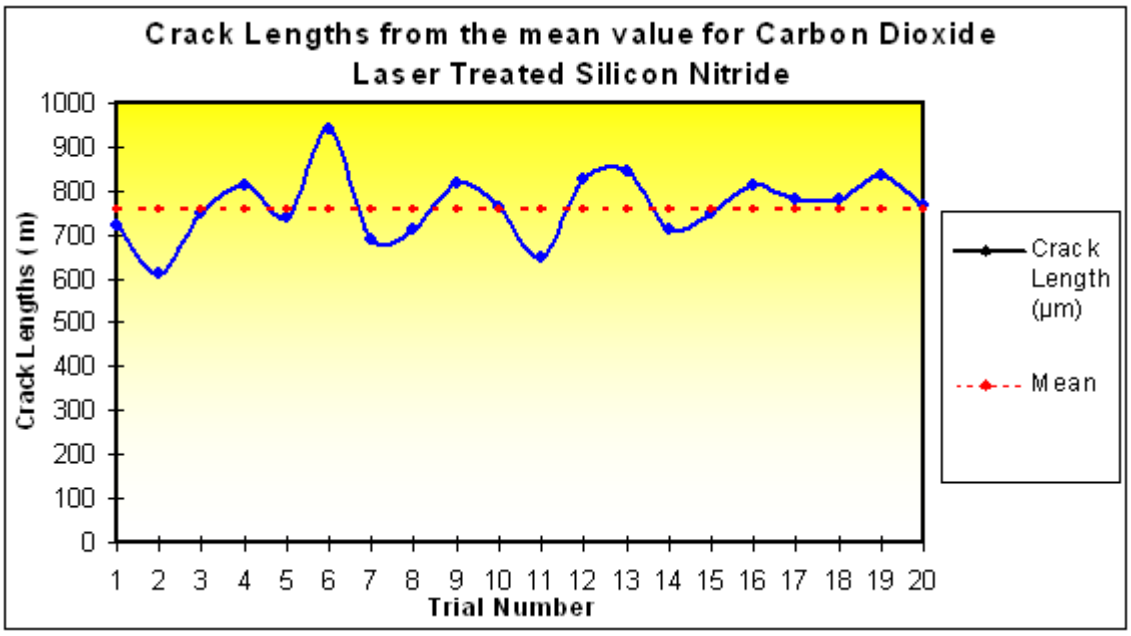


**Figure 6.14: Deviation of the crack lengths from its mean value of $CO_2$ treated $Si_3N_4$.**

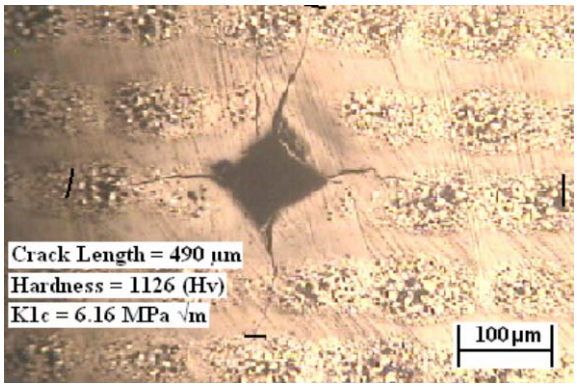


**Figure 6.15: Hardness indentation in HP $Si_3N_4$ and associated cracking. Surface treated at 45 w by $C0_2$ laser.**

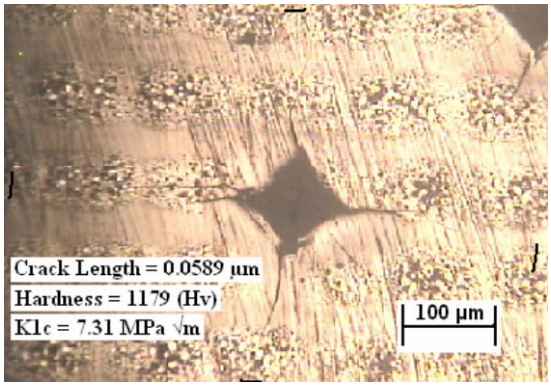


**Figure 6.16: $K_{1c}$, harness and the crack length of HP $Si_3N_4$ at 50 watts of laser power.**

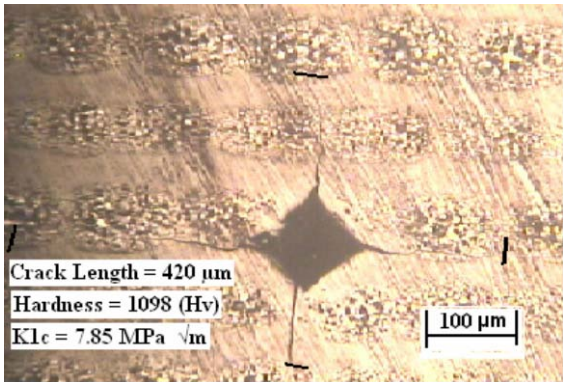


**Figure 6.17: $K_{1c}$, crack length, and the hardness obtained at over 55 watts of laser power.**

### *6.2.2: $K_{1c}$ of $CO_2$ Laser Treatment HP $Si_3N_4$*

| $K_{1c}$ (MPa √m) |
|---|
| 3.91 |
| 4.41 |
| 4.59 |
| 4.39 |
| 5.41 |
| 11.71 |
| 20.85 |
| 28.77 |
| 19.15 |
| 39.98 |
| 18.68 |
| 17.67 |
| 16.27 |
| 12.02 |
| 12.39 |
| 11.31 |
| 11.31 |
| 7.31 |
| 6.75 |
| 4.42 |

**Table 6.1: Calculation of the $K_{1c}$ using equation 10, after $CO_2$ Laser Treatment, 50 kg Vickers indenter load, on $Si_3N_4$.**

**Key:**

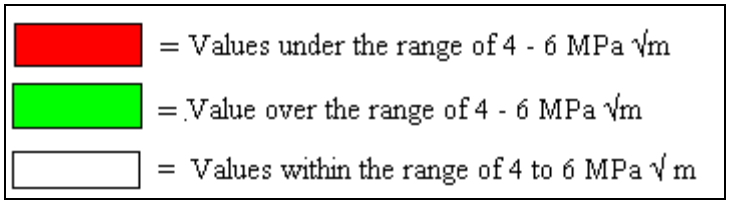


**Note:** The final $K_{1c}$ values were obtained from applying equation 10 (see chapter 5 for further details).

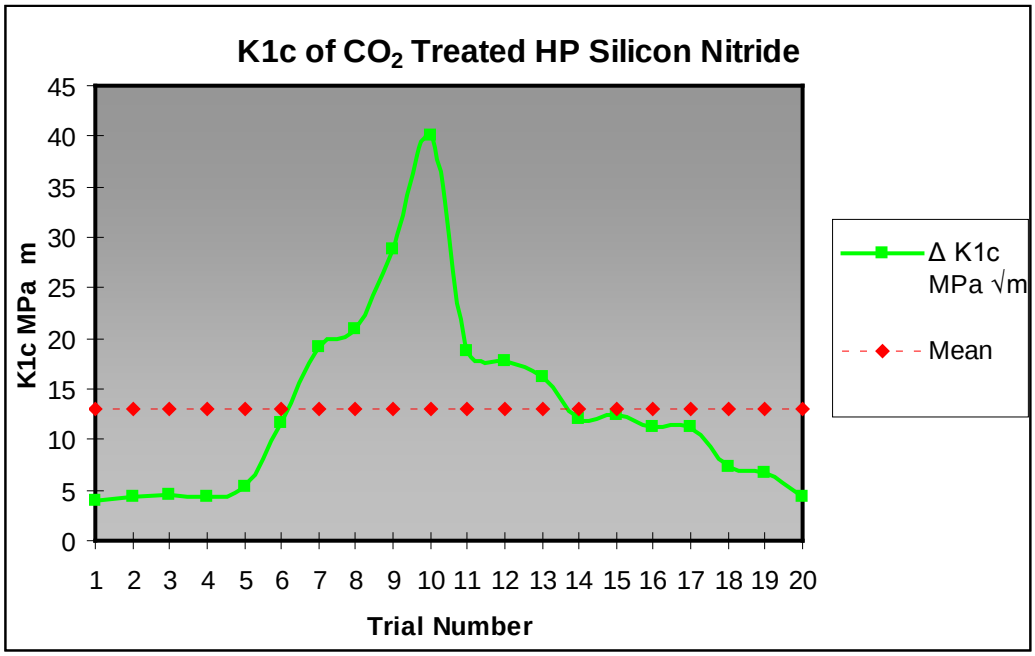


**Figure 6.18: $K_{1c}$ of $CO_2$ laser treated HP $Si_3N_4$.**

The values from Figure 6.18 present the change in hardness of the treated area (using pattern 4) with the spiral pattern in Chapter 4, section 4.3.3 (Figure 4.9). Due to the radius of pattern 4 (Figure 4.6) becoming progressively smaller, as the laser beam traversed in a spiral pattern, the temperature increased. This was because of the build up of heat in a smaller surface area as the radius of the laser path decreased. This consequently, caused the material to become softer however, not up to its melting temperature as there were minimum fumes extracted after the laser beam interaction with the material (initial experiments showed significant fumes extracted with local melting with HP $Si_3N_4$). It was found that the $K_{1c}$ of the (top) surface was enhanced as the hardness reduced and the material became softer. This softening correlates with smaller observed crack sizes from the Vickers indentations. The top layer of the ceramic has become ductile and a phase change that was mentioned in Malshe *et al's* work could have occurred [Malshe 2006]. Local softening of the minor glassy phase occurs at a temperature much below the Tm of the bulk material, although, the surface did not melt. Hence, rebinding and reflowing of the secondary

glassy phase [Malshe 2006] allowed the material to oxidise and transform. This was ideal since melting of the surface was not desired for this work as the material was found to have a rougher surface finish that would have enlarged the porosity and elongated the surface fractures. The surface integrity that was mentioned by Malshe *et al* was not analysed for this work since the SEM was unable to inspect the top surface layer with close range. This was due to the ceramic not able to conduct very well to complete an electrical loop that allowed the current to flow.

It is believed that a compositional change in the material has occurred, hence it could be argued that equation 10 is no longer valid as the equation in [Ponton 1989] is purely designed for $Si_3N_4$ in its original form, rather than oxidised material.

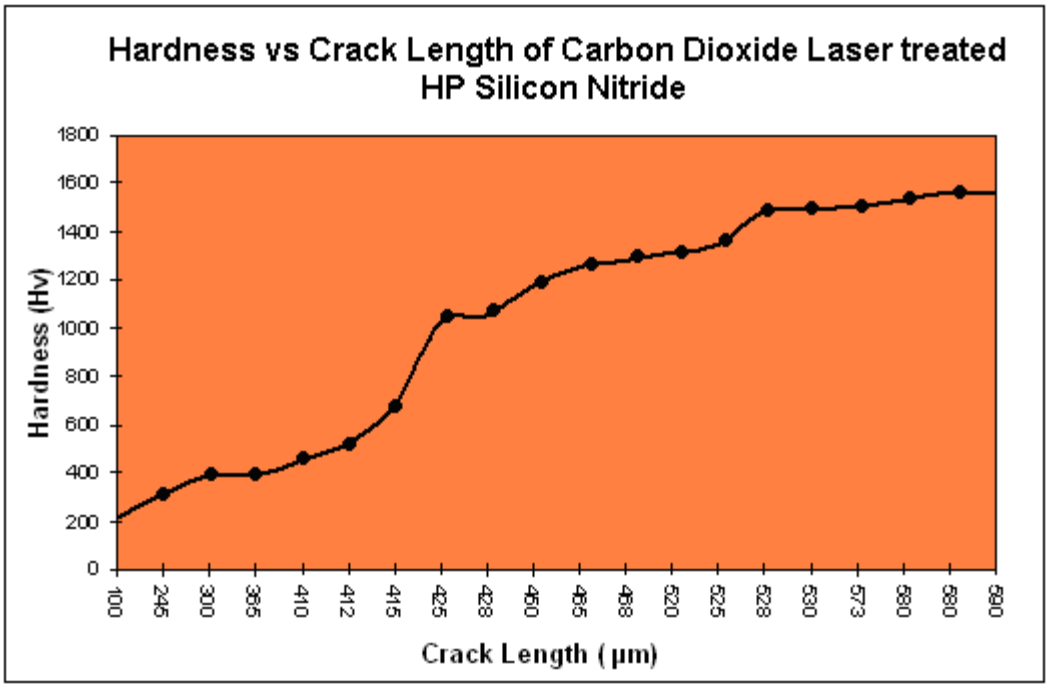


**Figure 6.19: Hardness v/s crack length of $CO_2$ Laser treated HP $Si_3N_4$ at 50 kg load.**

The graph in Figure 6.19 represents the results obtained for hardness v/s the crack length from the $CO_2$ laser treatment of HP $Si_3N_4$. With increasing hardness, the crack length had increased in size. As the load increases, a bigger "foot print" (size) of the diamond indent was observed. (So the resulting crack length for an indentation load of 50 kg on a particular surface with one condition should remain the same). However, change in temperature of the laser treated area had an effect on the surface condition, hence, different hardness values were obtained for the same indentation load. For uniform surface, crack size generated by indentation is directly proportional to the applied load.

It was already known that the flaw size or the crack lengths were found to be longer in size with increasing hardness from the results in Figure 6.19. The crack lengths also contribute to a greater extent in order to increase or decrease the ceramic's $K_{1c.}$ It was also found that the $K_{1c}$ of the HP $Si_3N_4$ tends to decrease as the crack lengths increase in size. Indentation

(associated cracks) size is directly proportional to the hardness. $K_{1c}$ being essentially a quantification of a material resistance to crack propagation is inversely proportional to generate particular crack size.

Increase in the hardness (after treatment) makes the material more brittle but wear resistant. The $K_{1c}$ was reduced due to an increase in the surface hardness. Softer surfaces are ductile; hence the tested material is more resistant to indentation and fracture. Hardness of the material has also influenced a change in the $K_{1c.}$ However, the rate of change of the hardness was not as influential as the crack lengths as the equation relates to these parameters.

## 6.3: $CO_2$ Laser Material Interaction

From the experimental observation(s) it was possible to propose what was happening at the point of interaction between the laser beam and the $Si_3N_4$ surface. The large power density at the focal spot produces high level of local thermal input. The surface did not melt at the point of interaction with the beam; the heat input was assumed between 1500 ºC to 2200ºC [Ponton 1989]. The meting temperature of the $Si_3N_4$ tends to be between 2550 ºC to 2700 ºC (see Appendix 11.5 section B, Table 11.4). This indicated that the temperature must have been below the melting point of the material.

The intense energy heated up the surface layer of the $Si_3N_4$ and produced dimples or fine craters on the surface as presented in Figure 6.20. The heat distributed around the treated area; however, was intense in the centre of the treated circle. As the laser beam stopped, the heat distributed over a larger surface allowing rapid cooling to take place.

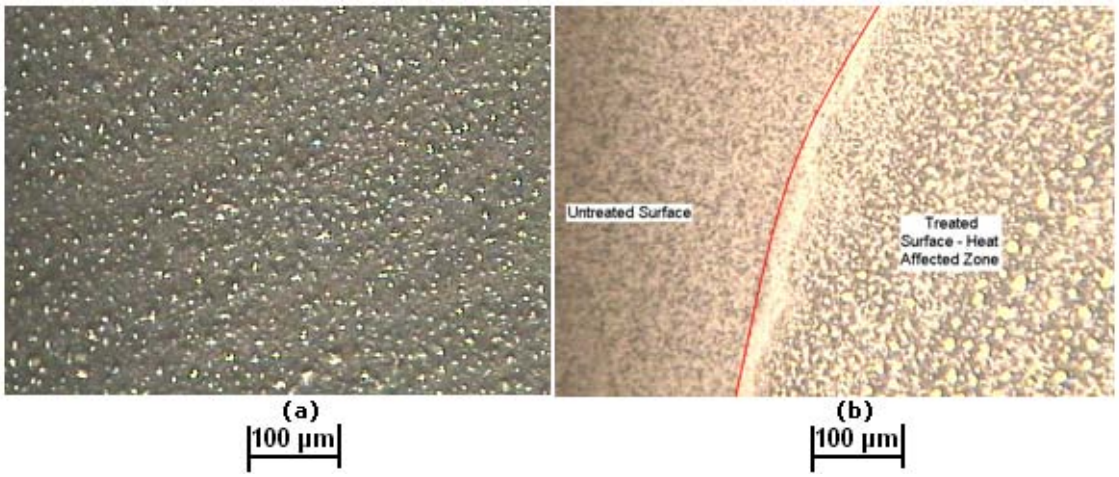


**Figure 6.20: $CO_2$ Laser treated Surface with evidence of dimples small craters by the beam (a) and the difference in the surface integrity between the polished virgin surface and $CO_2$ laser treated surface in (b).**

During $CO_2$ laser processing, the $Si_3N_4$ was exposed to the gases in the atmosphere. Therefore, it was possible that the surface of the $Si_3N_4$ was oxidised which could have

changed the composition of the top layer of the material, oxidation of $Si_3N_4$ results to silicon Dioxide.

The oxidation effect can be avoided if the laser treatment was conducted in a protective atmosphere by adding inert gases such as argon or helium. This was not possible with the low powered $CO_2$ laser marking system since the processing was conducted in a fibre glass shielded environment which could not accommodate for the set up of supplying an inert gas. Therefore, a protective environment was provided with Nd: YAG processing for the experiments that followed as it was technically feasible.

However, $CO_2$ laser treatment has shown an increase the $K_{1c}$ by up to 90 % of the HP $Si_3N_4$ value over 13 MPa √m (values taken from a larger pool of results, see Appendix 11.9), which indicated that the surface oxidation that occurred during processing was desirable in order to increase the $K_{1c}$. This was a consequence of the lesser hardness of the oxide. Surface cracking was not apparent after the $CO_2$ laser treatment. As the laser power was increased, both the degree of material removal also increased, however, the surface cracks appeared to be lesser from the microscopic images for this particular laser beam in comparison with Nd: YAG laser.

## 6.4: Nd: YAG Laser alone experiments

### *6.4.1: Topography*

It was found that the surface of the treated area became much finer as the power intensity of the beam increased. Figure 6.21 illustrates the Ra value of the Nd: YAG treated surface finish. Comparison of Figure 6.21, 6.22, 6.23 revealed that a much finer surface (lower Ra) was obtained after treatment at 575 W compared to that at 550 W. It was predicted that the surface roughness would reduce, as the laser power increased due to the increasing temperature induced into the material having a bigger influence as the input of heat is increased resulting into excessive thermal shocking.

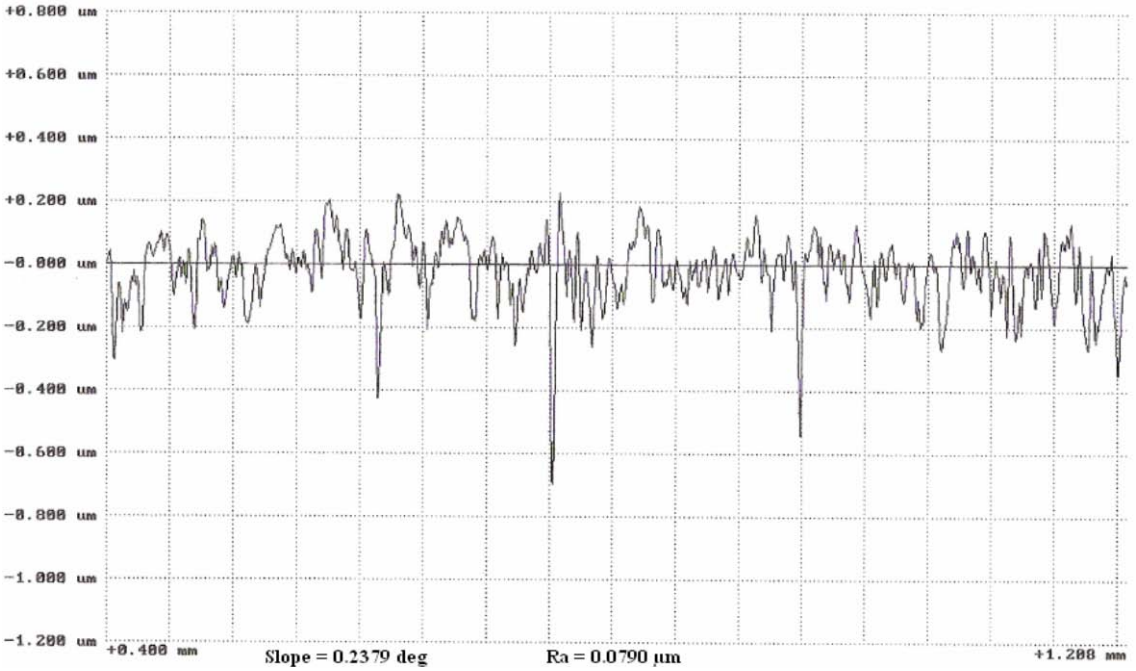


**Figure 6.21: Surface finish of HP $Si_3N_4$ treated by an Nd: YAG laser at 550 watts. The surface roughness is (Ra) 0.07 µm.**

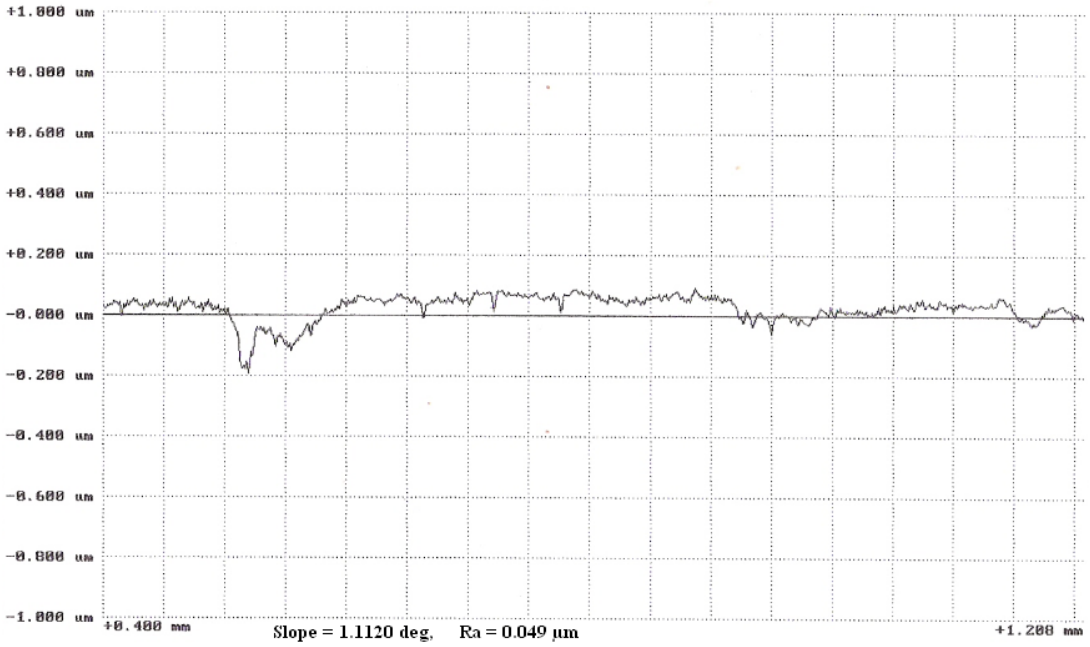


**Figure 6.22: Surface finish of HP $Si_3N_4$ treated by an Nd: YAG laser at 575 watts. The surface roughness is (Ra) 0.049 µm.**

This result in comparison with the virgin (untreated) ground & polished surface and "as machined" surface was much finer since the Nd: YAG laser treatment improved the surface finish from 4.8 µm (as machined) to 0.79µm (ground & polished). This indicated that the micro cracks existed on the surface after grinding and polishing of the virgin surface were minimized to gain a possible improvement in the materials hardness.

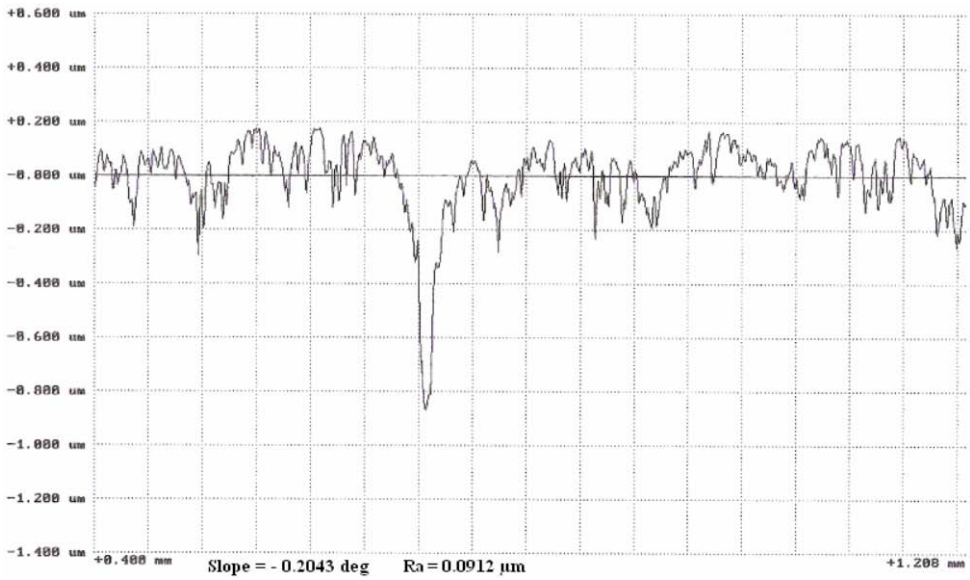


**Figure 6.23: Surface finish of HP $Si_3N_4$ treated by an Nd: YAG laser at 525 watts. The surface roughness is (Ra) 0.09 µm.**

### *6.4.2: Hardness*

Nd: YAG laser alone experiments were conducted using the 2 KW Nd: YAG laser operated in a pulsed mode as described in detail in Chapter 4 (section 4.4). Table 11.29 in Appendix 11.15.5 presents the hardness values found from the Vickers indentation test.

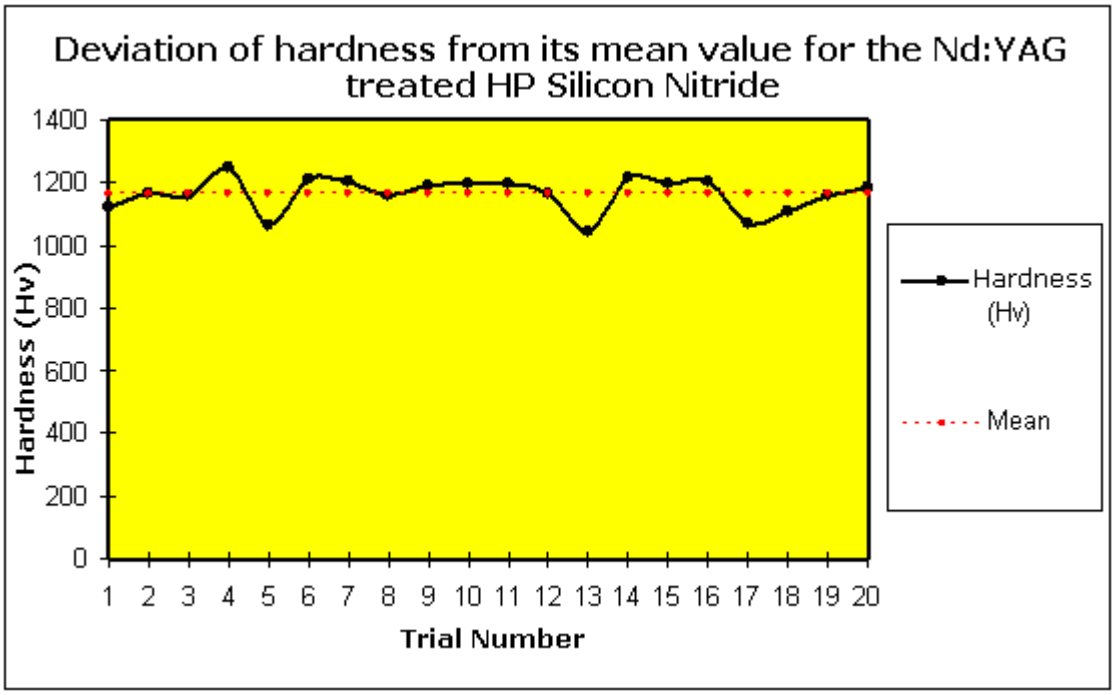


**Figure 6.24: Hardness of the Nd: YAG Laser treated HP $Si_3N_4$.**

Figure 6.24 presents the hardness values of the Nd: YAG laser treated HP $Si_3N_4$, along with the its mean value. When compared with the hardness (Hv) of the virgin surface; the treated surface showed a reduction in hardness. The mean deviation in the hardness was 16 % since the difference between the highest and the lowest value was 119 which was just above the

nominal 10 % "tolerance" (± 116). A possible reason for this is due to the material not being uniform throughout its surface area. The test samples that were obtained from the manufacturer were "as machined" pieces of $Si_3N_4$ with associated surface defects. This also suggests that both the laser beams during the treatment had not evenly penetrated into the surface of the test sample.

### *6.4.3: Analysis of the Crack Lengths*

The average crack length found from 20 samples was 766 µm. In comparison with the $CO_2$ laser treated samples, it was 44 % larger. Variation in the surface topography from the "as machined" material may influence power absorption as the surface asperities project above the focal plane. Variation in the crack length was expected due to the porous and brittle nature of the ceramic which was further complemented by the way in which the Nd: YAG laser beam was delivered (as a pulse/ thermal shock). The material removal with Nd: YAG processing was lower in comparison with the $CO_2$ laser treatment, which justifies the reason for improved surface finish obtained with Nd: YAG laser treatment. The hardness was found to be up to 10 % higher than the $CO_2$ laser treated surface which indicated that the Nd: YAG laser treated surface exhibit lower $K_{1c}$ and produced larger cracks after the treatment in comparison with the $CO_2$ laser processing.

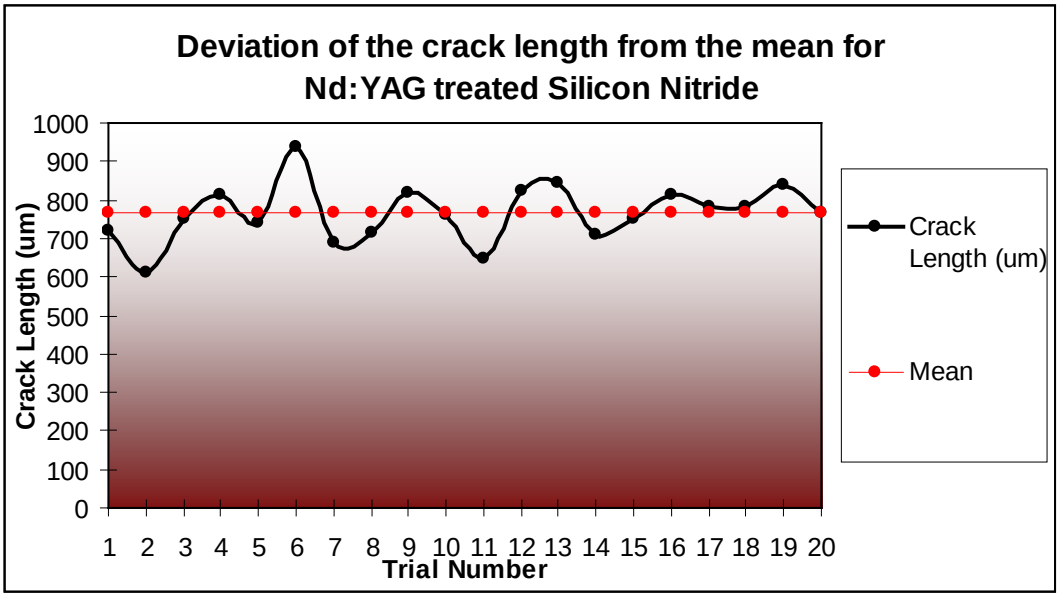


**Figure 6.25: Deviation of the crack lengths from the mean value of $Si_3N_4$, treated by the Nd: YAG laser.**

### *6.4.4: Calculation of $K_{1c}$*

| $K_{1c}$ (MPa √m) |
|---|
| 5.43 |
| 6.81 |
| 5.01 |
| 4.29 |
| 5.32 |
| 3.50 |
| 5.59 |

| |
|---|
| 5.43 |
| 4.36 |
| 4.82 |
| 6.14 |
| 4.42 |
| 4.41 |
| 5.31 |
| 4.93 |
| 4.36 |
| 4.91 |
| 5.29 |
| 4.25 |
| 4.78 |

**Table 6.2: Calculation of the $K_{1c}$ after the Nd: YAG laser treatment using the variable parameters stated in blue (50 kg Vickers indenter load).**

**Key:**

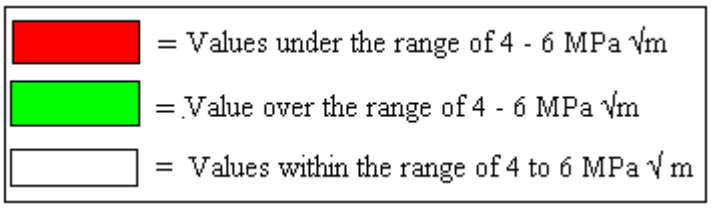


**Note:** The mean value in Figure 6.26 differs from the values presented in Appendix 11.11 since the results come from a bigger pool of data.

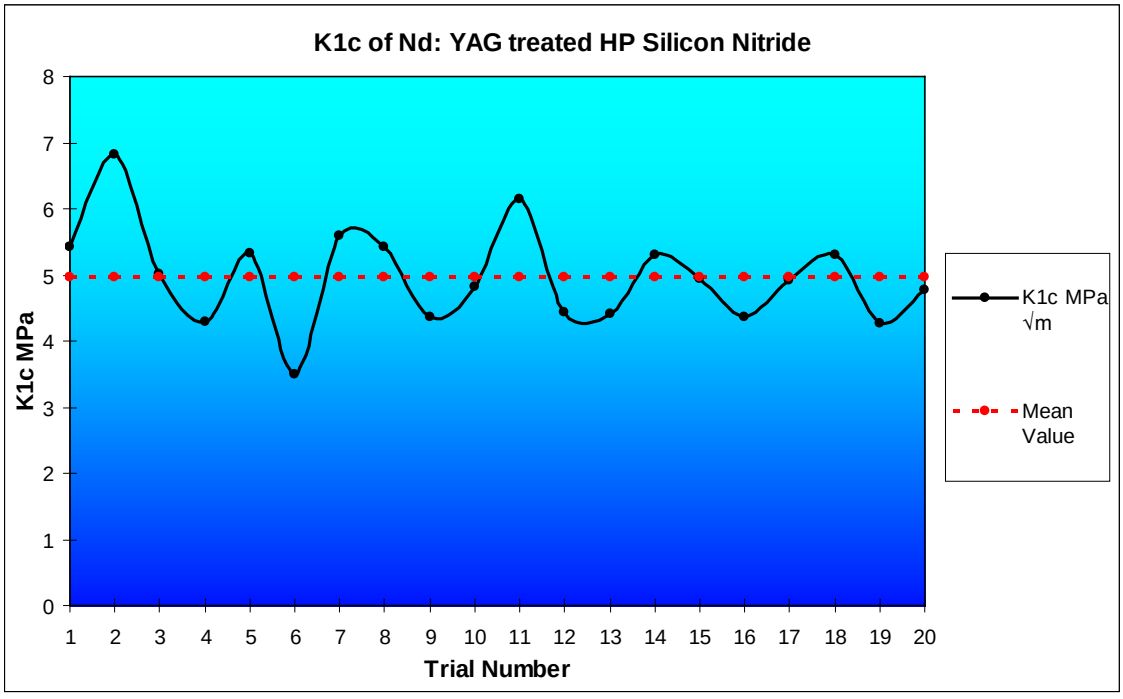


**Figure 6.26: $K_{1c}$ of Nd: YAG treated HP $Si_3N_4$.**

The average $K_{1c}$ from 20 indentations was found to be 4.97 MPa√m . As previously mentioned; the value of $K_{1c}$ was dependant on two major parameters (crack length (µm), and Hardness (Hv)) from equation 10 in chapter 5 [Ponton 1989]. Those two parameters are the crack length (flaw size) and the input of the harness value into the equation. This means

that the change in hardness results to a variation with the length of the cracks produced. For example, increase in the materials hardness will result in the material being much more brittle. Hence, the produce crack length from the Vickers indentation will also increase.

The Nd: YAG laser pulsing led to a local rapid cooling effect, producing a temperature gradient between just treated and as yet untreated zone. The untreated zone was at an ambient temperature, the input of heat expands the material which led to opening of a crack. Temporal pulsing the Nd: YAG generates thermal gradient between just treated and as yet un-treated material. Cooling of the $CO_2$ laser treated area was much slower in comparison with the Nd: YAG laser treatment which allowed the material to soften due to slower cooling and inhibiting surface cracks from developing. This did not occur in the same way with the Nd: YAG laser as surface cracking was developed after the laser processing.

Increase in hardness resulted in an increase in the crack length which then resulted to a reduction in the final $K_{1c}$ value. With increasing hardness, the material became brittle and its resistance to fractures became lower than the softer material surfaces. The fluctuation on the graph may have occurred from inaccurate measurements made from the method used (see Chapter 5). Crack size measurements were taken from scales that were printed and measured against the printed image of the crack length. Often it was difficult to identify the crack tip from the printed images; hence, it could have led to perform an inaccurate reading of the cracks. The accuracy of the result was purely dependant on the visual ability of the human eye.

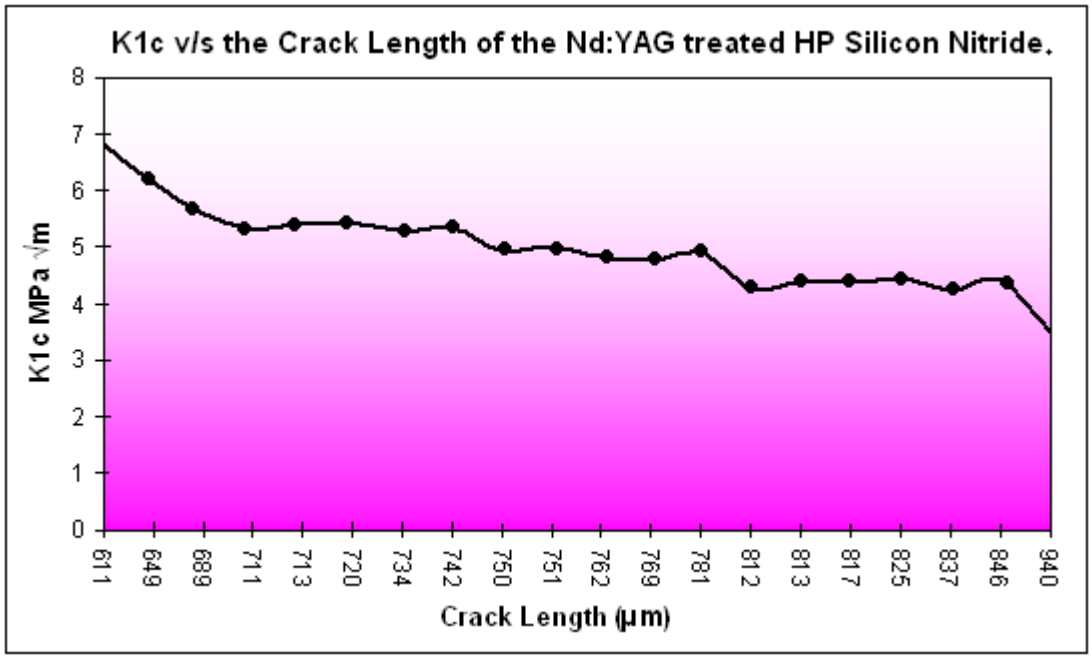


**Figure 6.27: $K_{1c}$ v/s Crack length relationship of Nd: YAG treated HP $Si_3N_4$.**

Longer cracks correspond to lower $K_{1c}$ value (Figure 6.27). This was in agreement with related results from $CO_2$ laser processing and indicated that the longer the crack length the lower the materials resistance to fracture. The average $K_{1c}$ value over 20 samples was also

much lower for Nd: YAG processing in comparison with the $CO_2$ processing. Change in the crack length by ± 100 µm can affect the $K_{1c}$ value ± 1.78 MPa √m.

Change in the materials hardness could also influence the final $K_{1c}$ value as revealed by equation 10. However, the change has to be of a high magnitude in order to have a major effect on the material's $K_{1c}$. For example, increase or decrease in the hardness value by ±100 Hv can change the final value of $K_{1c}$ by ± 0.25 MPa √m. As the hardness increases, there was not a significant change in the materials $K_{1c}$. However, fluctuation on the graph occurred due to the small variations in the results. Fluctuation in the $K_{1c}$ occurred due to the change in the crack length rather than a major change in the hardness. The nominal variation in hardness corresponds to a ± 1 MPa √m, fluctuations in the calculated values.

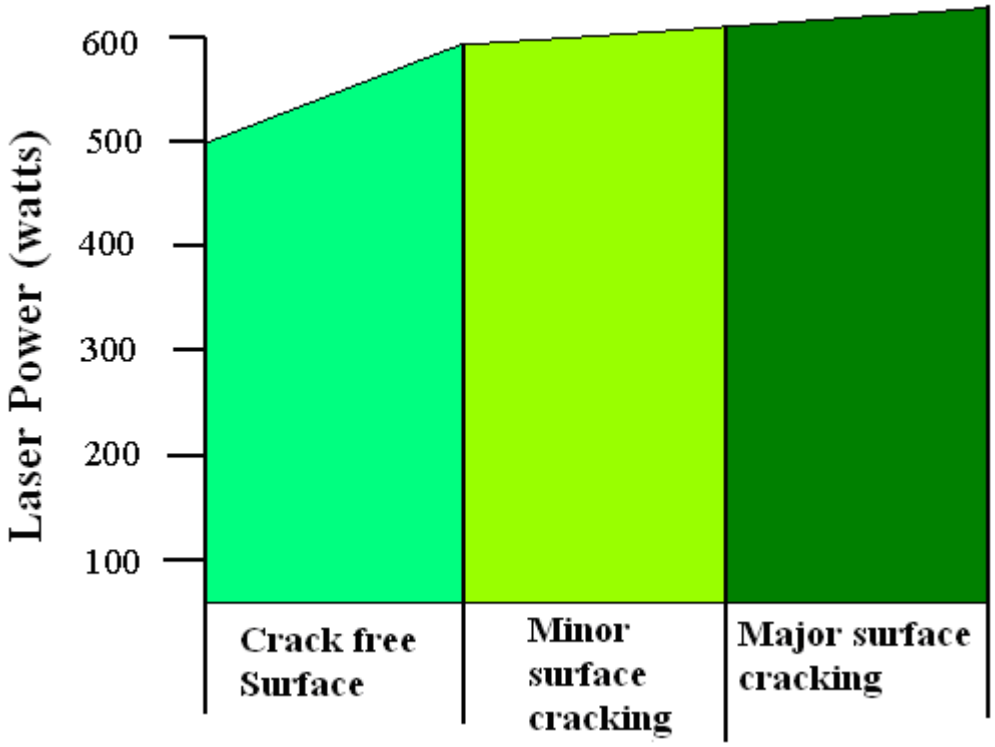


**6.28: Occurrence of surface cracks with increasing laser power on $Si_3N_4$ after Nd: YAG laser treatment.**

As the laser power increased, surface cracking levels also began to rise (illustrated in Figure 6.28). This was attributed to the rapid thermal shock produced by the Nd: YAG laser beam. The higher the power, the more energy was induced into the material, allowing the micro porosity and micro cracks to open as a consequence of local thermally induced expansion.

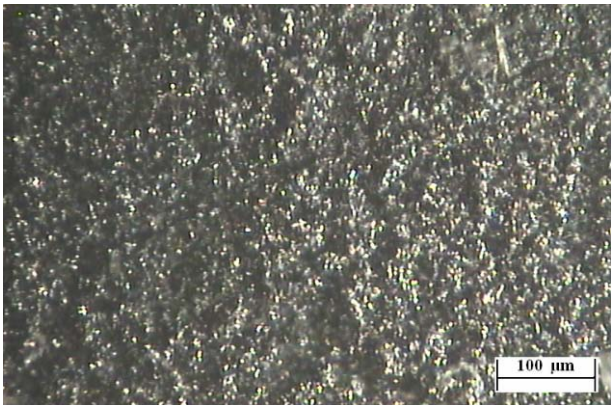


**Figure 6.29: Nd: YAG laser treated surface at 575 watts of laser power.**

Surface cracking was at minimum up to laser power of 575 W as presented in Figure 6.29. Beyond this point, large surface cracks began to appear as presented in Figure 6.30, cracks having developed from the centre of the fired laser spot. There was also a change in the colour of the material which reflected the localised heat induced into the material surface as illustrated in Figure 6.30 and the at the bottom of Figure 6.31. Figure 6.31 also presents an image of an indented surface by a Vickers diamond indentation test.

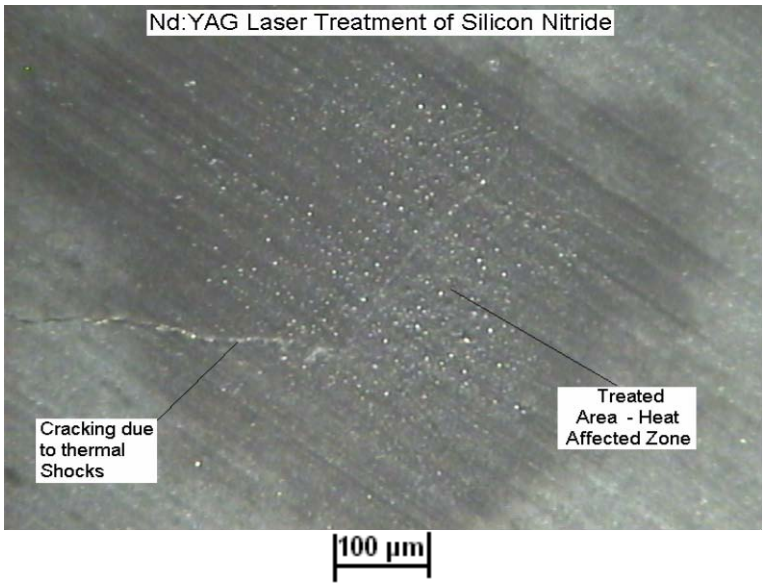


**Figure 6.30: Nd: YAG Laser treatment of $Si_3N_4$ at 600 watts of laser power.**

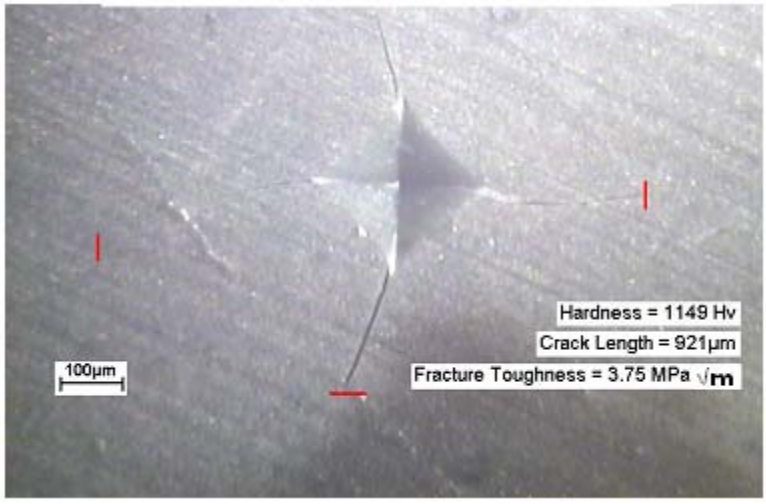


**Figure 6.31: Example of the hardness value, crack length and $K_{1c}$ obtained from an Nd: YAG laser treated surface at 600 watts of laser power.**

## 6.5: Nd: YAG Plasma pilot arc experiments

It was not possible to perform the plasma augmented laser processing (PALP) as a hybrid process. The work-piece therefore, was required to pass the electric current in order to complete the circuit. Despite $Si_3N_4$ having a degree of electrical conductivity; the current was not able to pass through. The test samples were then cleaned with acetylene prior to testing and still failed to conduct. Due to limited testing time available; these set of trials were not further investigated.

As an alternative, plasma arc laser processing was conducted and functioned successfully. As mentioned in Chapter 4, a non-transferred low current pilot arc, along with the laser beam pulsing for 10 ms was applied. From the optical microscopy, it was found that the surface cracks were minimised in comparison with the laser alone treatment at same laser power density. However, cracking began to appear beyond 580 W of laser power, where the laser beam has produced a thermal shock which led to crack propagation, further complemented by the extra heat input of the plasma pilot arc. Figure 6.32 illustrates a crack-free surface, treated at 550 W of laser power where it can be seen that the black areas are the HAZ's from the incident laser beam. In order to justify the laser material interaction, and SEM image or and EDX (Energy Dispersive X-Ray) analysis would have been more suitable rather than the optical microscopy.

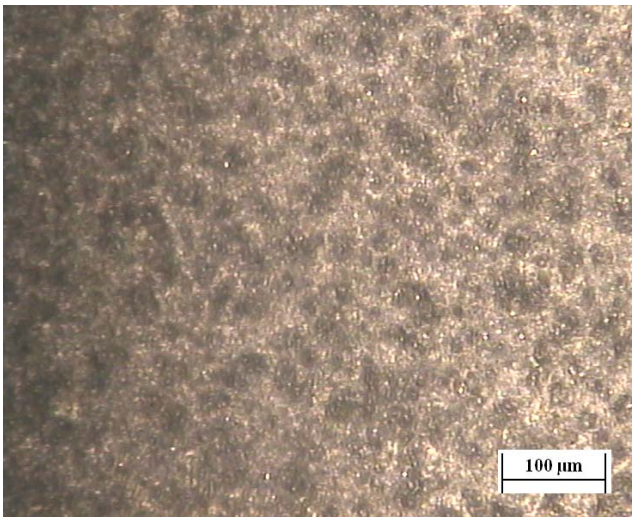


**Figure 6.32: Example of the Nd: YAG treated surface of the HP $Si_3N_4$, treated at 550 watts of laser power.**

### *6.5.1: Nd: YAG Laser and material Interaction*

The beam mode of the Nd: YAG laser was "Top Hat" due to fibre optic beam transmission. As the beam interacted with the material, some part of the beam reflected whilst some portion was absorbed. Absorption of the laser beam differs with a material composition. As the beam was absorbed there was an input of heat which produced vaporisation indicating that the ceramic has melted. Hence, the temperature of the material was assumed to be about 2300 ºC since the melting point of the $Si_3N_4$ is between 2300 and 2500 ºC [CES 2007]. The temperature was dependant on the pulse conditions. The longer the duty cycle meant that the input of heat at the material surface was also much higher.

During this phase, the pulsed beam induced high power density into a small surface area of the material. This caused expansion of the heat affected zone (HAZ) as illustrated in Figure 6.33. However, the surrounding material surface was much cooler (possibly at ambient temperature) which inhibited the HAZ expansion. The HAZ subsequently contracts due to rapid cooling. Due to the difference in the temperature between the HAZ and the surrounding surface; there was tension and compression induced alternatively. HAZ heats up tries to expand, however, it is restricted by cool bulk material (compressive stress). When the HAZ cools and contracts; it is restricted by the bulk material (tensile stress).

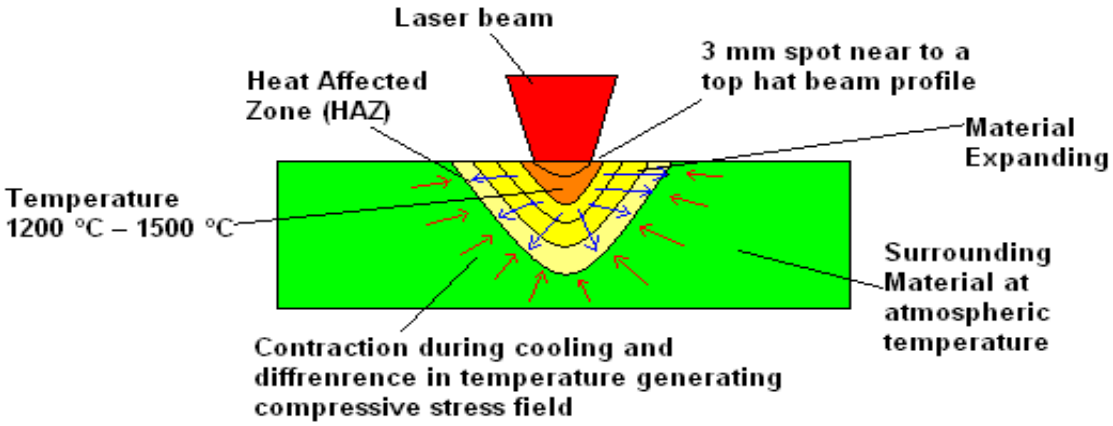


**Figure 6.33: Nd: YAG Laser Material Interaction.**

## 6.6: Variable Effects with Processing Gases

### *6.6.1: Types of Shield gases and their effects*

Typical gases that are used for laser processing are Argon, helium, nitrogen, oxygen or air which could potentially have a mixture of carbon dioxide and oxygen. Each of the gas types will have a different effect on the material surface. The choice of a shield gas is dependant on the desired treatment to be conducted along with the type of material. Most suitable gases that are regularly applied with ceramic processing are argon, helium and nitrogen. This is because the three gases mentioned are inert and aid to keep the ceramic material from changing its composition by oxidizing. Although, oxidation cannot be completely avoided by using the three inert gases mentioned during laser processing particularly in ambient atmosphere. However, oxidation can be avoided if processing was conducted in a vacuum chamber. Processing with air and oxygen is not very ideal as its effect would be much greater to the ceramic. As the oxygen is absorbed into the material surface, the effect of oxidation can occur to a greater limit as the material composition would change for example (Silicon Nitride changing to Silicon Oxide, Silicon nitroxide or potentially Silicon Dioxide). This is dependant on the content of gases existing in the atmosphere and their ionisation with the material.

The shield gas effects the processing by separating the keyhole particularly with welding applications, however, with ceramics the shield gas aids to control the level of oxidation being produced with the laser/ material and the atmospheric interaction. The shroud gas can generate a plasma plum at the material surface and in most cases also aids the material to absorb the laser beam much better, depending on the processing temperature and the ionization of the particular gas used.

### *6.6.2: Nozzle type and diameter and gas pressure*

The type of nozzle to use is dependant on the desired laser process and the work piece or the material being processed. For example a welding process requires a thicker beam which aids to distribute the laser energy and the weld joints to melt and adhere together.

Therefore, a larger diameter nozzle is desirable. A cutting process requires a finer beam, hence, a smaller diameter nozzle is chosen. A welding nozzle is equally desirable with surface treatment of ceramics. This is because a finer beam diameter is more ideal for cutting and will result into producing a cut line rather than only penetrating into the top layer of the ceramic. This could potentially produce a keyhole or a melt pool if the material has not already vaporised prior to generating the keyhole or the melt pool.

Therefore, the diameter of the nozzle controls the gas pressure and the gas flow rate. The smaller the diameter, the higher the pressure. Appropriate pressure is required to drive the plasma away from the laser head and the focusing unit and to protect the weld from the influence of the gas which could potentially result into the material being changed to a new composition. During the cutting process, high pressures are required to cut through the material. For welding and surface treatment applications, the pressure is required to be controlled to a lower flow rate which will assist with achieving a specific penetration, absorption and in case of ceramics; a possible phase transformation.

Variation in the gas pressure of the processing gas, could result into many differing effects. The shroud gas along with the laser material interaction during laser processing can lead to a build up of a plume. This plum can often stop the laser beam from providing a full coverage if it is not delivered to the correct pressure. Particularly with ceramics it can blow away a lot of debris from the material surface which results into a rougher finish and a potential propagation of surface cracks.

## 6.7: Chapter Summary

Table 6.3 justifies the outcome from analysing the application of each energy source to the $Si_3N_4$ in particular as it was the main material investigated. The table justifies the most successful energy beam from the investigations performed. As previously described in the discussion; both Nd: YAG hybrid with plasma arc and ultrasonic surface treatments were unsuccessful due to technical reasons. The plasma arc failed to function due to constraints with transferring the electrical current as the $Si_3N_4$ test samples failed to electrically conduct. The ultrasonic treatment was not thoroughly investigated to produce any useful results. Details of the ultrasonic treatment are presented in Appendix 11.7 section C.

| Contact- less Surface Treatments | Average Hardness (Hv) | Average Crack length after Vickers indentation (µm) | Average $K_{1c}$ (MPa √m) | Surface Finish (µm) | Appearance of cracks after treatment |
|---|---|---|---|---|---|
| **$CO_2$ Laser** | 1029 | 431.21 | 15.18 | 0.5812 | No Cracks |
| **Nd: YAG Laser alone and pilot arc** | 1161 | 765. 28 | 7.12 | 0.049 | 575 watts |
| **Nd: YAG Plasma augmented treatment** | N/A | N/A | N/A | N/A | N/A |
| **Ultrasonics Surface Treatment** | No Change | N/A | N/A | N/A | No Change to the surface. |

**Table 6.3: Difference in the results after applying the non-contact energy beams to the $Si_3N_4$.**

Comparing the $CO_2$ and the Nd: YAG laser sources; it can be stated that the $CO_2$ laser treatment performed better and was more successful from the two when observed from a view point of obtaining a higher $K_{1c}$ value. This was due to the fact that the $CO_2$ laser treatment reduced the hardness of the material and created a more ductile surface. Due to this; the cracks obtained from the Vickers indentation test were found to be shorter than the cracks obtained for the Nd: YAG laser treatment. Also, the surface cracks after treatment obtained from the Nd: YAG laser beam were not observed with the $CO_2$ laser beam. It was confirmed from observing the crack profile (Figure 6.15, 6.16, 6.17, 6.28, 6.30 and 6.31) for $CO_2$ and Nd: YAG treatment, that the cracks found were of half-penny median cracks (due to the high indenter load applied on the tested samples as stated in [Ponton 1989] and presented in Figure 3.4).

Despite the experimental conditions being the same for both materials, there were differences between the features of the two laser systems used which to an extent does not allow a true comparison of the results to be made. The differences perform as the reasons for the unfair comparison of the two systems and are stated as follows:

- The operating wavelengths of the two lasers being 10.6 µm for the $CO_2$ and 1.06 µm for an Nd: YAG laser. This indicates that the beam quality of the $CO_2$ laser is much superior in comparison with the Nd: YAG laser. This also means that there is significant heat going into the material due to the higher wavelength applied as well as more heat into the material than that of the Nd: YAG laser.

- The operating conditions of the two laser were also different as the $CO_2$ laser was executed with a CW beam and the Nd: YAG laser being executed with a pulsed beam. This also changed the time that the laser beam was acting on the material, since the pulsed beam from the Nd: YAG laser operated in ms and in comparison the $CO_2$ laser operated in seconds (spending longer time on the material surface). This also justifies the high temperature of heat being induced into the material by the $CO_2$ laser.

- The difference in the beam delivery system also had an effect on the results. This is another reason why a fair comparison cannot be made between the two systems. The $CO_2$ laser is delivered with a right angle beam delivery system and has a much finer spot size as it is precisely focused by the galvanometers and the optical lens (allowing a higher power density being focused on a smaller spot size in comparison with the Nd: YAG laser). The Nd: YAG laser is also transported by a 3 mm fibre cable and is therefore much bigger in diameter and comprises of the power density being focused on a larger surface area.

The above features therefore do not allow an equal comparison of the systems used, to a greater extent due to the differences in their features that changed the outcome of the experiments conducted.

## 7.0: Conclusion

Conventional shot peening is used to generate compressive surface residual stresses that enhance fatigue resistance in metallic materials. This is equally performed by using a laser beam with a great effectiveness with metals in particular. The principle is not valid and does not comply with respect to ceramic processing since the material does not tolerate plastic deformation. However, this work has established that laser treatment of ceramics (HP $Si_3N_4$ in particular) could be viable in order to improve the materials Fracture Toughness ($K_{1c}$). This was associated with softening the top layer, redistribution of glassy phase in the surface that feature cracks and possibly changing the materials composition which reduced the hardness of the material allowing a resistance towards indentation and cracking.

Comparison of the virgin ground and polished surfaces with the unpolished (virgin, "as machined) surface showed that the hardness was increased by up to an average of 18 % for the ground and polished surface of the HP $Si_3N_4$. This occurred due to grinding and polishing (progressive material removal) and minimisation of the existing surface flaws from machining that acted as tensile stress raisers. The length of the cracks obtained from the Vickers indentation tests were found up to 20 % longer for the virgin "as machined" surface in comparison with the ground and polished surface. Surface finish was enhanced for the ground and polished virgin surface (Ra = 0.07 µm) and untreated virgin surface being 4.82 µm. The $K_{1c}$ for the ground polished surface of HP $Si_3N_4$ was also improved by an average of over 30 % in comparison with the virgin as machined surface.

Surface treatment of HP $Si_3N_4$ using the $CO_2$ laser decreased the hardness by an average of up to 35 %. It is proposed that the build up of heat was softening the top surface layer of the material. This also led to surface oxidation which appeared to be ideal for enhancing the $K_{1c}$ as the composition of the material could have changed from $Si_3N_4$ to silicon oxide and a mixture of silicon dioxide. Best results were obtained using pattern 4 and laser power of 20 watts as the surface appeared to be "crack free" and the highest $K_{1c}$ value was obtained from a ductile surface.

$CO_2$ laser treatment increased the mean $K_{1c}$ from an average of 4.27 MPa$\sqrt{m}$ (virgin surface) to an average of over 13 MPa $\sqrt{m}$. Due to localised re-distribution and material removal during $CO_2$ processing; the surface condition obtained from ground and polished was lost and was measured to be 0.58 µm which was much rougher than the one produced by the Nd: YAG laser beam. However, the cracks were found to be longer with Nd: YAG laser due to thermal shocking where the laser beam acted as a sharp hot nail (hot rod) expanding the existing surface flaws.

According to the equation; a fluctuation in the crack length by 100 µm has led to a difference of 1.78 MPa $\sqrt{m}$ in the materials $K_{1c}$ and a fluctuation in hardness value by 100 Hv has a

difference of only 0.25 MPa√m. This shows that the hardness was not a very influential parameter to the final $K_{1c}$ value in comparison with the crack length.

Nd: YAG laser treatment of HP $Si_3N_4$ was found to decrease the hardness by an average of 27 % and increased the average crack length by 50 % when compared to the untreated ground and polished virgin surface. However, it was found that the HP $Si_3N_4$ surface, treated by the ND: YAG laser was very porous. It was believed that this occurred due to the rapid pulsing generated by the Nd: YAG laser where the peak power of up to 600 W was achieved in a very short period of time. Localised thermal input due to beam absorption by the surface produced rapid cooling locally to the bulk material acting as a heat sunk. This led the porosity within the HP $Si_3N_4$ to expand and become prone to cracking as the localised heat from the laser beam escaped during the rapid cooling of the treated material.

The Nd: YAG treatment of HP $Si_3N_4$ samples showed an increase in the $K_{1c}$ by 0.88 MPa √m in comparison with the virgin ground and polished surface and an average of 2.36 MPa √m increase in comparison with "as machined" surface. The average $K_{1c}$ value of the Nd: YAG treated HP $Si_3N_4$ samples was 7.12 MPa√m. The optimum power parameter window was between 550 W to 575 W; as the surface displayed an absence of cracking within this range.

Surface roughness was also enhanced after the Nd: YAG laser treatment. However, thermal shocking from the pulsed beam input generates local differential thermal expansions and contractions within the bulk material which accelerate micro cracking.

The plasma (pilot) arc reduced the effect of surface cracking due to the additional input of heat which minimised the effect of rapid cooling associated with the pulsed laser beam. This minimised local surface rapid expansion and contraction as the pilot arc was acting on the material continuously during the pulsing of the laser beam.

Enhancement in the $K_{1c}$ could allow the material to be used for many more demanding applications in both automotive and aerospace sectors. Despite being a surface treatment process, the $CO_2$ laser was more successful in comparison with the Nd: YAG laser for improving the materials $K_{1c}$. Although further work should be conducted using either an Nd: YAG laser or preferably an industrial Nd: YLF laser applicable to the engineering ceramics.

## 8.0: Recommendation for Future Work

Due to lack of availability of X – ray diffraction equipment; residual stress was not calculated for the laser treated $Si_3N_4$. Therefore, it was not possible to investigate if the material was under tension or compression.

Viewing the ceramic samples under the SEM was a problem, this occurred due to the samples failing to charge in order to form an electrical circuit which affected the image quality. This problem can be eliminated by coating the sample surface with a thin layer of gold which is a highly conductive material and could improve the image quality. It was not possible to carry out this procedure due to time constraints. To overcome this issue, samples were cleaned with methane and acetylene, however, the image quality was poor, and hence, it is very important to coat the samples in a fine gold layer if the investigation was to be carried out again for further development.

It is also recommended that the depth of penetration of ceramic is investigated, since it was not possible with unavailability of a diamond cutter to section the ceramic samples in half, in order to observe the depth of penetration. From conducting this investigation, it would be helpful to establish how deep and wide the laser beam has penetrated into the material.

Limited experiments were carried out with $ZrO_2$ (not mentioned in the main body of the thesis) ceramics since there was minimum availability of the material. It would be interesting to investigate the effective result of varying the parameters has on the $K_{1c}$. Trials on $ZrO_2$ induced excessive input of laser power into the material which produced the surface cracks. The cracks could be minimised by controlling the power density and the amount of material removal from the surface. It would also be interesting to discover how the material behaves under Vickers indentation test and what range of $K_{1c}$ value is obtained since $ZrO_2$ could absorb the laser energy well.

“As machined” test samples showed of variation in their surface roughness after grinding and polishing. The grinding and polishing was conducted for equal time span, however, due to their initial condition not being identical to each other; the polished samples comprised of variations in its Ra value. This resulted in the material surface having small and large surface flaws in different areas which then led to variation in the hardness (obtained from conducting the Vickers indentation test), crack length and $K_{1c}$. If the test samples were polished to an equal Ra value rather than equal time span, there could be a possibility of improving the results.

The $Si_3N_4$ tested samples failed to conduct the electrical current when placed under the SEM. It was therefore, required that every sample is coated with gold since it is a good electrical

conductor. It was not possible to coat the samples in gold due to the time constraints and availability of equipment for this work.

Trials could also be conducted on $Si_3N_4$ using the conventional shot peening technology. The results then could be compared with the laser treated samples. A comparison of the residual stress induced, surface finish and Vickers indentation test using both surface conditions could be performed. Comparison of the materials $K_{1c}$ should also be conducted in order to investigate if there is a difference between the surface conditions. This particular task was not performed due to unavailability of the conventional shot peening machinery within the university to carryout the trials and due to cost issues (if it was to be done by job shops or a sub-contractor).

Experimental work could be conducted using the Holographic Diffractive Optical Elements (HDOE) which could be complemented with both of the laser system used for this work. HDOE are computer generated holographic optical elements which replace the conventional lenses and converge with the beam delivery system in order to control the shape, size and the end profile of the active laser beam [Kell 2006]. HDOE could be made to transform into a "top hat" "ruby post" or a "peaked edge line" as presented in Figure 7.1. The difference between a Gaussian beam and a HDOE beam is controllability to a desired shape and still keeping the same area of the beam distribution. Surface treatment using circular beam is produced by the Gaussian beam mode $TEM_{00}$. This was because it ideally replicated the conventional shot peening process. The interesting issue is the effect which it has on the material surface such as the depth and width of penetration as well as the thermal stress induced into the material surface.

**(a) (b) (c) (d)**

**Figure 7.1: Distribution of various laser beam profiles (a) Gaussian beam, (b) "top hat", (c) "Rugby post" (DOE), (d) peak edge line (DOE) [Kell 2006].**

A diffractive Optical Element (DOE) is a small mirror which consist of thousands of 6 µm squares that are set below the surface at various submicron depths [Kell 2006]. As the raw beam of 20 mm diameter is fired at the DOE, the mirrors execute a particular wave. The waves then combine and interfere with each other to generate a premeditated beam shape. HDOE are placed into the beam delivery system as shown in Figure 7.2.

**(a)** **(b)**

**Figure 7.2: (a) Beam delivery system for Gaussian beam and (b) Holographic Diffractive Optical Elements [Kell 2006].**

HDOE offer advantages such as large focal depth in comparison with the conventional lenses, hence, the working distance automatically becomes less critical. Conventional lenses require regular maintenance. This is not required with HDOE if it is well protected from fumes and dust. HDOE also reduces the amount of moving parts required such as galvanometers within the $CO_2$ laser systems as well as the flexibility to shape the beam. It is ideal for the surface treatment applications since it allows the motion system to traverse around the part at high speed and flexibility and a sufficient depth of penetration. The more surface area that is covered by the laser pulse (shock) would reduce the cost of the operation as the process time of the treatment is reduced. This is more beneficial especially when processing larger parts.

# 9.0: References

Advance Joining Centre [*c.* October 2006] *Plasma Augmented Laser Processing* Coventry: Coventry University Press

Ahn. Chandrasekhar, Y. Farris, S. (1996) 'Determination of surface residual stress in machined ceramics using indentation fracture'. *Journal of manufacturing science and engineering* Vol 118, p483-489

Altenburger, I. (2002a) 'Alternative Mechanical surface treatment micro residual stress & fatigue behaviour'. 10th Conference on shot peening France, p 150

Altenberger, I. Noster, V. (2002b) 'High Temperature, fatigue of mechanical surface treated materials'. *10th conference on shot Peening, France n*. vol, P 206

Blundell, B. Bifiin, Johnson, T. J. Page, C. (1998) 'High Speed Augmented – Laser Welding of thin sheet metals'. *5th International conference on the trends in welding research*, PP 483- 487

Bryden, B. (2002) 'High power diode, laser transmission welding'. *Assembly Automation* Vol 20, (No 2) P136 – 139

Braisted, W. Brockman. R, (1998) 'Finite Element of Laser Shock Peening', *International journal of fatigue* V 21, p 719 – 724

British Standards (2005) 'Vickers Hardness Test- Part 2- Verification and Calibration of testing Machines'. *Metallic Materials - ISO 6507-1 n.* Vol, *n.* pp

Bush, G. J. Almen, O. Danse, A. Heiss, J. (1962) 'How, when and whom was Mechanical Prestressing Discovered'. *SAE Division XX Presentation,* P 11 [online] available from <http://www.shotpeener.com/library/tsp_articles.php>[1962]

Charschan, S.S. (1972) *Lasers in Industry*. Toledo Ohayo: Western Electronic Company Publication

Clauer, A. (1996) 'Laser Shock Peening for fatigue resistance in surface treatment of titanium alloys'. *The metal society of AIME conference n*. vol, pp 1-14 [online] available from <http://www.stellarwind.com/LSPT/pub1014.pdf> [*c.* 2006]

Coorstek Amazing Solutions (2007) *Nitrides* [online] available from <http://www.coorstek.com/materials/ceramics/nitrides.asp> [c. February 2007]

Cortes, R. Villagomez, R. Coello, V. Lopez, R. (2008) 'Laser beam quality factor ($M^2$) measured by distorted Fresnel zone plates'. *Revista Mexican de fisica* Vol 54, (4) PP 279 – 283

Dynamic Ceramic (2007) *Ceramic Materials* [online] available from <http://www.dynacer.com/silicon_nitride.htm>[*c*. January 2007]

Elgamec Company Ltd (09 January 2007) *Conventional shot peening trials on silicon nitride* Hants (see Appendix 11.13 onwards)

Granta Design Ltd (2007) *Cambridge Engineering Material Selector (CES).* Cambridge: Cambridge University

Hackel, L. (2005) 'Shaping the future-laser peening technology has come of age'. *Metal Improvement Company Ltd* Vol 19, (Issue 3) *n.* pp

Herbert, E.G. (1927) 'The work hardening of steel by abrasion'. *Engineering Iron steel institute of Glasgow n.* vol Pp 440- 472

Joel Advanced Technology (2005) 'SEM'. *Instruction Manual,* Cambridge

Kalpakjian, S (2001) *Manufactuing Engineering and Technology 4th edition*. New Jersey: Prentice Hall Press

Kell, J. Tyrer, J. Higginson, R. Thomson, R. Jones, J. Noden, S. (2006) 'Holographic Diffractive Optical Elements Allow Improvements in Conduction Laser Welding of Steels'. *Proceedings of the 25th International Conference on Applications of Lasers and Electro- Optics*, P1-6

Lawn, B. Wilshaw, T. (1975) 'Indentation fracture: principles and application'. *Journal of material science* V 10, P 1049 – 1081

London Travel (2007) *The list of References illustrated* [online] available from <http://golondon.about.com/od/londonmuseums/ig/British-Museum Highlights/Tomb-of-Ur-Helmet.htm>(*c.* March 2007)

Mannava. (1997) *Laser Shock Peened gas turbine engines and fan blades edges* [online] available from <http://www.shotpeener.com>[1997]

Mangels, J. Mikijelj, B. (2006) *Ceradyne's Silicon Nitride for Automotive Application* [online] available from <http://www.ceradyne.com>[*c*. 2006]

Mangels, J. (2006) *Advanced Technical Ceramics Improve Performance and Reduce Life Cycle Cost* [online] available from <http://www.ceradyne.com>[*c*. 2006]

Mangels, J. (2006) Silicon Nitride – *A Proven Ceramic Material For Engine Applications* [online] available from <http://www.ceradyne.com>[*c*. 2006]

Mikijelj, B. Mangels, J. (2005) *Effect of Silicon Nitride cam rollers on Cam Lobe Life* [online] available from <http://www.ceradyne.com>[*c*. 2005]

Malshe, A. Sun Li. Jiang, W. McCluskey, P. (July 2006) 'Effect of $CO_2$ Laser Surface Processing on Fracture Behaviour of silicon Nitride Ceramic'. *Journal of engineering materials and technology* Vol 128, p460 – 467

Marsh, K. J. (1993) *Shot Peening: Technique and Applications*. United Kingdom: Chameleon Press Ltd

McColm, I. (1990) *Ceramic Hardness*. New York: Platinum Press

McGeachie, I. (2002) *Laser Peening of Metals* [online] available from <http://www.metalmprovement.com> [c. July 2002]

Metal Improvement Company. (2005) *Shot Peening Applications* [online] available from <http://www.metalmprovement.com> [c. 2005]

Metal Improvement Company Ltd (2006) *Laser Peening* [online] available from <http://www.metalimprovement.com>[*c*. October 2006]

Metal Improvement Company Ltd (12th July 2007) *Typical Costs of laser Shock Peening* Derby (See appendix 11.12 onwards)

Morgan Advanced Ceramics (2006) *Technical data Sheets* [online] available from <http://www.morganadvancedceramics.com/aboutceramics.htm> [*c*. November 2006]

Ocana, J. Morales, M. Molpeceres, C. Porro, J. (2005) 'Laser shock processing as a method of surface properties modification of metallic materials'. *Surface Characteristics, 9th International conference of shot peening*, pp 466- 471

Orange, G. Liang, K. Fantozzi, G. (1987) 'Crack Resistance and fracture toughness of alumina and Zirconia ceramics: comparison of notched beam and indentation technique'. *Science of ceramics* Vol 14, (PT 7 – 9) PP 709 – 14

Page, C. Devermann, T. Biffin, J. Blundell, N. (2002) 'Plasma Augmented Welding and its Application'. *Science and Technology of Welding and Joining* Vol 7, (No 1) P1-9

Peng, H. (2004) 'Spark Plasma Sintering of $Si_3N_4$ Based Ceramics'. *Doctoral Desertion, Department of Inorganic Chemistry,* Stockholm Sweden: Stockholm University press

Pfeiffer. Frey, W. (2002) 'Shaping the future- damage or benefits'. *Fraunhofer Institute for mechanics of materials ICSP-8*, Germany

Ponton. Rawlings, C. (1989) 'Vickers indentation fracture toughness test, Part 1 - Review of literature and formulation of standardised indentation toughness equations'. *Materials Science Technology* Vol. 5, p865- 872

Precision Ceramics Ltd (2007) *Precision Ceramic Manufacturing* [online] available from <http://www.precision-ceramics.co.uk/manufacturing.htm> [*c*. January 2007]

Prevey, P. (2000) 'The effect of cold work on the Thermal stability of residual compression in surface enhancement'*. IN718, 20th ASM Material Solutions Conference & Exposition* St Louis, Missouri *n*. vol, *n*. pp

Prevey, P. Jayaraman, N. (2005) 'Overview of plastic burnishing for mitigation of fatigue damage and mechanism'. *Fatigue and facture of steels, 9th International conference of shot peening*, pp 267- 272

Qureshi, M. Malik, M. Dubey, R. (2001) 'Use of lasers for Shot peening'. *International conference on shot peening and blast cleaning*, P 171

Rofin Sinar (*c*. 2006) *The list of References Illustrated* [online] available from <http://rofin.com/index-e.htm> (*c*. 2006)

Shukla, P. P. Wu, H. Johnson, T.A. (2007) 'Effects of High Speed Laser Welding on Thin Sheet Steels as Applicable to Manufacture Three Piece Packaging Cans'. *National Conference of Futuristic Trends in Mechanical Engineering (NCME) 2007*, Shree Ram Collage of Engineering and Management (SRCEM), Banmore (Gwalior), India, P49- 55

Specht, R. Harris, F. (2002) *'Process Control Technique for laser peening of metals.' 6th European conference on residual stress*, p1-6

Spiricon (2007) *The list of References illustrated* [online] <http://spiricon.com/techinfo/publications/scientific/propagation_factor_laser_performance.pdf>[*c*. April 2007]

Solomah, A. Mannik, A. Brown, S. (1993) 'Laser Machining of Silicon Nitride Ceramics'. *Proceedings of the international conference on machining of advanced materials n*. vol, *n.* pp

Steen, W. (1998) *Laser Material Processing 2nd Edition* London: Springer Publication

Strakna, T. Jahanmir, S. Allor, R. Kumar, K. (1996) 'Influence of grinding direction on Fracture Strength of Silicon Nitride'. *Journal of Engineering Materials and Technology* Vol 118, p335- 342

Sun Li. Malshe, A.P. Ping, J. Mccluskey, P. (2006) 'Experimental Investigation of Laser Surface Processing of Flexure Silicon Nitride Ceramics'. *Transaction of Nonferrous Metals Society of China* Vol 16, PP 558 – 65

Timothy, J. Strakna. Jahanmir, S. Allor, R. Kumar, K. (1995) 'Influence of Grinding Direction on Fracture Strength of Silicon Nitride'. *ASME- Machining of Advanced Materials* Vol 208, PP 53 – 64

Verpoort, C. Gerdes, C. (1989) 'Influence of Shot Peening on material properties and the controlled shot peening of turbine blades'. *Metal behaviour and surface engineering IITT international n*. Vol , *n*. p

# Appendices

## 11.0: Appendices

***Section A***

### 11.1: Project Introduction

**Name:** Pratik Shukla

**Course:** MSc by Research

**Project Title**: Shot peening of Ceramics using Contact-Less Energy Beams

**Principle Aim:** The feasibility of surface treating silicon nitride ($Si_3N_4$) Using contact-Less energy beams.

### Project Objectives:

**i**. To evaluate the differences between mechanical and non-contact surface-treatment processes from literature.

**ii.** Experimental trials on silicon nitride with non- contact energy beams such as industrial lasers, non transferred plasma arc, hybrid laser plasma arc, and ultrasonic beam.

**iii.** Analysis of the observed changes in mechanical properties using experimental and analytical approaches.

### 11.2: Risk assessment

- By following the guidelines set for operating laser associated equipment in the Centre for advanced Joining laboratory. I am authorised to use the machines, however, only on the basis of full assistance provided from a laboratory technician.
- Ensure that the interlocked access doors are fully closed & secured. The LED indicators illuminate when the door interlocks are made. Verify their operation.
- Ensure that working area is free of unnecessary clutter, trailing wires etc. Whenever possible position the laser control panel to avoid trip hazard from its trailing lead.
- Ensure correct use of personal protective equipment at all times and being aware of all safety aspects.

- Identified the risks involved with the use of Class four lasers and acted accordingly when conducting welding experiments in the laser laboratory.
- Monitor machine performance at all times and always be prepared to execute an emergency shut down.
- Following general health and safety guidelines set out by the university guidelines.
- Considered my own safety as well as safety of others and never to leave a potentially hazardous situation unattended.
- Use of protective gear such as protective gloves when handling welded test specimens and associated chemicals.

## 11.3: Gantt Chart Version 1 produced on 11th October 2006.

**Table 11.1: Initial project time plan commencing October 2006**

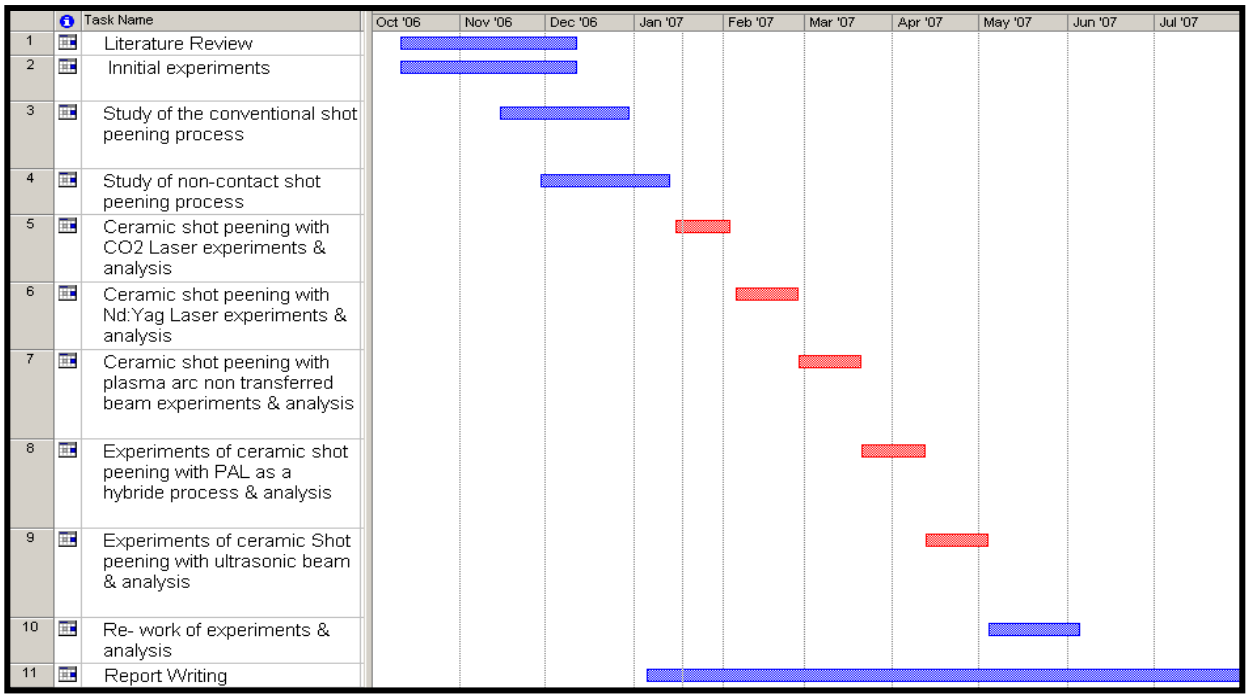

### 11.4: Gantt Chart Version 2 produced in 31st January 2007

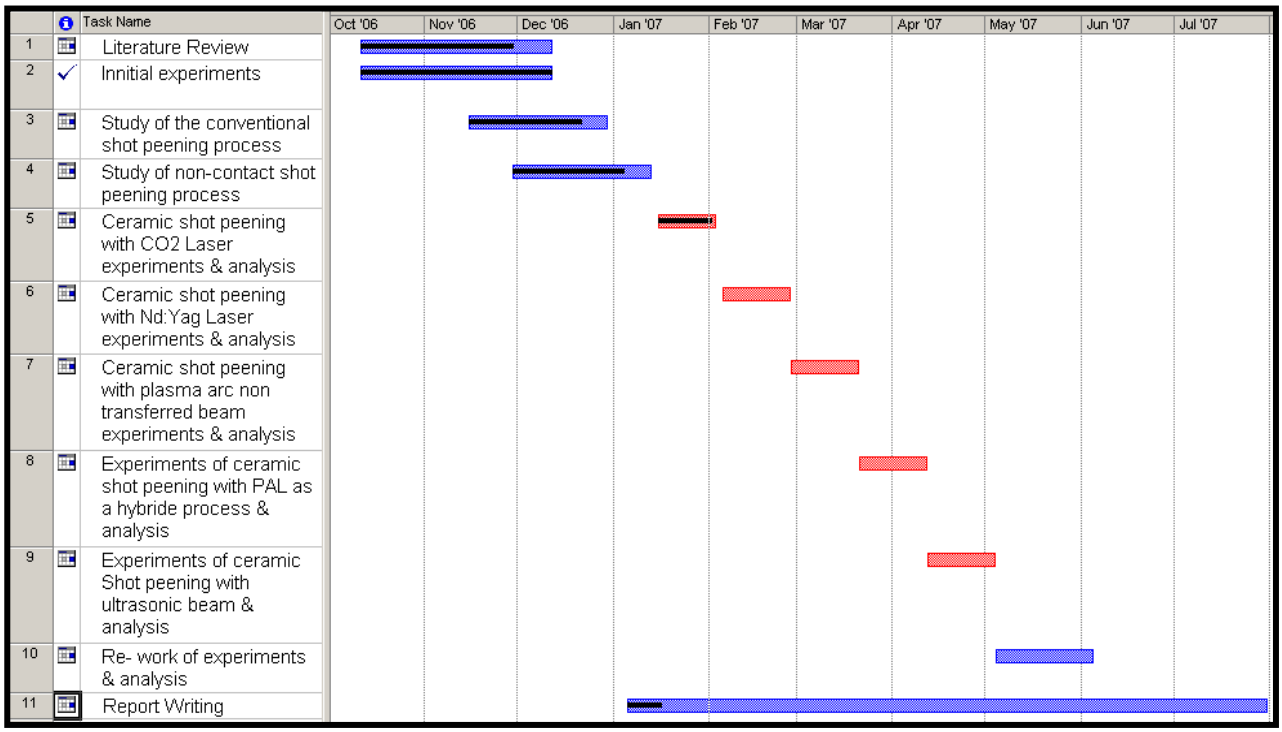


**Table 11.2: Project status in January 2007**

### 11.4: Gantt Chart Version 3 produced on 15th December 200

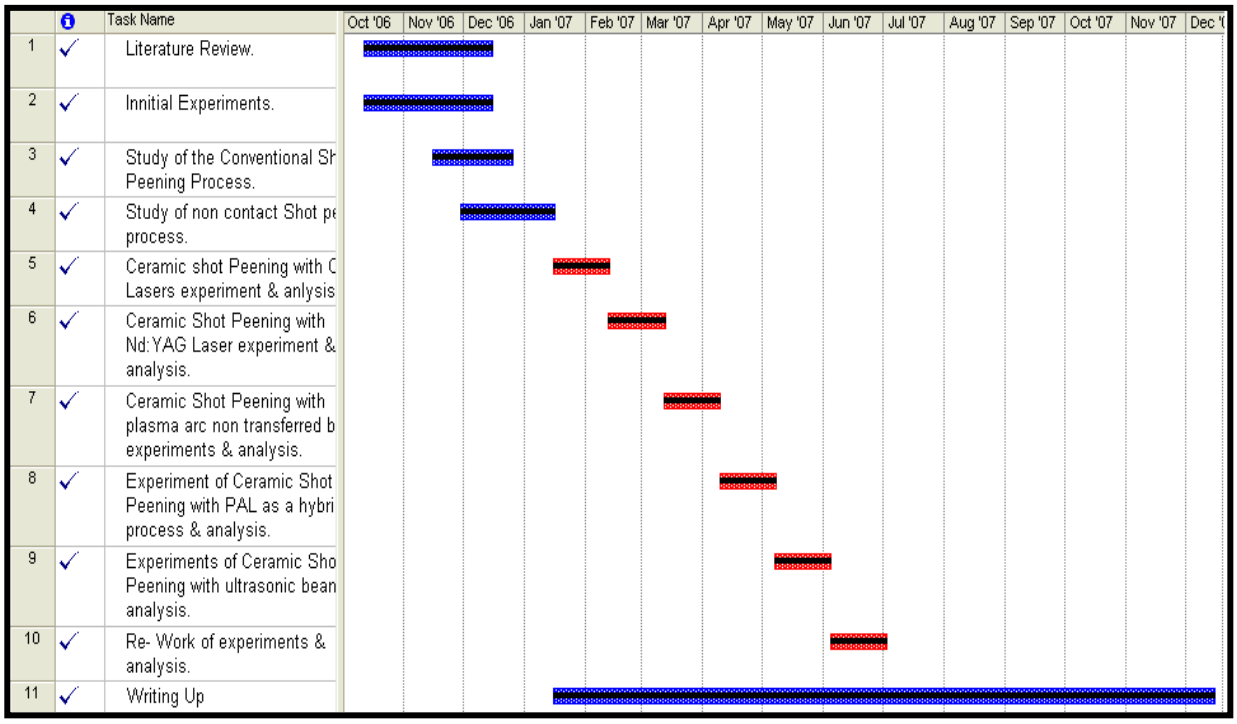


**Table 11.3: Final status of the project ending in December 2007**

## 11.5: Physical Properties of HP $Si_3N_4$

***Section B***

| Properties | | Units |
|---|---|---|
| Density | 3210-3280 | Kg/ $m^3$ |
| Price | 20.17 – 30.85 | GBP/ kg |
| **Composition** | | |
| Base | Nitride | |
| $Si_3N_4$ (silicon nitride) | 99 | % |
| **Mechanical Properties** | | |
| Bulk Modulus | 198 -208 | GPa |
| Compressive Strength | 3450 – 4833 | MPa |
| Elongation | 0 | % |
| Fatigue strength @ $10^7$ cycles | 330.8 – 385.9 | MPa |
| Fracture toughness | 4 – 6 | MPa. $m^{1/2}$ |
| Hardness | 1523 – 1680 | Hv |
| Mechanical loss coefficient | 2e-5 – 5e-5 | MPa |
| Modulus of rupture | 414 – 580 | |
| Poisson's ratio | 0.26 – 0.27 | |
| Shape factor | 15 | |
| Shear modulus | 107.5 – 112.9 | GPa |
| Tensile Strength | 345 – 483.3 | MPa |
| Yield strength (elastic limit) | 345 – 483.3 | MPa |
| Young's modulus | 273.1 – 287 | GPa |
| **Thermal Properties** | | |
| Maximum service temperature | 1220 -1280 | C |
| Melting point | 2388 – 2496 | C |
| Minimum service temperature | -273 | C |
| Specific heat | 882 – 918 | J/kg.k |
| Thermal conductivity | 1404 - 15.6 | W/m.k |
| Thermal expansion coefficient | 3.2 – 3.3 | µstain/C |
| **Other Properties** | | |
| Electrical Resistivity | 3.16e16 – 1e18 | µohm.cm |
| Transparency | Opaque | |
| Wear resistance | Very Good | |

**Table 11.4: Properties of sintered $Si_3N_4$**

## 11.5.1: Physical properties of Zirconia.

| Properties | | Units |
|---|---|---|
| Density | 6030 – 6160 | Kg/ $m^3$ |
| Price | 10.68 -15.43 | GBP/ kg |
| **Composition** | | |
| Base | Oxide | |
| $Si_3N_4$ (silicon nitride) | 100 | % |
| **Mechanical Properties** | | |
| Bulk Modulus | 93.49 – 98.2 | GPa |
| Compressive Strength | 1415 – 2070 | MPa |
| Elongation | 0 | % |
| Fatigue strength @ $10^7$cycles | 107.2 – 125 | MPa |
| Fracture toughness | 1 – 2.5 | MPa.$m^{1/2}$ |
| Hardness | 1107 – 1218 | Hv |
| Mechanical loss coefficient | 5e-4 – 1e-3 | MPa |
| Modulus of rupture | 177 – 195 | |
| Poisson's ratio | 0.24 – 0.28 | |
| Shape factor | 15 | |
| Shear modulus | 53.42 – 56.1 | GPa |
| Tensile Strength | 125 – 140 | MPa |
| Yield strength (elastic limit) | 125 – 140 | MPa |
| Young's modulus | 134.6 – 141.5 | GPa |
| **Thermal Properties** | | |
| Maximum service temperature | 2151 – 2249 | C |
| Melting point | 2550 – 2700 | C |
| Minimum service temperature | - 273 | C |
| Specific heat | 418 – 436 | J/ kg.k |
| Thermal conductivity | 1.7 – 2 | W/ m.k |
| Thermal expansion coefficient | 6 – 8.8 | µstain/ C |
| **Other Properties** | | |
| Electrical Resistivity | 3.16e14 – 3.16e15 | µohm. cm |
| Transparency | Opaque | |
| Wear resistance | Very Good | |

**Table 11.5: Properties of sintered $Si_3N_4$**

## 11.6: Application of $K_{1c}$ Equations

***Section C***

**Key:**

= Invalid and unacceptable values

= Acceptable values, hence the equation is accurate and usable

**$K_{1c} = 0.0101\ P/\ (ac^{1/2})$ .....(1)**

| Geometrical Value | Load (Kg) | Load P (N) | c | c/m | a | $(a^* c^{1/2})$ | $k^*P/(a^* c^{1/2})$ | $K_{1c}$ (MPa √m) |
|---|---|---|---|---|---|---|---|---|
| **Lawn and Swain Equation (1974)** | | | | | | | | |
| Silicon Nitride: Virgin Surface | | | | | | | | |
| 0.0101 | 50 | 490.5 | 0.000755 | 0.0003775 | 0.00151 | 5.70025E-07 | 8690934.608 | **8.69** |
| 0.0101 | 50 | 490.5 | 0.00060 | 0.0002975 | 0.00119 | 3.54025E-07 | 13993503.28 | **13.76** |
| 0.0101 | 50 | 490.5 | 0.00064 | 0.00032 | 0.00128 | 4.096E-07 | 12094848.63 | **12.09** |
| 0.0101 | 50 | 490.5 | 0.000622 | 0.000311 | 0.001244 | 3.86884E-07 | 12805000.98 | **12.80** |
| 0.0101 | 50 | 490.5 | 0.00062 | 0.00031 | 0.00124 | 3.844E-07 | 12887747.14 | **12.88** |

**Table 11.6: Calculations from the Lawn and Swain Equation (1974).**

**Comment:** the values obtained using the above $K_{1c}$ equation highlighted in red are too high for the required range.

**$K_{1c} = 0.0515\ P/C^{3/2}$ .....(2)**

| Geometrical Value | Load (Kg) | Load P (N) | c | $c^{3/2}$ | $k^*P/(a^*c^{3/2})$ | $K_{1c}$ (MPa √m) |
|---|---|---|---|---|---|---|
| **Lawn and Fuller Equation (1975)** | | | | | | |
| Silicon Nitride: Virgin Surface | | | | | | |
| 0.0515 | 50 | 490.5 | 0.000755 | 0.001125 | 22454 | **0.02** |
| 0.0515 | 50 | 490.5 | 0.00060 | 0.0008925 | 28303.36 | **0.02** |
| 0.0515 | 50 | 490.5 | 0.00064 | 0.00096 | 26313.28 | **0.02** |
| 0.0515 | 50 | 490.5 | 0.000622 | 0.000933 | 27074.76 | **0.02** |
| 0.0515 | 50 | 490.5 | 0.00062 | 0.00093 | 27162.1 | **0.02** |

**Table 11.7: Calculations from using Lawn and Fuller Equation (1975).**

**Comment:** the values obtained are very low so the equation is not acceptable.

**$K_{1c} = 0.0824\ P/c^{3/2}$ .....(3)**

| Geometrical Value | Load (Kg) | Load P (N) | c | $c^{3/2}$ | $k^*P/(a^*c^{3/2})$ | $K_{1c}$ (MPa √m) |
|---|---|---|---|---|---|---|
| **Evans and Charles (1976)** | | | | | | |
| Silicon Nitride: Virgin Surface | | | | | | |
| 0.0824 | 50 | 490.5 | 0.000755 | 2.15184E-10 | 1.88E+11 | **187825.85** |
| 0.0824 | 50 | 490.5 | 0.00060 | 1.05322E-10 | 3.84E+11 | **374233.33** |
| 0.0824 | 50 | 490.5 | 0.00064 | 1.31072E-10 | 3.08E+11 | **308358.76** |
| 0.0824 | 50 | 490.5 | 0.000622 | 1.20321E-10 | 3.36E+11 | **335911.64** |
| 0.0824 | 50 | 490.5 | 0.00062 | 1.19164E-10 | 3.39E+11 | **339172.90** |

**Table 11.8: Calculation from using the Evans and Charles equation (1976).**

**Comment:** this equation is also not acceptable since the values are very high.

$K_{1c} = 0.0134\ (E/Hv)^{1/2}\ (P/c^{3/2})$ ……(4)

| Geometrical Value | Load (kg) | Load P (N) | H | E/Hv | A | c/m | $C^{3/2}$ | $P/(c^{3/2})$ | $K_{1c}$ (MPa √m) |
|---|---|---|---|---|---|---|---|---|---|
| **Lawn, Evans and Marshall Equation (1980)** | | | | | | | | | |
| Silicon Nitride: Virgin Surface | | | | | | | | | |
| 0.0134 | 50 | 490.5 | 1521 | 16.4365549 | 0.000755 | 0.0003775 | 7.33458E-06 | 66874966.54 | **3.63** |
| 0.0134 | 50 | 490.5 | 1583 | 15.79279848 | 0.0006 | 0.0002975 | 5.13134E-06 | 95589140.5 | **5.02** |
| 0.0134 | 50 | 490.5 | 1583 | 15.79279848 | 0.00064 | 0.00032 | 5.72433E-06 | 85686823.67 | **4.56** |
| 0.0134 | 50 | 490.5 | 1583 | 15.79279848 | 0.000622 | 0.000311 | 5.48454E-06 | 89433129.51 | **4.76** |
| 0.0134 | 50 | 490.5 | 1583 | 15.79279848 | 0.00062 | 0.00031 | 5.45811E-06 | 89866219.26 | **4.78** |

**Table 11.9: Calculations from using the Lawn, Evans and Marshall equation (1998)**

**Comment:** the values are reasonable and lie within the range (4 – 6 MPa √m); hence this equation was acceptable and can be considered for use if other equations do not present better consistency.

$K_{1c} = 0.0330\ (E/Hv)^{2/5}\ (P/c^{3/2})$ ……(5)

| Geometrical Value | Load (kg) | Load P (N) | H | E/Hv | A | c/m | $c^{3/2}$ | $P/(c^{3/2})$ | $K_{1c}$ (MPa √m) |
|---|---|---|---|---|---|---|---|---|---|
| **Niihara, Morena, and Hasselman Equation (1982)** | | | | | | | | | |
| Silicon Nitride: Virgin Surface | | | | | | | | | |
| 0.033 | 50 | 490.5 | 1521 | 0.002161283 | 0.000755 | 0.0003775 | 7.33458E-06 | 66874966.54 | **0.18** |
| 0.033 | 50 | 490.5 | 1583 | 0.0019953 | 0.0006 | 0.0002975 | 5.13134E-06 | 95589140.5 | **0.25** |
| 0.033 | 50 | 490.5 | 1583 | 0.0019953 | 0.00064 | 0.00032 | 5.72433E-06 | 85686823.67 | **0.23** |
| 0.033 | 50 | 490.5 | 1583 | 0.0019953 | 0.000622 | 0.000311 | 5.48454E-06 | 89433129.51 | **0.24** |
| 0.033 | 50 | 490.5 | 1583 | 0.0019953 | 0.00062 | 0.00031 | 5.45811E-06 | 89866219.26 | **0.24** |

**Table 11.10: Niihara, Morena and Hasselman equation (1982).**

**Comment:** Values for the equation are high, hence the equation is unacceptable.

$K_{1c} = 0.0363\ (E/Hv)^{2/5} (P/a^{1.5})\ (a/c)^{1.56}$ ……(6)

| Geometrical Value | Load (kg) | Load P (N) | H | E/Hv | a | $a^{1.5}$ | c/m | $P/(a^{1.5})$ | $(a/c)^{1.56}$ | $K_{1c}$ (MPa√m) |
|---|---|---|---|---|---|---|---|---|---|---|
| **Lankford Equation (1982)** (31) | | | | | | | | | | |
| **Silicon Nitride: Virgin Surface** | | | | | | | | | | |
| 0.0363 | 50 | 490.5 | 1521 | 0.002161283 | 0.000755 | 2.07453E-05 | 0.0003775 | 23643871.17 | 2.948538435 | **0.0031** |
| 0.0363 | 50 | 490.5 | 1583 | 0.0019953 | 0.0006 | 1.45136E-05 | 0.0002975 | 33795864.73 | 2.948538435 | **0.0041** |
| 0.0363 | 50 | 490.5 | 1583 | 0.0019953 | 0.00064 | 1.61909E-05 | 0.00032 | 30294867.04 | 2.948538435 | **0.0037** |
| 0.0363 | 50 | 490.5 | 1583 | 0.0019953 | 0.000622 | 1.55126E-05 | 0.000311 | 31619386.17 | 2.948538435 | **0.0039** |
| 0.0363 | 50 | 490.5 | 1583 | 0.0019953 | 0.00062 | 1.54379E-05 | 0.00031 | 31772506.52 | 2.948538435 | **0.0039** |

**Table 11.11: Lankford equation (1982).**

**Comment:** values are too low hence, the unacceptable equation.

$K_{1c} = 0.095 (E/Hv)^{2/3} (P/c^{3/2})$ ……(7)

| k | Load (kg) | Load P (N) | H | E/Hv | a | c/m | $c^{3/2}$ | $P/(c^{3/2})$ | $K_{1c}$ (MPa √m) |
|---|---|---|---|---|---|---|---|---|---|
| **Laugier Equation (1985)** | | | | | | | | | |
| Silicon Nitride: Virgin Surface | | | | | | | | | |
| 0.095 | 50 | 490.5 | 1521 | 90.05344564 | 0.000755 | 0.0003775 | 7.33458E-06 | 66874966.54 | **572.12** |
| 0.095 | 50 | 490.5 | 1583 | 83.13749465 | 0.0006 | 0.0002975 | 5.13134E-06 | 95589140.5 | **745.55** |
| 0.095 | 50 | 490.5 | 1583 | 83.13749465 | 0.00064 | 0.00032 | 5.72433E-06 | 85686823.67 | **676.75** |
| 0.095 | 50 | 490.5 | 1583 | 83.13749465 | 0.000622 | 0.000311 | 5.48454E-06 | 89433129.51 | **706.34** |
| 0.095 | 50 | 490.5 | 1583 | 83.13749465 | 0.00062 | 0.00031 | 5.45811E-06 | 89866219.26 | **709.76** |

**Table 11.12: Laugier equation (1985).**

**Comment:** the values found are too high hence, the equation is unacceptable.

$K_{1c} = 0.022 (E/Hv)^{2/3} (P/c^{3/2})$ ……(8)

| K | Load /kg | Load P (N) | H | E/Hv | a | c/m | $c^{3/2}$ | $P/(c^{3/2})$ | $K_{1c}$ (MPa√m) |
|---|---|---|---|---|---|---|---|---|---|
| **Laugier Equation (1985)** | | | | | | | | | |
| Silicon Nitride: Virgin Surface | | | | | | | | | |
| 0.022 | 50 | 490.5 | 1521 | 90.05344564 | 0.000755 | 0.0003775 | 7.33458E-06 | 66874966.54 | **132.49** |
| 0.022 | 50 | 490.5 | 1583 | 83.13749465 | 0.0006 | 0.0002975 | 5.13134E-06 | 95589140.5 | **172.65** |
| 0.022 | 50 | 490.5 | 1583 | 83.13749465 | 0.00064 | 0.00032 | 5.72433E-06 | 85686823.67 | **156.72** |
| 0.022 | 50 | 490.5 | 1583 | 83.13749465 | 0.000622 | 0.000311 | 5.48454E-06 | 89433129.51 | **163.57** |
| 0.022 | 50 | 490.5 | 1583 | 83.13749465 | 0.00062 | 0.00031 | 5.45811E-06 | 89866219.26 | **164.36** |

**Table 11.13: Laugier equation (1985).**

**Comment:** Unacceptable equation since the values do not lie within the required range.

$K_{1c} = 0.035 (E/Hv)^{1/4} (P/c^{3/2})$ ……(9)

| Geometrical Value | Load /kg | Load P (N) | H | E/Hv | a | c/m | $c^{3/2}$ | $P/(c^{3/2})$ | $K_{1c}$ (MPa√m) |
|---|---|---|---|---|---|---|---|---|---|
| **Tanak Equation (1987)** | | | | | | | | | |
| Silicon Nitride: Virgin Surface | | | | | | | | | |
| 0.022 | 50 | 490.5 | 1521 | 4.109138725 | 0.000755 | 0.0003775 | 7.33458E-06 | 66874966.54 | **6.04** |
| 0.022 | 50 | 490.5 | 1583 | 3.948199621 | 0.0006 | 0.0002975 | 5.13134E-06 | 95589140.5 | **8.19** |
| 0.022 | 50 | 490.5 | 1583 | 3.948199621 | 0.00064 | 0.00032 | 5.72433E-06 | 85686823.67 | **7.44** |
| 0.022 | 50 | 490.5 | 1583 | 3.948199621 | 0.000622 | 0.000311 | 5.48454E-06 | 89433129.51 | **7.76** |
| 0.022 | 50 | 490.5 | 1583 | 3.948199621 | 0.00062 | 0.00031 | 5.45811E-06 | 89866219.26 | **7.80** |

**Table 11.14: Calculations from the Tanak equation (1987).**

**Comment:** the figures are close to the required values, however, they are still considered too high, so the equation is yet unacceptable.

$K_{1c} = 0.016 (E/Hv)^{1/2} (P/c^{3/2})$ ……(10)

| Geometrical Value | load /kg | Load (N) | H | E/Hv | a | c/m | $c^{3/2}$ | $P/(c^{3/2})$ | $K_{1c}$ (MPa √m) |
|---|---|---|---|---|---|---|---|---|---|
| **Anstis, Chantikul, Lawn and Marshall equation (1981)** | | | | | | | | | |
| Silicon Nitride: Virgin Surface | | | | | | | | | |
| 0.016 | 50 | 490.5 | 1521 | 16.4365549 | 0.000755 | 0.0003775 | 7.33458E-06 | 66874966.54 | **4.33** |
| 0.016 | 50 | 490.5 | 1583 | 15.79279848 | 0.00060 | 0.0002975 | 5.13134E-06 | 95589140.5 | **6.00** |
| 0.016 | 50 | 490.5 | 1583 | 15.79279848 | 0.00064 | 0.00032 | 5.72433E-06 | 85686823.67 | **5.44** |
| 0.016 | 50 | 490.5 | 1583 | 15.79279848 | 0.000622 | 0.000311 | 5.48454E-06 | 89433129.51 | **5.68** |
| 0.016 | 50 | 490.5 | 1583 | 15.79279848 | 0.00062 | 0.00031 | 5.45811E-06 | 89866219.26 | **5.71** |

**Table 11.15: Anstis, Chantikul, Lawn and Marshall equation (1981).**

| Geometrical Value | Load / Kg | Load P(N) | H | E / H | a | c / m | $c^{3/2}$ | $P/(c^{3/2})$ | K1c / Mpa √m |
|---|---|---|---|---|---|---|---|---|---|
| **Anstis, Chantikul, Lawn and Marshall equation** | | | | | | | | | |
| Silicon Nitride: Treated Surface, $CO_2$ Laser marker treatment, Pattern 4 | | | | | | | | | |
| 0.016 | 50 | 490.5 | 1368 | 21.92982 | 0.000628 | 0.000314 | 5.55745E-06 | 88259896 | **6.61** |
| 0.016 | 50 | 490.5 | 1368 | 21.92982 | 0.00058 | 0.00029 | 4.93852E-06 | 99321213 | **7.44** |
| 0.016 | 50 | 490.5 | 1368 | 21.92982 | 0.000625 | 0.000313 | 5.52427E-06 | 88789984 | **6.65** |
| 0.016 | 50 | 490.5 | 1368 | 21.92982 | 0.000615 | 0.000308 | 5.39222E-06 | 90964373 | **6.81** |
| 0.016 | 50 | 490.5 | 1368 | 21.92982 | 0.00059 | 0.000295 | 5.06679E-06 | 96806827 | **7.25** |

**Table 11.16: Calculation of $K_{1c}$ for $CO_2$ Laser Treated $Si_3N_4$.**

## 11.7: Ultrasonic Treatment

An ultrasonic probe was used to treat the surface of the $Si_3N_4$, initially at very low power (10 Watts). The distance of the probe from the material surface was 3 mm. The time which the treatment was carried out for was 60 seconds on one particular surface. The treated surface was then observed under the optical microscopy and tested for any change in the hardness. No change in the material colour or hardness was found. Therefore, second set of experiments were done using a higher power ultrasonic probe with the following experimental conditions presented in table 11.17.

| Experimental Settings |
|---|
| Pool of Distilled water |
| Ultrasound Probe (20 Hertz) |
| Amplitude 50 % |
| Power – 40 Watts |
| Temperature 40 c |

**Table 11.17: Parameters used for the Ultrasonic treatment on $Si_3N_4$.**

## 11.8: Results

Results from the ultrasonic treatment were found to have no effect on the HP $Si_3N_4$ surface. An ultrasonic probe using the processing parameters given in chapter 5 was applied for the treatment. At 40 watts of power and the water temperature being 40 ºC, the material had no visual effective change on the surface. Vickers hardness test was then conducted to investigate if there was a change in the materials hardness. No change in the hardness was found with the treated area as the hardness value for the virgin surface was similar to the treated area. The hardness of the treated HP $Si_3N_4$ was found to be 1592 Hv and the mean hardness of the virgin surface was calibrated to be 1604 Hv. This shows that there was no significant difference between the hardness values of the two surfaces which can be considered for calculating the change in the $K_{1c}$ value for comparison. Therefore, further trials were not conducted for the investigation. It would be interesting to conduct further experiments by increasing the power and the temperature of the water in the pool to observe the effects.

## 11.9: Experimental Results and Discussion

### *11.9.1: Hardness of as machined and ground, polished HP $Si_3N_4$ Surfaces. Indentation Load = 50 Kg*

| Trial No | Hardness (Hv) | |
|---|---|---|
| | As machined virgin surface | Ground & Polished virgin surface |
| 1 | 1357 | 1549 |
| 2 | 1379 | 1569 |
| 3 | 1215 | 1640 |
| 4 | 1345 | 1589 |
| 5 | 1226 | 1640 |
| 6 | 1416 | 1626 |
| 7 | 1426 | 1646 |
| 8 | 1478 | 1649 |
| 9 | 1486 | 1520 |
| 10 | 1401 | 1549 |
| 11 | 1191 | 1564 |
| 12 | 1197 | 1605 |
| 13 | 1350 | 1564 |
| 14 | 1390 | 1549 |
| 15 | 1445 | 1640 |
| 16 | 1326 | 1546 |
| 17 | 1501 | 1616 |
| 18 | 1287 | 1648 |
| 19 | 1380 | 1545 |
| 20 | 1306 | 1483 |
| **Average** | 1346.928571 | 1586.85 |

**Table 11.18: Hardness values calibrated from the Vickers indentation test for the ground, polished and as machined virgin surfaces.**

### *11.9.2: Crack lengths from the Vickers indentation tests for the virgin ground, polished surface and as machined virgin surface.*

| Trial No | Crack Length (µm) | |
|---|---|---|
| | As machined virgin surface | Ground Polished virgin surface |
| 1 | 835 | 622 |
| 2 | 728 | 572 |
| 3 | 798 | 582 |
| 4 | 826 | 595 |
| 5 | 692 | 560 |
| 6 | 826 | 589 |
| 7 | 762 | 600 |
| 8 | 756 | 562 |
| 9 | 654 | 638 |
| 10 | 750 | 657 |
| 11 | 745 | 535 |
| 12 | 631 | 583 |
| 13 | 710 | 622 |
| 14 | 690 | 640 |
| 15 | 837 | 597 |
| 16 | 855 | 430 |
| 17 | 710 | 410 |
| 18 | 654 | 589 |
| 19 | 726 | 560 |
| 20 | 719 | 595 |
| **Average** | 745.2 | 596.92857 |

**Table 11.19: Crack lengths found form the Vickers indentation tests for the virgin ground, polished surface and as machined virgin surface.**

**Note:** The indentation load = 50 kg (490.5 Newtons) for both type of samples presented on Table 11.19.

### *11.9.3: $K_{1c}$ of virgin ground, polished and as machined virgin Surfaces*

| Trial No | Δ $K_{1c}$ MPa √m | |
|---|---|---|
| | As machined virgin surface | Polished virgin surface |
| 1 | **3.95** | **5.68** |
| 2 | **4.85** | **6.44** |
| 3 | **4.23** | **6.27** |
| 4 | **4.02** | **6.07** |
| 5 | **5.24** | **6.67** |
| 6 | **4.02** | **6.16** |
| 7 | **4.53** | **5.99** |
| 8 | **4.59** | **6.61** |
| 9 | **5.7** | **5.47** |
| 10 | **4.64** | **5.23** |
| 11 | **4.69** | **7.12** |
| 12 | **6.01** | **6.26** |
| 13 | **5.04** | **5.68** |
| 14 | **5.26** | **5.44** |
| 15 | **3.94** | **6.04** |
| 16 | **3.81** | **7.5** |
| 17 | **5.04** | **7.42** |
| 18 | **5.7** | **6.16** |
| 19 | **4.88** | **6.65** |
| 20 | **4.95** | **6.07** |
| **Average** | **4.769285714** | **6.2465** |

**Table 11.20: $K_{1c}$ deviation of the virgin ground, polished and as machined surfaces.**

### *11.9.4: Hardness of the $CO_2$ Laser Treated HP $Si_3N_4$*

| Trial No | Hardness (Hv) |
|---|---|
| 1 | 1569 |
| 2 | 1492 |
| 3 | 1564 |
| 4 | 1486 |
| 5 | 1505 |
| 6 | 1283 |
| 7 | 1049 |
| 8 | 524 |
| 9 | 454 |
| 10 | 212 |
| 11 | 386 |
| 12 | 387 |
| 13 | 306 |
| 14 | 675 |
| 15 | 1027 |
| 16 | 1179 |
| 17 | 1253 |
| 18 | 1345 |
| 19 | 1314 |
| 20 | 1564 |
| **AVERAGE** | 1028.7 |

**Table 11.21: Hardness of the $CO_2$ Laser treated HP $Si_3N_4$.**

| Trial No | Hardness / Hv |
|---|---|
| 1 | 1118 |
| 2 | 1162 |
| 3 | 1158 |
| 4 | 1249 |
| 5 | 1062 |
| 6 | 1208 |
| 7 | 1204 |
| 8 | 1158 |
| 9 | 1187 |
| 10 | 1196 |
| 11 | 1194 |
| 12 | 1162 |
| 13 | 1042 |
| 14 | 1215 |
| 15 | 1197 |
| 16 | 1201 |
| 17 | 1071 |
| 18 | 1109 |
| 19 | 1158 |
| 20 | 1184 |
| **AVERAGE** | 1161.75 |

**Table 11.22: Hardness of the Nd: YAG Laser treated samples with its standard deviation.**

### *11.9.5: Crack lengths of the Nd: YAG laser treated $Si_3N_4$*

| Trial No | Crack Length (µm) |
|---|---|
| 1 | 720 |
| 2 | 611 |
| 3 | 751 |
| 4 | 812 |
| 5 | 742 |
| 6 | 940 |
| 7 | 689 |
| 8 | 713 |
| 9 | 817 |
| 10 | 762 |
| 11 | 649 |
| 12 | 825 |
| 13 | 846 |
| 14 | 711 |
| 15 | 750 |
| 16 | 813 |
| 17 | 781 |
| 18 | 781 |
| 19 | 837 |
| 20 | 768 |
| **AVERAGE** | 765.90 |

**Table 11.23: Crack lengths of the Nd: YAG laser treated $Si_3N_4$ with the deviation values from the mean.**

# 11.10: Results from $CO_2$ Laser Processing of HP $Si_3N_4$

***Section D***

| |
|---|
| P = Load |
| C = Crack Size |
| a = 2c |
| E = 25000 |

| Empirical Value | Load / kg | Load P (N) | H | E / Hv | A | c / m | $c^{3/2}$ | $P / ( c^{3/2})$ | $K_{1c}$ (MPa $\sqrt{m}$) |
|---|---|---|---|---|---|---|---|---|---|
| **Anstis, Chantikul, Lawn and Marshall equation (1981)** | | | | | | | | | |
| $Si_3N_4$: $CO_2$ Laser Treated Surface | | | | | | | | | |
| 0.016 | 50 | 490.5 | 1529 | 16.35056 | 0.00053 | 0.000265 | 4.31389E-06 | 68221529 | **4.41** |
| 0.016 | 50 | 490.5 | 1492 | 16.75603 | 0.00052 | 0.00026 | 4.19237E-06 | 70198889 | **4.59** |
| 0.016 | 50 | 490.5 | 1564 | 15.98465 | 0.000528 | 0.000264 | 4.2834E-06 | 68707091 | **4.39** |
| 0.016 | 50 | 490.5 | 1486 | 16.82369 | 0.00058 | 0.00029 | 4.93852E-06 | 59592728 | **3.91** |
| 0.016 | 50 | 490.5 | 1505 | 16.6113 | 0.000465 | 0.000233 | 3.54515E-06 | 83014857 | **5.41** |
| 0.016 | 50 | 490.5 | 1283 | 19.48558 | 0.000412 | 0.000206 | 2.95666E-06 | 165896866 | **11.16** |
| 0.016 | 50 | 490.5 | 1049 | 23.83222 | 0.0003 | 0.00015 | 1.83712E-06 | 266994382 | **20.85** |
| 0.016 | 50 | 490.5 | 524 | 47.70992 | 0.000245 | 0.000123 | 1.35583E-06 | 361771940 | **39.98** |
| 0.016 | 50 | 490.5 | 454 | 55.06608 | 0.000573 | 0.000286 | 4.84304E-06 | 101279318 | **12.02** |
| 0.016 | 50 | 490.5 | 212 | 117.9245 | 0.000101 | 5.05E-05 | 3.5887E-07 | 1.367E+09 | **237.47** |
| 0.016 | 50 | 490.5 | 386 | 64.76684 | 0.000468 | 0.000234 | 3.57378E-06 | 137249756 | **17.67** |
| 0.016 | 50 | 490.5 | 387 | 64.59948 | 0.00045 | 0.000225 | 3.375E-06 | 145333333 | **18.68** |
| 0.016 | 50 | 490.5 | 306 | 81.69935 | 0.000365 | 0.000183 | 2.46544E-06 | 198950350 | **28.77** |
| 0.016 | 50 | 490.5 | 675 | 37.03704 | 0.00041 | 0.000205 | 2.93515E-06 | 167112224 | **16.27** |
| 0.016 | 50 | 490.5 | 1027 | 24.34275 | 0.000428 | 0.000214 | 3.12507E-06 | 156956688 | **12.39** |
| 0.016 | 50 | 490.5 | 1179 | 21.20441 | 0.00058 | 0.00029 | 4.93852E-06 | 99321213 | **7.31** |
| 0.016 | 50 | 490.5 | 1253 | 19.95211 | 0.000425 | 0.000213 | 3.09769E-06 | 158343635 | **11.31** |
| 0.016 | 50 | 490.5 | 1345 | 18.58736 | 0.000415 | 0.000208 | 2.98901E-06 | 164101239 | **11.31** |
| 0.016 | 50 | 490.5 | 1314 | 19.02588 | 0.00059 | 0.000295 | 5.06679E-06 | 96806827 | **6.75** |
| 0.016 | 50 | 490.5 | 1564 | 15.98465 | 0.000525 | 0.000263 | 4.25299E-06 | 69198439 | **4.42** |
| 0.016 | 50 | 490.5 | 1368 | 18.27485 | 0.00053 | 0.000265 | 4.31389E-06 | 68221529 | **4.66** |
| 0.016 | 50 | 490.5 | 1368 | 18.27485 | 0.000585 | 0.000293 | 5.00252E-06 | 58830353 | **4.02** |
| 0.016 | 30 | 294.3 | 1440 | 17.36111 | 0.00063 | 0.000315 | 5.5907E-06 | 52641036 | **3.50** |
| 0.016 | 30 | 294.3 | 1315 | 19.01141 | 0.000515 | 0.000258 | 4.13205E-06 | 71223680 | **4.96** |
| 0.016 | 30 | 294.3 | 1356 | 18.43658 | 0.000535 | 0.000267 | 4.36894E-06 | 67361801 | **4.62** |
| 0.016 | 30 | 294.3 | 1437 | 17.39736 | 0.000835 | 0.000418 | 8.5307E-06 | 34498923 | **2.30** |
| 0.016 | 30 | 294.3 | 1416 | 17.65537 | 0.000693 | 0.000346 | 6.44295E-06 | 45677843 | **3.07** |
| 0.016 | 30 | 294.3 | 1281 | 19.516 | 0.000592 | 0.000296 | 5.08613E-06 | 57863291 | **4.08** |
| 0.016 | 50 | 490.5 | 1325 | 18.86792 | 0.000885 | 0.000443 | 9.30829E-06 | 52694962 | **3.66** |
| 0.016 | 50 | 490.5 | 1387 | 18.02451 | 0.000875 | 0.000438 | 9.15097E-06 | 53600881 | **3.64** |
| 0.016 | 50 | 490.5 | 1304 | 19.17178 | 0.000795 | 0.000398 | 7.92512E-06 | 61891828 | **4.33** |
| 0.016 | 50 | 490.5 | 1382 | 18.08973 | 0.000805 | 0.000403 | 8.07512E-06 | 60742153 | **4.13** |
| 0.016 | 50 | 490.5 | 1397 | 17.89549 | 0.000895 | 0.000448 | 9.4665E-06 | 51814278 | **3.50** |
| 0.016 | 50 | 490.5 | 1304 | 19.17178 | 0.000758 | 0.000379 | 7.37104E-06 | 66544176 | **4.66** |
| 0.016 | 50 | 490.5 | 1229 | 20.34174 | 0.000915 | 0.000458 | 9.78558E-06 | 50124767 | **3.61** |
| 0.016 | 50 | 490.5 | 1443 | 17.32502 | 0.000589 | 0.000295 | 5.05392E-06 | 97053469 | **6.46** |
| 0.016 | 50 | 490.5 | 1304 | 19.17178 | 0.000815 | 0.000408 | 8.22605E-06 | 59627636 | **4.17** |
| 0.016 | 50 | 490.5 | 1325 | 18.86792 | 0.000863 | 0.000432 | 8.96337E-06 | 54722737 | **3.80** |
| 0.016 | 50 | 490.5 | 1310 | 19.08397 | 0.000795 | 0.000398 | 7.92512E-06 | 61891828 | **4.32** |
| 0.016 | 50 | 490.5 | 1449 | 17.25328 | 0.000805 | 0.000403 | 8.07512E-06 | 60742153 | **4.03** |
| 0.016 | 50 | 490.5 | 1358 | 18.40943 | 0.000815 | 0.000408 | 8.22605E-06 | 59627636 | **4.09** |
| 0.016 | 30 | 294.3 | 1277 | 19.57713 | 0.000593 | 0.000296 | 5.09903E-06 | 96194773 | **6.80** |
| 0.016 | 30 | 294.3 | 1460 | 17.12329 | 0.000625 | 0.000313 | 5.52427E-06 | 88789984 | **5.87** |
| 0.016 | 30 | 294.3 | 1281 | 19.516 | 0.00069 | 0.000345 | 6.40809E-06 | 76543862 | **5.41** |
| 0.016 | 30 | 294.3 | 1415 | 17.66784 | 0.000465 | 0.000233 | 3.54515E-06 | 138358096 | **9.30** |
| 0.016 | 30 | 294.3 | 1277 | 19.57713 | 0.00078 | 0.00039 | 7.70188E-06 | 63685726 | **4.50** |
| 0.016 | 30 | 294.3 | 1134 | 22.04586 | 0.000615 | 0.000308 | 5.39222E-06 | 90964373 | **6.83** |
| 0.016 | 50 | 490.5 | 1263 | 19.79414 | 0.000585 | 0.000293 | 5.00252E-06 | 98050589 | **6.97** |
| 0.016 | 30 | 294.3 | 1281 | 19.516 | 0.00075 | 0.000375 | 7.26184E-06 | 67544830 | **4.77** |
| 0.016 | 30 | 294.3 | 1420 | 17.60563 | 0.000702 | 0.000351 | 6.57598E-06 | 74589610 | **5.00** |
| 0.016 | 30 | 294.3 | 1263 | 19.79414 | 0.000652 | 0.000326 | 5.88608E-06 | 83332155 | **5.93** |
| 0.016 | 30 | 294.3 | 1196 | 20.90301 | 0.000235 | 0.000118 | 1.27367E-06 | 385107709 | **28.17** |
| 0.016 | 30 | 294.3 | 1230 | 20.3252 | 0.00042 | 0.00021 | 3.04319E-06 | 161179599 | **11.62** |
| 0.016 | 30 | 294.3 | 1325 | 18.86792 | 0.00039 | 0.000195 | 2.72303E-06 | 180130434 | **12.51** |
| 0.016 | 50 | 490.5 | 1330 | 18.79699 | 0.000585 | 0.000293 | 5.00252E-06 | 98050589 | **6.80** |
| 0.016 | 30 | 294.3 | 1372 | 18.22157 | 0.000425 | 0.000213 | 3.09769E-06 | 158343635 | **10.81** |
| 0.016 | 30 | 294.3 | 1256 | 19.90446 | 0.00062 | 0.00031 | 5.45811E-06 | 89866219 | **6.41** |
| 0.016 | 30 | 294.3 | 1665 | 15.01502 | 0.000444 | 0.000222 | 3.30773E-06 | 148289209 | **9.19** |

| | | | | | | | | | |
|---|---|---|---|---|---|---|---|---|---|
| 0.016 | 30 | 294.3 | 1254 | 19.9362 | 0.000468 | 0.000234 | 3.57378E-06 | 137249756 | **9.80** |
| 0.016 | 30 | 294.3 | 1404 | 17.80627 | 0.000517 | 0.000259 | 4.15615E-06 | 118017984 | **7.96** |
| 0.016 | 30 | 294.3 | 1372 | 18.22157 | 0.0003 | 0.00015 | 1.83712E-06 | 266994382 | **18.23** |
| 0.016 | 30 | 294.3 | 1196 | 20.90301 | 0.000445 | 0.000223 | 3.31891E-06 | 147789639 | **10.81** |

**Table 11.24: Calculation of $K_{1c}$ for $CO_2$ Laser treated $Si_3N_4$.**

## 11.11: Results from Nd: YAG Processing of HP $Si_3N_4$

| |
|---|
| P = Load |
| C = Crack Size |
| a = 2c |
| E = 25000 |

| Geometrical Value | Load (kg) | Load P (N) | H | E/Hv | A | c/m | $c^{3/2}$ | $P/(c^{3/2})$ | $K_{1c}$ (MPa $\sqrt{m}$) |
|---|---|---|---|---|---|---|---|---|---|
| **Anstis, Chantikul, Lawn and Marshall equation (1981)** | | | | | | | | | |
| $Si_3N_4$: $CO_2$ Laser Treated Surface | | | | | | | | | |
| 0.016 | 50 | 490.5 | 1118 | 16.35056 | 0.00072 | 0.000265 | 4.31389E-06 | 68221529 | **5.43** |
| 0.016 | 50 | 490.5 | 1162 | 16.75603 | 0.000611 | 0.00026 | 4.19237E-06 | 70198889 | **6.81** |
| 0.016 | 50 | 490.5 | 1158 | 15.98465 | 0.000751 | 0.000264 | 4.2834E-06 | 68707091 | **5.01** |
| 0.016 | 50 | 490.5 | 1249 | 16.82369 | 0.000812 | 0.00029 | 4.93852E-06 | 59592728 | **4.29** |
| 0.016 | 50 | 490.5 | 1062 | 16.6113 | 0.000742 | 0.000233 | 3.54515E-06 | 83014857 | **5.32** |
| 0.016 | 50 | 490.5 | 1208 | 19.48558 | 0.00094 | 0.000206 | 2.95666E-06 | 165896866 | **3.50** |
| 0.016 | 50 | 490.5 | 1204 | 23.83222 | 0.000689 | 0.00015 | 1.83712E-06 | 266994382 | **5.59** |
| 0.016 | 50 | 490.5 | 1152 | 47.70992 | 0.000713 | 0.000123 | 1.35583E-06 | 361771940 | **5.43** |
| 0.016 | 50 | 490.5 | 1187 | 55.06608 | 0.000817 | 0.000286 | 4.84304E-06 | 101279318 | **4.36** |
| 0.016 | 50 | 490.5 | 1196 | 117.9245 | 0.000762 | 5.05E-05 | 3.5887E-07 | 1.367E+09 | **4.82** |
| 0.016 | 50 | 490.5 | 1194 | 64.76684 | 0.000649 | 0.000234 | 3.57378E-06 | 137249756 | **6.14** |
| 0.016 | 50 | 490.5 | 1119 | 64.59948 | 0.000825 | 0.000225 | 3.375E-06 | 145333333 | **4.42** |
| 0.016 | 50 | 490.5 | 1042 | 81.69935 | 0.000846 | 0.000183 | 2.46544E-06 | 198950350 | **4.41** |
| 0.016 | 50 | 490.5 | 1215 | 37.03704 | 0.000711 | 0.000205 | 2.93515E-06 | 167112224 | **5.31** |
| 0.016 | 50 | 490.5 | 1197 | 24.34275 | 0.00075 | 0.000214 | 3.12507E-06 | 156956688 | **4.93** |
| 0.016 | 50 | 490.5 | 1201 | 21.20441 | 0.000813 | 0.00029 | 4.93852E-06 | 99321213 | **4.36** |
| 0.016 | 50 | 490.5 | 1071 | 19.95211 | 0.000781 | 0.000213 | 3.09769E-06 | 158343635 | **4.91** |
| 0.016 | 50 | 490.5 | 1109 | 18.58736 | 0.000734 | 0.000208 | 2.98901E-06 | 164101239 | **5.29** |
| 0.016 | 50 | 490.5 | 1158 | 19.02588 | 0.000837 | 0.000295 | 5.06679E-06 | 96806827 | **4.25** |
| 0.016 | 50 | 490.5 | 1184 | 15.98465 | 0.000769 | 0.000263 | 4.25299E-06 | 69198439 | **4.78** |
| 0.016 | 50 | 490.5 | 1114 | 18.27485 | 0.00079 | 0.000265 | 4.31389E-06 | 68221529 | **4.73** |
| 0.016 | 50 | 490.5 | 1038 | 18.27485 | 0.000672 | 0.000293 | 5.00252E-06 | 58830353 | **6.25** |
| 0.016 | 30 | 294.3 | 1107 | 17.36111 | 0.00072 | 0.000315 | 5.5907E-06 | 52641036 | **5.46** |
| 0.016 | 30 | 294.3 | 1239 | 19.01141 | 0.00078 | 0.000258 | 4.13205E-06 | 71223680 | **4.57** |
| 0.016 | 30 | 294.3 | 918 | 18.43658 | 0.00073 | 0.000267 | 4.36894E-06 | 67361801 | **5.87** |
| 0.016 | 30 | 294.3 | 1203 | 17.39736 | 0.00076 | 0.000418 | 8.5307E-06 | 34498923 | **4.82** |
| 0.016 | 30 | 294.3 | 1162 | 17.65537 | 0.000568 | 0.000346 | 6.44295E-06 | 45677843 | **7.60** |
| 0.016 | 30 | 294.3 | 1051 | 19.516 | 0.000784 | 0.000296 | 5.08613E-06 | 57863291 | **4.93** |
| 0.016 | 50 | 490.5 | 1208 | 18.86792 | 0.000834 | 0.000443 | 9.30829E-06 | 52694962 | **4.19** |
| 0.016 | 50 | 490.5 | 1356 | 18.02451 | 0.000732 | 0.000438 | 9.15097E-06 | 53600881 | **4.81** |
| 0.016 | 50 | 490.5 | 1187 | 19.17178 | 0.000656 | 0.000398 | 7.92512E-06 | 61891828 | **6.06** |
| 0.016 | 50 | 490.5 | 1305 | 18.08973 | 0.000869 | 0.000403 | 8.07512E-06 | 60742153 | **3.79** |
| 0.016 | 50 | 490.5 | 1076 | 17.89549 | 0.000887 | 0.000448 | 9.4665E-06 | 51814278 | **4.05** |
| 0.016 | 50 | 490.5 | 1174 | 19.17178 | 0.000692 | 0.000379 | 7.37104E-06 | 66544176 | **5.62** |
| 0.016 | 50 | 490.5 | 1114 | 20.34174 | 0.000725 | 0.000458 | 9.78558E-06 | 50124767 | **5.38** |
| 0.016 | 50 | 490.5 | 1110 | 17.32502 | 0.000834 | 0.000295 | 5.05392E-06 | 97053469 | **4.37** |
| 0.016 | 50 | 490.5 | 1166 | 19.17178 | 0.000921 | 0.000408 | 8.22605E-06 | 59627636 | **3.67** |
| 0.016 | 50 | 490.5 | 1183 | 18.86792 | 0.000689 | 0.000432 | 8.96337E-06 | 54722737 | **5.64** |
| 0.016 | 50 | 490.5 | 1393 | 19.08397 | 0.000712 | 0.000398 | 7.92512E-06 | 61891828 | **4.94** |
| 0.016 | 50 | 490.5 | 1460 | 17.25328 | 0.000675 | 0.000403 | 8.07512E-06 | 60742153 | **5.23** |
| 0.016 | 50 | 490.5 | 1272 | 18.40943 | 0.000742 | 0.000408 | 8.22605E-06 | 59627636 | **4.86** |
| 0.016 | 30 | 294.3 | 1191 | 19.57713 | 0.000865 | 0.000296 | 5.09903E-06 | 96194773 | **3.99** |
| 0.016 | 30 | 294.3 | 1003 | 17.12329 | 0.000862 | 0.000313 | 5.52427E-06 | 88789984 | **4.37** |
| 0.016 | 30 | 294.3 | 1088 | 19.516 | 0.00072 | 0.000345 | 6.40809E-06 | 76543862 | **5.50** |
| 0.016 | 30 | 294.3 | 1110 | 17.66784 | 0.000697 | 0.000233 | 3.54515E-06 | 138358096 | **5.72** |
| 0.016 | 30 | 294.3 | 1107 | 19.57713 | 0.00085 | 0.00039 | 7.70188E-06 | 63685726 | **4.25** |
| 0.016 | 30 | 294.3 | 1172 | 22.04586 | 0.00071 | 0.000308 | 5.39222E-06 | 90964373 | **5.41** |
| 0.016 | 50 | 490.5 | 1071 | 19.79414 | 0.00074 | 0.000293 | 5.00252E-06 | 98050589 | **5.32** |
| 0.016 | 30 | 294.3 | 1199 | 19.516 | 0.000745 | 0.000375 | 7.26184E-06 | 67544830 | **4.98** |
| 0.016 | 30 | 294.3 | 1134 | 17.60563 | 0.00082 | 0.000351 | 6.57598E-06 | 74589610 | **4.43** |
| 0.016 | 30 | 294.3 | 1189 | 19.79414 | 0.00072 | 0.000326 | 5.88608E-06 | 83332155 | **5.26** |
| 0.016 | 30 | 294.3 | 1156 | 20.90301 | 0.00065 | 0.000118 | 1.27367E-06 | 385107709 | **6.22** |

| | | | | | | | | | |
|---|---|---|---|---|---|---|---|---|---|
| 0.016 | 30 | 294.3 | 1164 | 20.3252 | 0.00069 | 0.00021 | 3.04319E-06 | 161179599 | **5.67** |
| 0.016 | 30 | 294.3 | 1198 | 18.86792 | 0.00076 | 0.000195 | 2.72303E-06 | 180130434 | **4.83** |
| 0.016 | 50 | 490.5 | 1210 | 18.79699 | 0.000637 | 0.000293 | 5.00252E-06 | 98050589 | **6.27** |
| 0.016 | 30 | 294.3 | 1201 | 18.22157 | 0.000742 | 0.000213 | 3.09769E-06 | 158343635 | **5.01** |
| 0.016 | 30 | 294.3 | 1169 | 19.90446 | 0.000787 | 0.00031 | 5.45811E-06 | 89866219 | **4.64** |
| 0.016 | 30 | 294.3 | 1154 | 15.01502 | 0.000876 | 0.000222 | 3.30773E-06 | 148289209 | **3.98** |
| 0.016 | 30 | 294.3 | 1208 | 19.9362 | 0.000659 | 0.000234 | 3.57378E-06 | 137249756 | **5.96** |
| 0.016 | 30 | 294.3 | 1204 | 17.80627 | 0.000864 | 0.000259 | 4.15615E-06 | 118017984 | **3.98** |
| 0.016 | 30 | 294.3 | 1158 | 18.22157 | 0.000785 | 0.00015 | 1.83712E-06 | 266994382 | **4.68** |
| 0.016 | 30 | 294.3 | 1187 | 20.90301 | 0.000754 | 0.000223 | 3.31891E-06 | 147789639 | **4.92** |
| 0.016 | 50 | 490.5 | 1196 | 20.90301 | 0.000876 | 0.000438 | 9.16666E-06 | 53509125 | **3.91** |
| 0.016 | 50 | 490.5 | 1163 | 21.49613 | 0.000865 | 0.000433 | 8.99454E-06 | 54533057 | **4.04** |
| 0.016 | 50 | 490.5 | 1101 | 22.70663 | 0.000675 | 0.000338 | 6.20027E-06 | 79109447 | **6.03** |
| 0.016 | 50 | 490.5 | 1123 | 22.2618 | 0.000764 | 0.000382 | 7.46612E-06 | 65696762 | **4.95** |
| 0.016 | 50 | 490.5 | 1143 | 21.87227 | 0.000854 | 0.000427 | 8.82352E-06 | 55590067 | **4.15** |
| 0.016 | 50 | 490.5 | 1162 | 21.51463 | 0.00067 | 0.000335 | 6.13151E-06 | 79996650 | **5.93** |
| 0.016 | 50 | 490.5 | 1158 | 21.58895 | 0.000782 | 0.000391 | 7.73152E-06 | 63441563 | **4.71** |
| 0.016 | 50 | 490.5 | 1249 | 20.01601 | 0.000765 | 0.000383 | 7.48078E-06 | 65567987 | **4.69** |
| 0.016 | 50 | 490.5 | 1062 | 23.54049 | 0.000695 | 0.000348 | 6.47787E-06 | 75719336 | **5.87** |

Regards

Pratik Shukla

## 11.14: Acceptance of Publications

**National Conference on**
***"Recent Developments & Futuristic Trends in Mechanical Engineering"***
**(NCME-2007)**
**April 28-29, 2007**

Department of Mechanical Engineering
**Shri Ram College of Engineering & Management**
(An ISO 9001:2000 Certified Institute)
A. B. Road, Banmore, Morena, MP. Website: www.srcem.org, E-Mail ID: ncme.srcem@gmail.com, Ph: 07532 255798, 255024, 255873, Fax: 07532 255893



To

**Mr. Pratik P. Shukla**

Sub: - Acceptance Letter – NCME 2007

Dear Sir,

Congratulations! It gives me immense pleasure to inform you that, your abstract has been accepted for full-length paper submission in the National Conference on Recent Developments & Futuristic Trends in Mechanical Engineering (NCME-2007) to be held during 28th to 29th April, 2007 at Banmore (India). The details of the paper are as follows,

| Name of the author/s | Title of the paper/s | Ref. No. |
|---|---|---|
| **Pratik P. Shukla** | Effects of High Speed Laser Welding, on tin plated steels applicable to manufacture three piece packaging Cans<br><br>**Determination of Fracture Toughness using Vickers Indentation method applied to Laser Treated Engineering Ceramics.** | **PD 81, PD 49** |

Please find an attachment of Author Guidelines for preparing full-length paper. All the required formatting details are mentioned in it. Please send one hard copy of the same by post also. Kindly mention your Ref. No hereafter with every communication.

Please keep in mind that for publication of your paper in the NCME 2007 Proceedings, it is mandatory that you register yourself for the conference before **April 20, 2007.** The registration form is also attached here with. Please fill the registration form completely and attach the Demand Draft, in favour of "**The Principal, SRCEM, Banmore**, Payable at **Gwalior** of registration fee (mentioning your name and affiliation on the back side of D.D.); send it by post so as to reach on or before **April 20, 2007**.

| | |
|---|---|
| Vice Chairman<br>ShriRam Group of Colleges, Banmore<br><br>**Shri Harendra Sharma**<br>Secretary<br>ShriRam Group of Colleges, Banmore<br><br>**Org. Chairman:**<br>**Prof. H.B. Khurasia**<br>Director, SRCEM, Banmore | Feel free to enquire about any details regarding this. We are very much thankful for your highly valued contribution to this event.<br><br>With warm regards,<br>**P.S. Chauhan**<br>Convener, NCME-2007<br><br>Assistant Professor & Head, Department of Mechanical Engineering, ShriRam College of Engineering & Management, A. B. Road, Banmore, Near Gwalior, Madhya Pradesh , Web Site: www.srcem.org , E Mails: ncme_srcem@rediffmail.com, ncme.srcem@gmail.com, Ph: 07532 - 255798, 255873, 255024, Fax: 07532 – 255893, M: 094257 12291 |

## 11.15: Meetings with Colin Page

Meetings were held on weekly basis to discuss the status of the project. Colin Page provided support from start to the finish of the complete project by means of one to one discussions telephone conversations and obtaining feedback via email during my time off campus.

## 11.16: Meetings with Dr Wu

Meetings were held on a regular basis as Dr Wu introduced the project. However, due to his transfer to Loughborough University, minimum support was attained. However, I paid visits according to availability from both sides.

***January 2007***

The method of analysis

- Reliability and consistency of the results
- Laser / material interaction

***April 2007***

- Plan of action for a conference publication
- Investigate oxidation issues by:
- Conducting experiments on stainless steel

Use stainless steel (austenitic) to compare with $Si_3N_4$ and test its micro hardness, observe what is happening at the laser / material interface to come up with a conclusion for $Si_3N_4$.

***May 2007***

- Learn how to operate the SEM in order to take images of the test samples and also observe if there is some evidence of oxidation.

- Try to reduce the laser power density while processing. Possibly by changing either power, mark speed or the focal spot size as one individual parameter.

- If time permits; conduct a finite stress element analysis (FEA) on the laser treated sample simply to examine the heat distribution after the laser treatment.

## 11.17: Determination of Fracture Toughness using Vickers Indentation method applied to Laser Treated Engineering Ceramics.

**Author: Pratik P. Shukla**
Coventry University, Faculty of Engineering and Computing, Sir Frank Whittle Building, Priory Street, Coventry, CV1 – 5FB, United Kingdom, Tel: 0044 02476 888550, 0044 7739461805, Email: cey245@coventry.ac.uk ; pratik.shukla@21com

**Contributors: Dr Colin Page and Dr Houzheng Z. Wu**

**Abstract**
The aim of this study is to investigate the fracture toughness ($K_{1c}$) of Silicon nitride ($Si_3N_4$) ceramics by employing $CO_2$ and Nd: YAG (niodinium, yittrium, aluminium garnet) industrial lasers. Vickers indentation method is used to determine the $K_{1c}$ of hot pressed and reaction bonded $Si_3N_4$.

Vickers macro indenter was employed to create diamond indents into the treated and un-treated surface layer of the $Si_3N_4$ to obtain the hardness. Indents were created using 5 kg, 20 kg, 30 kg and 50 kg loads. Hardness of the material and cracks produced by the indentations were measured and recorded. The values obtained for the two parameters are placed into the equation* to calculate the $K_{1c}$. Diverse equations calibrated for ceramic materials were applied to the indented virgin surface to first obtain the true $K_{1c}$ value of the $Si_3N_4$. From this study, it was proven that the best possible equation for $Si_3N_4$ as derived by [Antis, Chantikul, Lawn and Marshall, 1981] is: $*K_{1c} = 0.016\ [E/H]^{1/2} \times [P/C^{3/2}]$ and confirmed to be accurate.

Test samples were ground then polished using diamond and abrasive wheels at 10 µm, 6 µm and 3 µm prior to the surface treatment. Scanning electron microscopy (SEM) and optical microscopy were used to analyse the surface morphology and to present the results by the aid of micrographs.

Surface treatment using the $CO_2$ laser decreased the hardness by 26 percent. 45 percent of the tested samples showed increase in $K_{1c}$ by an average of 8.19 MPa $M^{1/2}$. Nd: YAG treatment of $Si_3N_4$ decreased the hardness by 24 percent. Measured crack lengths from Vickers indentation are much larger than the cracks from $CO_2$ laser processing. This decreased the $K_{1c}$ value of the samples treated by Nd: YAG laser processing. It is believed that the composition of the $Si_3N_4$ surface layer has transformed due to oxidation during $CO_2$ laser processing. This has led to the difference in the crack generation between the two lasers treatments processed, as further discussed in the paper.

$K_{1c}$ = Fracture Toughness, 0.016 = Calibrated value for $Si_3N_4$, E = Young's Modulus of $Si_3N_4$, H = Material hardness [Hv], P = Load [Vickers Indentation (N)], C = Average crack size [Meters]

***Keywords***: *Fracture Toughness ($K_{1c}$), surface cracks, $CO_2$ and Nd: YAG laser processing, Vickers indentation.*

**Date: 12/02/07**
*Abstract accepted and published for the NCME 2007 (National Conference of Futuristic Trends in Mechanical Engineering, Gwalior, India. Paper not written due to time constraints.*

# 11.18: Shot Peening of Ceramics Using Non- Contact Energy Beams

**Pratik P. Shukla***
Advance Joining Centre, Coventry University, Coventry, U.K

**Dr Colin Page**
Advance Joining Centre, Coventry University, Coventry, U.K

**Dr Houzheng Wu**
IPTME, Loughborough University, U.K

**Abstract**
Laser Shot Peening is a comparable process to the conventional peening technique applied on various types of metal surfaces. Commercial advantages offered by the laser systems such as flexibility, deep penetration, shorter process times, high speeds, accuracy and aesthetics are attractive in comparison with the conventional peening technique. This research aims to start the process of addressing the gap in knowledge by applying industrial lasers and energy beams to Silicon Nitride ($Si_3N_4$) in particular as a typical ceramic. The investigation was highlighted on the feasibility of shot peening $Si_3N_4$ using the non- contact energy beams and analysing the fracture toughness ($K_{1c}$) of the $Si_3N_4$ ceramic.

$CO_2$, Nd: YAG (Niodinium, Yittrium, Aluminium Garnet) industrial lasers and plasma augmented processing were employed. $K_{1c}$ of the hot pressed ($HPSi_3N_4$) and reaction bonded $Si_3N_4$ ($RBSi_3N_4$) was calculated by using the Vickers indentation method.

Surface treatment using the $CO_2$ laser showed decrease in hardness by 26 percent. 45 percent of the tested samples showed increase in $K_{1c}$ by 8.19 MPa $M^{1/2}$. Nd: YAG treatment of $Si_3N_4$ decreased the hardness by 24 percent. Measured crack lengths from Vickers indentation were much larger than the cracks from $CO_2$ laser processing. This decreased the $K_{1c}$ value of the samples treated by Nd: YAG laser processing. Increase in $K_{1c}$ was found using the $CO_2$ laser processing in comparison with the other energy beams.

Justification of the enhancement in $K_{1c}$ by the $CO_2$ laser and the interaction between the material and the energy beams in comparison with the conventional shot peening is further discussed in this paper, along with the feasibility of shot peening $Si_3N_4$ by the employed energy beams.

***Key word:*** *Non-contact energy beams, $CO_2$ and Nd: YAG Laser, Plasma Augmented Processing, $Si_3N_4$, Fracture Toughness ($K_{1c}$), Vickers Indentation Method.*

**Date: 15/05/07**
*Paper to be written for the 10th International conference of Shot peening science in September 2008.*